UNIVERSITÀ DEGLI STUDI DI TRIESTE

XXXV CICLO DEL DOTTORATO DI RICERCA IN

Earth Science, Fluid-Dynamics, and Mathematics.
Interactions and Methods

Borsa MIUR

Geometry and kinematics of the Cyprus Arc system

Settore scientifico-disciplinare: GEO/03

DOTTORANDO

Nicolò Bertone

COORDINATORE

PROF. Stefano Maset

SUPERVISORE DI TESI

PROF. Pini Gian Andrea

CO-SUPERVISORI DI TESI

PROF. Lorenzo Bonini

DOTT. Anna Del Ben

ANNO ACCADEMICO 2021/2022

CONTENTS

Sommario

ABSTRACT

Convergent margins are areas where two or more tectonic plates collide. The tectonic characteristics of these areas can vary depending on the type of plate involved. For example, a convergent margin where an oceanic plate collides with a continental plate is different from a margin where two continental plates collide. In general, convergent margins can start with intraoceanic subduction and end with a continent-continent collision that creates an orogen. One way to study these systems is to analyze ancient convergent systems, for example by examining exposed rocks along an orogenic belt. However, this approach can be challenging, especially for old phases. An alternative approach is to select an area where different types of convergent margins are active today. The Cyprus Arc system in the eastern Mediterranean is an example of this, as it contains different types of convergent margins, from oceanic subduction to continent-continent collision.

During the Cretaceous, a regional phase of compression began, leading to a rearrangement of the rifted blocks. The Afro-Arabian plate collided with the Eurasian plate and formed suprasubduction ophiolite complexes, which were later obducted and led to the closure of the southern Neo-Tethys. The compressive phase continued until the Eocene, creating the Syrian Arc when continental collision began on the Arabian margin. Meanwhile, The Red Sea began to open in the middle Miocene, forming the Dead Sea Transform Fault. All these different movements are now associated with the tectonic escape of the Anatolian microplate, strong uplift of the margins and sinistral strike-slip activity which mainly controls the tectonics today.

The Levant Basin, an extensional basin in the southeastern Mediterranean, has received much attention due to its hydrocarbon resources. However, the geometry of the main structures and their kinematics remain controversial, as previous studies have proposed different models to explain the tectonic evolution of the area.

The aim of this thesis is to shed new light on the Cenozoic tectonic evolution of the eastern Mediterranean Sea by analysis the tectonic characteristics of different types of crust which collide along a single convergent boundary. We therefore propose the division of the Cyprus Arc system into three segments with different structural framework: active oceanic subduction beneath the Florence Rise, incipient continental collision beneath the Cyprus Arc and suture thickening via transpression beneath the Latakia Ridge.

Studying new data or re-evaluating existing data can help clarify some of the contentious issues and improve knowledge of the geometries and timing of the major structures in this sector of the Mediterranean Sea. To this aim, we have used three regional seismic reflection profiles crossing the main structures of the area. They offer insights into the region's geological history and a new example of how convergent margins evolve when different plate types are involved.

The seismic datasets used for this study are vintage seismic reflection datasets: the MS and the Strakhov-5 surveys. These two surveys consist of regional and deep seismic profiles acquired during the first geophysical exploration phase of the Mediterranean Sea.

From 1969 to 1982, the National Institute of Oceanography and Applied Geophysics (OGS) in Trieste (Italy) acquired several multichannel seismic profiles with the National Research Council ship "Marsili" as part of an Italian scientific program to explore the entire Mediterranean. In recent years, the OGS has used modern seismic processing techniques to reprocess and time-migrate all the seismic sections.

In 1987, GEOMAR (i.e., Helmholtz Center for Ocean Research Kiel), in collaboration with the Russian Academy of Sciences acquired 1700 km of multichannel seismic reflection data over the Cyprus Arc system from the Florence Rise to the Syrian coast during the 5th cruise of the research vessel Akademik Nikolay Strakhov. This was the first comprehensive geophysical data acquisition around the Cyprus Arc system and, more generally, in the northern Levant Basin. This dataset includes the stack version, the depth-migrated version of the seismic profiles, and the velocity analysis.

Regardless of the reprocessing phase, the resolution for the first 3/7 seconds (TWT) is good, depending on the water depth. However, these seismic sections have a good penetration depth to visualize the entire Cenozoic deposits and deeper structures than other seismic profiles in the study area. The first phase was dedicated to the seismic interpretation of the time-migrated sections. We interpreted the main seismic packages and faults, as we aim to build an evolutionary tectonic model of the area that describes the Cenozoic evolution. We use the velocity analysis of the seismic profile and previous estimates of the velocities of the seismo-stratigraphic packages to create geological sections that match our seismic profiles. The depth profiles are a prerequisite for building an evolutionary model that describes the major tectonostratigraphic phases.

This study focuses on three transects crossing the main offshore structures (i.e., Florence Rise, Cyprus Arc and Latakia Ridge) from west to east.

The Western Transect (MS53) shows how the Herodotus Basin's oceanic crust subducts northward beneath the Eurasian plate. The Florence Rise is the leading edge of the system, and the Antalya Basin is its forearc basin. Near the Turkish coast, a buried block appears to act as a backstop for the offshore system, and some out-of-sequence thrusts have been interpreted north of it. The strain is partitioned between the Florence Rise and the Taurides front.

The Central Transect (Strakhov-8) is located south of Cyprus. This profile shows the Eratosthenes Seamount, the Cyprus Trench, and its accretionary wedge from south to north. The Eratosthenes Seamount is faulted by active extensional faults due to the weight of the overriding upper plate. As this seamount has a thicker crust than the surrounding Levant Basin (thinned continental crust) and the Herodotus Basin (oceanic crust), it now acts as an inhibitor to the forward propagation of the Cyprus accretionary wedge. The uppermost reflectors also witness this inhibitory behaviour in the Cyprus Trench. The lower part of the Plio-Quaternary succession is characterized by growth strata that flatten in the upper part. This effect is related to a minor forward propagation of the Cyprus Arc in this sector. In fact, from the Pleistocene onwards, the island of Cyprus experienced a substantial uplift due to the docking of this thick continental block, which stopped the horizontal spreading and triggered vertical movements.

The Eastern Transect (MS56) crosses the Latakia Ridge, i.e., the northern boundary of the Levant Basin. The seismic line continues north into the Cyprus and Latakia basins, crosses the Kyrenia Ridge and reaches the Turkish coast. On the seismic section, we interpreted the Mesozoic subduction front which is now hindered by strike-slip motions on the Latakia Ridge. Another prominent transpressive structure is the Kyrenia Ridge, which is interpreted as an active transpressive structure with a well-imaged thrust system in front of it.

Our data allowed an accurate reconstruction of the evolution of the Cyprus Arc system from the Messinian in the Western and Central Transects and from the Paleogene in the Eastern Transect. Moving from west to east with respect to Cyprus, it was possible to analyze the evolution from oceanic subduction to the continent-continent collision along the same convergent margin. The characteristic features are a thinner accretionary wedge to the west and a thicker and more deformed wedge toward the east. The trenches also vary along strike: the Herodotus Basin has a poorly developed trench due to the small amount of sediment that can reach it as the Florence Rise is a structural barrier. South of Cyprus, the trench is well developed and records the recent evolution of this system, and on the Eastern Transect, there is no trench as strike-slip movements dominate

today. This interpretation is also supported by the earthquake location, which becomes shallower from west to east and is in good agreement with the gravimetric and magnetic studies. In conclusion, the tectonic evolution of the eastern Mediterranean is a complex process that is the result of the interaction between different plates, with different types of convergent margins.

RIASSUNTO

I margini convergenti sono aree in cui due o più placche tettoniche si scontrano. Le caratteristiche tettoniche di queste aree possono variare a seconda del tipo di placca coinvolta. Ad esempio, un margine convergente in cui una placca oceanica si scontra con una placca continentale è diverso da un margine in cui due placche continentali si scontrano. In generale, i margini convergenti possono iniziare con la subduzione intraoceanica e terminare con una collisione continente-continente che crea un orogeno. Un modo per studiare questi sistemi è quello di analizzare antichi sistemi convergenti, ad esempio esaminando le rocce esposte lungo una cintura orogenetica. Tuttavia, questo approccio può essere impegnativo, soprattutto per le vecchie fasi. Un approccio alternativo consiste nel selezionare un'area in cui oggi sono attivi diversi tipi di margini convergenti. Il sistema dell'Arco di Cipro nel Mediterraneo orientale ne è un esempio, in quanto contiene diversi tipi di margini convergenti, dalla subduzione oceanica alla collisione continente-continente.

Durante il Cretaceo, iniziò una fase regionale di compressione, che portò ad un riarrangiamento dei blocchi riftati. La placca afro-arabica entrò in collisione con la placca eurasiatica e formò complessi ofiolitici di soprasubduzione, che furono successivamente obdotti e portarono alla chiusura della Neotetide meridionale. La fase di compressione continuò fino all'Eocene, creando l'Arco siriano, quando iniziò la collisione continentale sul margine arabo. Il Mar Rosso cominciò ad aprirsi nel Miocene medio, formando la faglia trasforme del Mar Morto.

Tutti questi diversi movimenti sono ora associati all’estrusione tettonica della microplacca anatolica, e il forte sollevamento dei margini e la trascorrenza sinistra controllano principalmente la tettonica odierna. Il bacino di Levante, un bacino estensionale nel Mediterraneo sud-orientale, ha ricevuto molta attenzione a causa delle sue risorse di idrocarburi. Tuttavia, la geometria delle strutture principali e la loro cinematica rimangono controverse, poiché studi precedenti hanno proposto diversi modelli per spiegare l'evoluzione tettonica dell'area.

Studiare nuovi dati o rivalutare quelli esistenti può aiutare a chiarire alcune di queste questioni controverse e migliorare la conoscenza delle geometrie e dei tempi delle principali strutture in questo settore del Mar Mediterraneo. A tal fine, abbiamo utilizzato tre profili regionali di riflessione sismica che attraversano le principali strutture dell'area di studio. Queste sezioni permettono di approfondire la storia geologica della regione e dare un nuovo esempio di come i margini convergenti si evolvono quando sono coinvolti diversi tipi di placche.

I dataset di dati sismici utilizzati per questo studio sono composti da dati di riflessione sismica vintage: le campagne di acquisizione MS e Strakhov-5. Queste due campagne di acquisizione consistono in profili sismici regionali e profondi acquisiti durante la prima fase di esplorazione geofisica del Mar Mediterraneo.

Dal 1969 al 1982, l'Istituto Nazionale di Oceanografia e Geofisica Applicata (OGS) di Trieste (Italia) ha acquisito diversi profili sismici multicanale con la nave del Consiglio Nazionale delle Ricerche "Marsili" come parte di un programma scientifico italiano per esplorare l'intero Mediterraneo. Negli ultimi anni, l'OGS ha utilizzato moderne tecniche di elaborazione sismica per rielaborare e migrare in tempi tutte le sezioni sismiche.

Nel 1987, GEOMAR (cioè Helmholtz Center for Ocean Research Kiel), in collaborazione con l'Accademia Russa delle Scienze ha acquisito 1700 km di dati di sismica a riflessione multicanale attraverso il sistema dell'arco di Cipro (dal Florence Rise alla costa siriana) durante la 5a crociera della nave da ricerca Akademik Nikolay Strakhov. Questa è stata la prima acquisizione completa di dati geofisici intorno al sistema dell'arco di Cipro e, più in generale, nel bacino settentrionale del Levante. Questo dataset include la versione stack, la versione migrata in profondità dei profili sismici e le analisi di velocità.

Indipendentemente dalla fase di rielaborazione, la risoluzione per i primi 3/7 secondi (TWT) è buona, a seconda della profondità della colonna d'acqua. Tuttavia, queste sezioni sismiche hanno una buona profondità di penetrazione per visualizzare l'intero deposito cenozoico e le strutture più profonde rispetto ad altri profili sismici nell'area di studio. La prima fase è stata dedicata all'interpretazione sismica delle sezioni migrate in tempo. Abbiamo interpretato i principali pacchetti sismici e faglie, poiché il nostro obiettivo è quello di costruire un modello tettonico evolutivo dell'area che descriva l'evoluzione cenozoica. Abbiamo poi utilizzato l'analisi di velocità del profilo sismico e le precedenti stime delle velocità dei pacchetti sismo-stratigrafici per creare sezioni geologiche che corrispondano ai nostri profili sismici. I profili di profondità sono un prerequisito per costruire un modello evolutivo che descriva le principali fasi tettonostratigrafiche.

Questo studio si concentra su tre transetti che attraversano le principali strutture offshore (cioè Florence Rise, Cyprus Arc e Latakia Ridge) da ovest a est.

Il transetto occidentale (MS53) mostra come la crosta oceanica del bacino di Erodoto subduca verso nord sotto la placca eurasiatica. Il Florence Rise è il fronte del sistema e il bacino di Antalya è il suo

bacino di forearc. Vicino alla costa turca, un blocco sepolto sembra fungere da backstop per il sistema offshore, e alcune faglie inverse fuori sequenza sono state interpretate a nord di esso. La deformazione è partizionata tra il Florence Rise e il fronte delle Tauridi.

Il transetto centrale (Strakhov-8) si trova a sud di Cipro. Questo profilo mostra il seamount di Eratostene, la fossa di Cipro e il suo cuneo di accrezione da sud a nord. Il seamount di Eratostene è affetto da faglie estensionali attive dovute al peso della placca superiore che sovrascorre quella inferiore. Poiché questo blocco ha una crosta continentale più spessa rispetto al bacino di Levante circostante (crosta continentale assottigliata) e al bacino di Erodoto (crosta oceanica), ora agisce come inibitore della propagazione del cuneo di accrezione cipriota. I riflettori più superficiali del Plio-Quaternario testimoniano anche questo comportamento inibitorio nella fossa di Cipro. La parte inferiore della successione Plio-Quaternaria è caratterizzata da strati di crescita che si appiattiscono nella parte superiore. Questo effetto è legato a una propagazione minore dell'arco di Cipro in questo settore. Infatti, dal Pleistocene in poi, l'isola di Cipro subì un notevole sollevamento dovuto all'ingresso di questo spesso blocco continentale, che ne fermò la propagazione orizzontale e innescò movimenti verticali.

Il transetto orientale (MS56) attraversa il Latakia Ridge, cioè il confine settentrionale del bacino di Levante. La linea sismica prosegue verso nord nel bacino di Cipro e di Latakia, attraversa il Kyrenia Ridge e raggiunge la costa turca. Sulla sezione sismica abbiamo interpretato il fronte di subduzione mesozoica, che ora è “compromesso” da movimenti trascorrenti sul Latakia Ridge. Un'altra importante struttura traspressiva è il Kyrenia Ridge, che viene interpretato come una struttura attiva con un sistema di thrust ben visibile al suo fronte.

I nostri dati hanno permesso un'accurata ricostruzione dell'evoluzione di questi margini convergenti dal Messiniano al Quaternario nei Transetti Occidentali e Centrali e dal Paleogene nel Transetto Orientale. Spostandosi da ovest a est rispetto a Cipro, è stato possibile analizzare l'evoluzione di questo margine convergente dalla subduzione oceanica alla collisione continente-continente. Le caratteristiche sono un cuneo di accrescimento più sottile a ovest e un cuneo più spesso e deformato verso est. Anche le fosse/avanfosse variano lungo il margine convergente: il bacino di Erodoto ha una fossa poco sviluppata a causa dello scarso apporto di sedimenti che può raggiungerlo in quanto il Florence Rise è una barriera strutturale. A sud di Cipro, l’avanfossa è ben sviluppata e registra la recente evoluzione di questo sistema, e sul transetto orientale, non c'è alcuna avanfossa attiva dato che domina la traspressione sul Latakia Ridge. Questa interpretazione

è supportata anche dalla localizzazione di terremoti, che diventano meno profondi da ovest a est ed è in buon accordo anche con gli studi gravimetrici e magnetici. In conclusione, l'evoluzione tettonica del Mediterraneo orientale è un processo complesso risultante dall'interazione tra diverse placche, con diversi tipi di margini convergenti coinvolti.

CHAPTER 1: INTRODUCTION

Convergent margins are areas where two or more tectonic plates collide. Their behaviour may depend on several factors as the type of lithospheres involved, their ages, the stress orientation and the number of plates involved among others. The oceanic lithosphere is denser than the continental one and, when plates of different densities collide, the denser plate (i.e., oceanic) is pushed below the more buoyant one (i.e., continental) in the process called subduction.

Subduction zones are also called destructive margins because here is where the oceanic crust is consumed. Subduction initiation is still a matter of study (e.g., Stern et al., 2004) when spontaneous or induced and what is the role of the type of plate involved. In a general evolutionary scheme, a convergent margin may begin with intraoceanic subduction and end with a continent-continent collision that produces an orogen over geologic time.

The study of convergent margins is of fundamental importance for the earthquake and ensuing tsunami risk assessment and also to understand the orogenetic processes. The most common approach to studying these systems is to analyze a fossil and exhumed convergent system, for example, by examining exposed rocks along an orogenic belt. However, the accuracy of paleogeographic reconstructions, which depends on the sequential restoration of tectonic phases in these areas can be challenging, especially for ancient phases.

One way to overcome this limitation is to select an area where different types of convergent margins are active today, i.e., an area where one can study convergent ocean-ocean, ocean-continent, and continent-continent margins.

The eastern Mediterranean Sea is a suitable natural laboratory to study the different stages of convergent margins along strike (Fig.1). The diachroneity of the closure of the oceanic crust in the eastern Mediterranean (Gürer & van Hinsbergen, 2019; Darin & Umhoefer, 2022) permits to study from west to east the passage from oceanic subduction, incipient continental collision to continental collision. Moreover, it is also intriguing to study this area because it has been shaped by the superposition of extensional (i.e., Tethys rifting), compressional (i.e., Alpine and Syrian Arc collisions) and strike-slip (i.e., Anatolian escape) tectonics to get the present days configuration (Fig.1).

Along the Cyprus Arc system, there is the coexistence of different tectonic plates involved in the convergence between Africa and Eurasia. The aim of this thesis is to shed new light on the Cenozoic tectonic evolution of the eastern Mediterranean Sea by analysis the tectonic characteristics of different types of crust which collide along a single convergent boundary. We therefore propose the division of the Cyprus Arc system into three segments with different structural framework: active oceanic subduction beneath the Florence Rise, incipient continental collision beneath the Cyprus Arc and suture thickening via transpression beneath the Latakia Ridge (Fig.1).

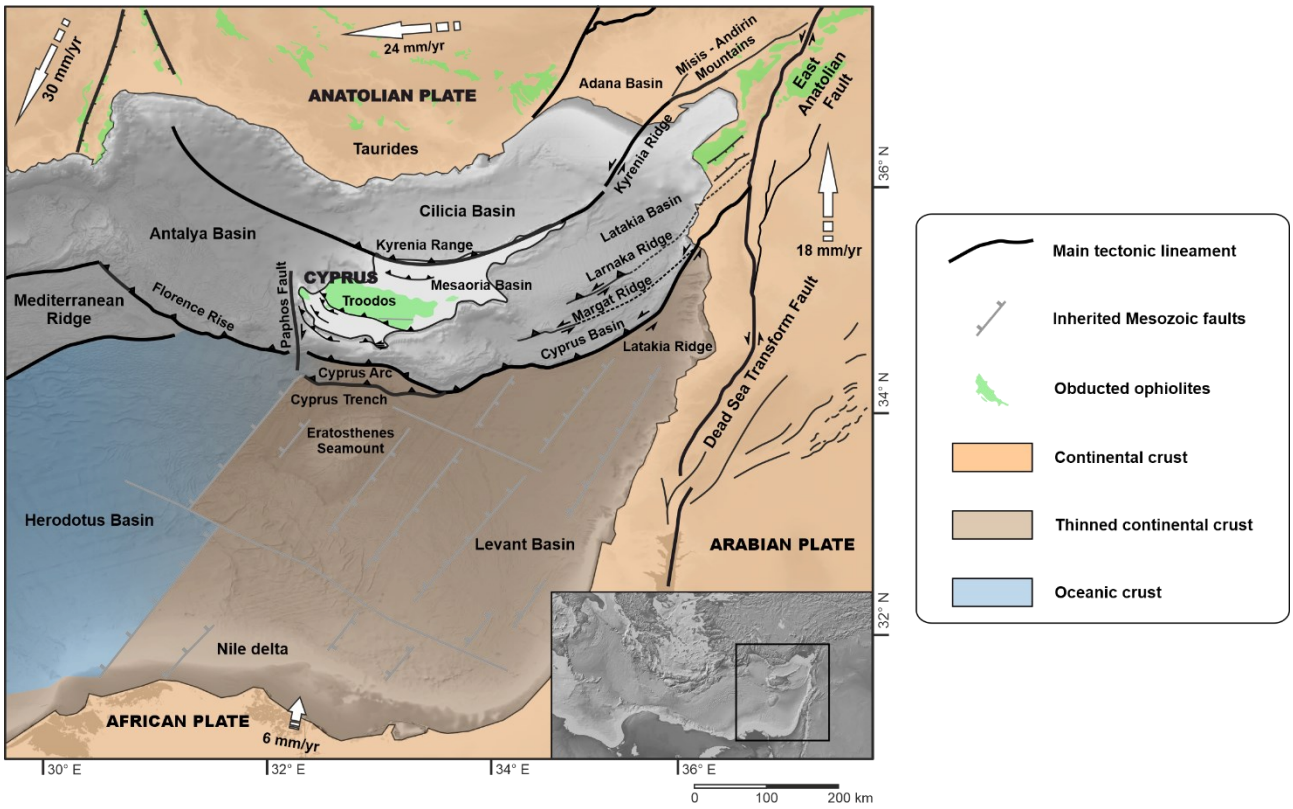

Figure 1: Tectonic map of the eastern Mediterranean. Green spots are the obducted ophiolites from Mc Phee & van Hisbergen, 2019. Extensional faults in the Levant Basin are inherited from the Tethyan rifting phase. The white arrows show the GPS velocity of the plates from McClusky et al. (2000). Tectonic lineaments from Montadert et al. (2014); Longacre et al. (2007) and Mc Phee & van Hisbergen (2019). The crustal domains beneath the Herodotus and Levant Basins are drawn from (Longacre et al., 2007; Granot, 2016). Bathymetry from EMODNet. Topography from GEBCO. Bottom right map inset from GeoMapApp.

We propose a novel model for the Cenozoic tectonic evolution of the Cyprus Arc system to provide new insights into the geologic history of the area and a new example of how convergent margins develop when different plate types are involved. The thesis take advantage from vintage

multichannel seismic reflections lines which cross this convergent margin. Part of these seismic lines has been reprocessed with modern processing techniques to improve the seismic imaging and to valorize the intrinsic value of these vintage data that are unique for their high depth of investigation and length. Then, the seismic interpretation was cross-checked with bibliographic information, magnetic and gravimetric anomalies and inserted into the wider tectonic framework of the studied area.

The core of this thesis is subdivided into:

- Results of the seismic sections interpretation on the time migrated version for the MS dataset and depth migrated version for the Strakhov dataset (Chapter 4.2 – Detailed interpretation of the tectonostratigraphic setting).
- Depth conversion of the time migrated seismic sections (Chapter 4.3 – Depth Conversion).
- Structural modeling of the three proposed transects (Chapter 5.1 – Geological model building).
- Seismic tying between depth converted and depth migrated seismic sections (Chapter 5.2 – Geological model discussion).
- Contextualization of the geological models within the geodynamic context of the eastern Mediterranean Sea (Chapter 5.3 – Linking the transects).

CHAPTER 2: GEOLOGICAL SETTING

2.1 – Geography and physiography of the eastern Mediterranean area

The eastern Mediterranean Sea stretches from the Ionian Sea to the coast of the Middle Eastern countries (Fig.2). It hosts the convergent margin between the African and Eurasian plates, represented by the Calabrian prism formed by Calabrian subduction, the Mediterranean Ridge formed by Hellenic subduction, and the Cyprus Arc system, where different crustal types meet along a convergent boundary. To the south, there are the relatively undeformed basins such as the Ionian Basin and the Herodotus Basin, which are floored by the oldest oceanic crust of the Earth (Triassic age), and the Levant Basin, which consists of transitional crust (Longacre et al., 2007; Granot, 2016; Smaily, 2017). The main physiographic elements are the inherited normal faults on the northern African margin, the positively inverted basins along the convergent margin and the recent extension in the back-arc area of the Hellenic subduction zone (i.e., the Aegean Sea - Fig.2).

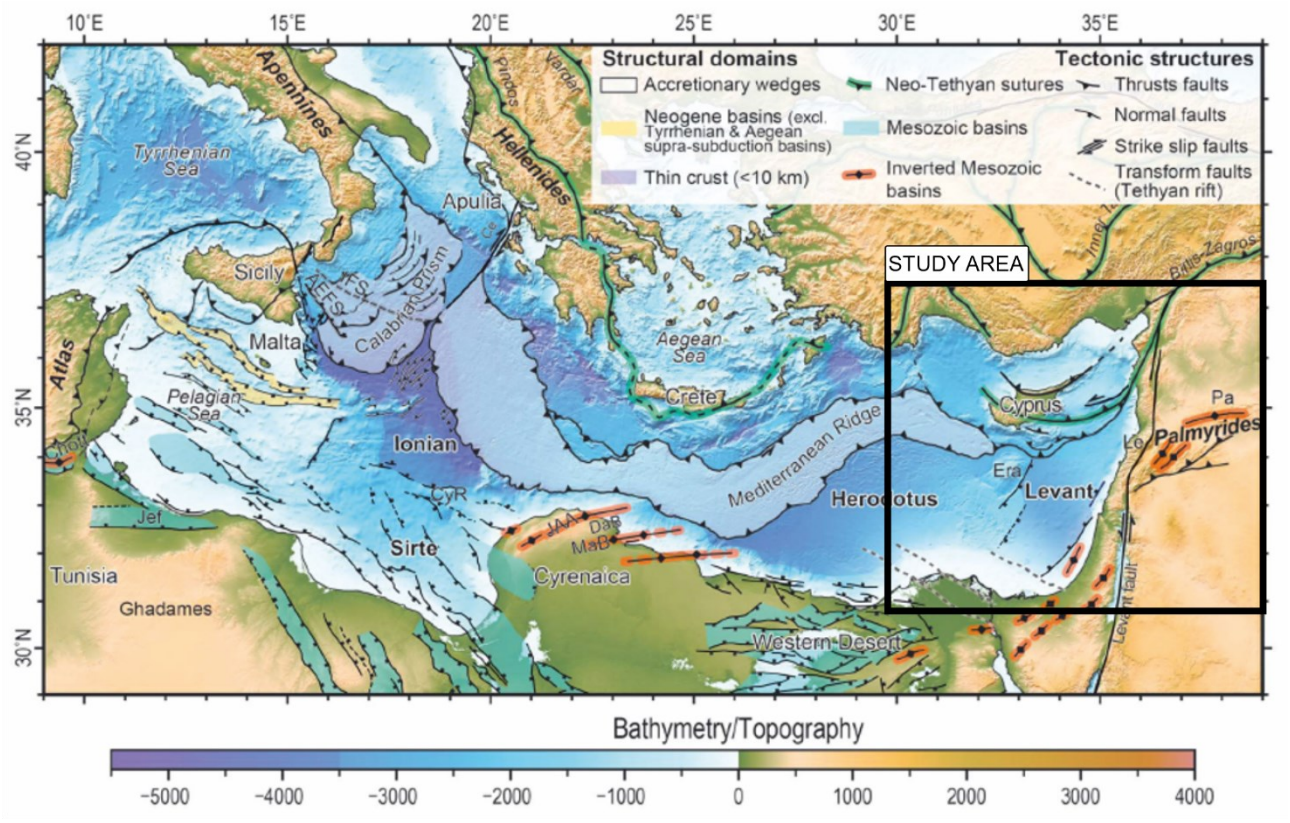

Figure 2: Tectonic map of the eastern Mediterranean Sea showing the main tectonic structures. At the northern margin of Africa, the Mesozoic basins are colored green. The inverted Mesozoic basins formed by the Syrian Arc compression are colored orange, while the Neogene extensional basins are light yellow. The green line represents the Neo-Tethyan sutures formed by the Alpine collision. The accretionary prisms are shown in whitish colors. The purple areas indicate the remnants of the Neo-

Tethys oceanic crust in the Ionian and Herodotus basins. In the northeastern Mediterranean, there is a mixture of structures of different ages: the Mesozoic extensional faults in the Levant Basin, the inverted Mesozoic basins, and the Neo-Tethys suture. Figure modified from Tugend et al. (2019).

In the northeastern corner of the eastern Mediterranean there is the triple junction between the African plate, the Arabian plate and the Anatolian microplate, a smaller plate considered to be part of the Eurasian plate. The main physiographic features of the northeastern Mediterranean are the island of Cyprus and the Cyprus Arc system south of it. The Cyprus Arc system can be divided into three segments: the Florence Rise to the west of Cyprus, the Cyprus Arc (*sensu stricto*) to the south and the Latakia Ridge to the east. South of the island of Cyprus there is the Eratosthenes Seamount, which is the most prominent feature in the bathymetry, and the Nile Delta, which is located at the southern end of the basin (Fig.2).

2.2 – General tectonic overview

The present tectonic structure of the eastern Mediterranean is the result of a long history of deformation, characterized by the alternation of extensional, contractional, and strike-slip phases, and the coexistence of different plate boundaries and crustal types involved in these processes.

2.2.1 - Rifting and post-rifting phase (Triassic – middle Cretaceous)

The formation of the eastern Mediterranean began in the late Paleozoic - early Mesozoic and is related to the opening of the Southern Neo-Tethys Ocean. The rifting of the northern margin of the Gondwana “supercontinent” led to the separation of several continental fragments, such as the Tauride microcontinent or the Eratosthenes Seamount (or continental block). Rifting lasted from the Permo-Triassic to the Middle Jurassic (Gardosh et al. 2010; Montadert et al. 2014) and led to the opening of the Southern Neo-Tethys Ocean with a NW-SE extension. This created an oceanic basin separated by several continental fragments with NE-SW trending normal faults (Fig.3 - Gardosh & Druckman, 2006; Robertson et al., 2012).

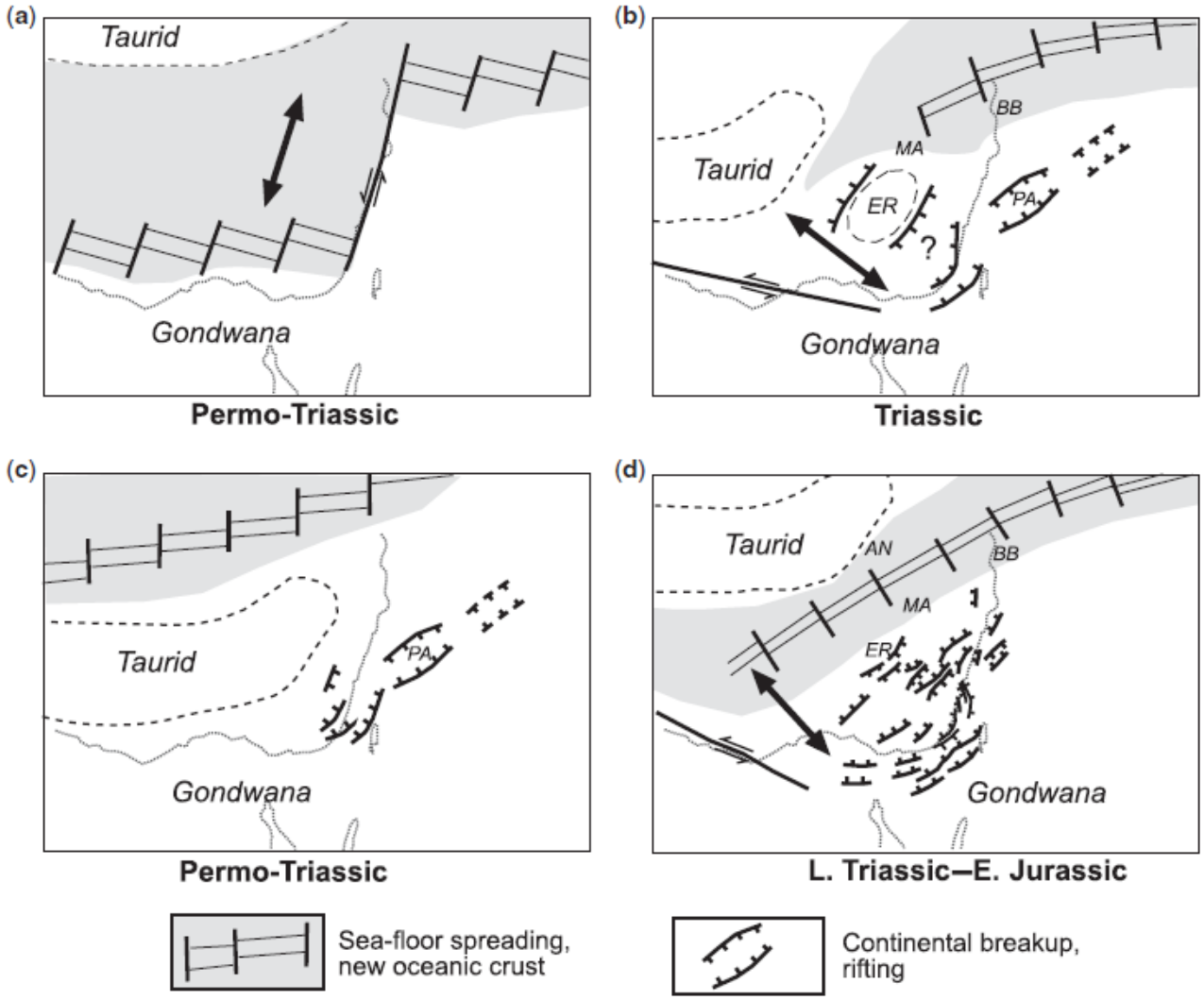

Figure 3: Alternative tectonic reconstructions proposed to explain the Tethyan rifting in the Levant area. a) from Dewey et al. (1973) and Stampfli & Borel (2002), representing a N-S extension involving an eastern transform margin. b) from Garfunkel & Derin (1984) and Garfunkel (1998), representing a NW-SE extension involving a southern transform margin. c) and d) from Gardosh et al. (2010) showing two phases of extension, with the Levant Basin not affected by seafloor spreading and oceanic crust formation. This suggests thinned continental crust beneath the Levant Basin and oceanic crust in the present-day Herodotus Basin between the Eratosthenes Seamount and the Tauride Block. AN = Antalya, MA = Mamonia Complex, BB = Baer-Bassit Massif, ER = Eratosthenes Seamount, Pa = Palmirides Range. Figure from Gardosh et al. (2010).

Rifting in the Levant Basin stopped in an early stage. Gardosh and Druckman (2006) found no evidence of seafloor spreading and oceanic crust emplacement south and east of the Eratosthenes Seamount, only north and west of it in the Herodotus Basin (Fig.3 - Gardosh et al. 2010). Therefore,

a stretched and thinned transitional continental crust is thought to form the floor of the Levant Basin. In contrast, the basement of the Herodotus Basin west of the Eratosthenes Seamount is composed of oceanic crust (Granot, 2016; Smaily, 2017; Netzeband et al. 2006; Longacre et al., 2007; Segev & Rybakov, 2010).

The Triassic rocks outcropping and drilled in the boreholes onshore along the Levant margin consist of dolomites, shallow-water carbonates and evaporites deposited during the rifting phase (Bowman, 2011; Ghalayini et al., 2018). The older drilled offshore rocks are instead shallow-water carbonates and siliciclastic sediments from the Upper Triassic to Lower Jurassic, as found in the Israeli offshore (Gardosh et al., 2008). The data from Israel indicate a north-dipping shallow-water carbonate platform interbedded with shale deposits with evidence of 10 cycles of marine transgression and regression (Gardosh et al., 2008). In contrast, outcrops in the southern Taurides and Mamonia Complex in Cyprus provide evidence of the condition of the northern margin of this basin, which was in a deep-water environment (Fig.3 - Harrison et al., 2008; Bowman, 2011). The Middle Triassic consists of volcanic rocks with MORB affinity, mixed with sandstones, calcarenites and metamorphic rocks (Harrison et al., 2008). The Late Triassic deposits on the southern margin of the Tauride block consist of pelagic limestones and radiolarites (Bowman, 2011). On Cyrpus, the Mamonia Complex has Late Triassic rocks and consists of dolomites and recrystallized limestones (Harrison et al., 2008; Robertson et al., 2012).

The rifting phase probably continued during the Early to Middle Jurassic and eventually led to the break-up of the continent (Robertson et al., 2012; Gardosh et al., 2010). This phase is evidenced by extensive magmatism along the margin and possible intrusions in the Eratosthenes Seamount and the Jonah High in the Levant Basin associated with magmatic anomalies (Rybakov et al., 2011).

The section from the Late Jurassic to the Middle Cretaceous is related to the post-rifting phase, thermal cooling, and the formation of the Afro-Arabian passive margin, which was characterized by more intense subsidence in the basin than at the margins (Fig.4).

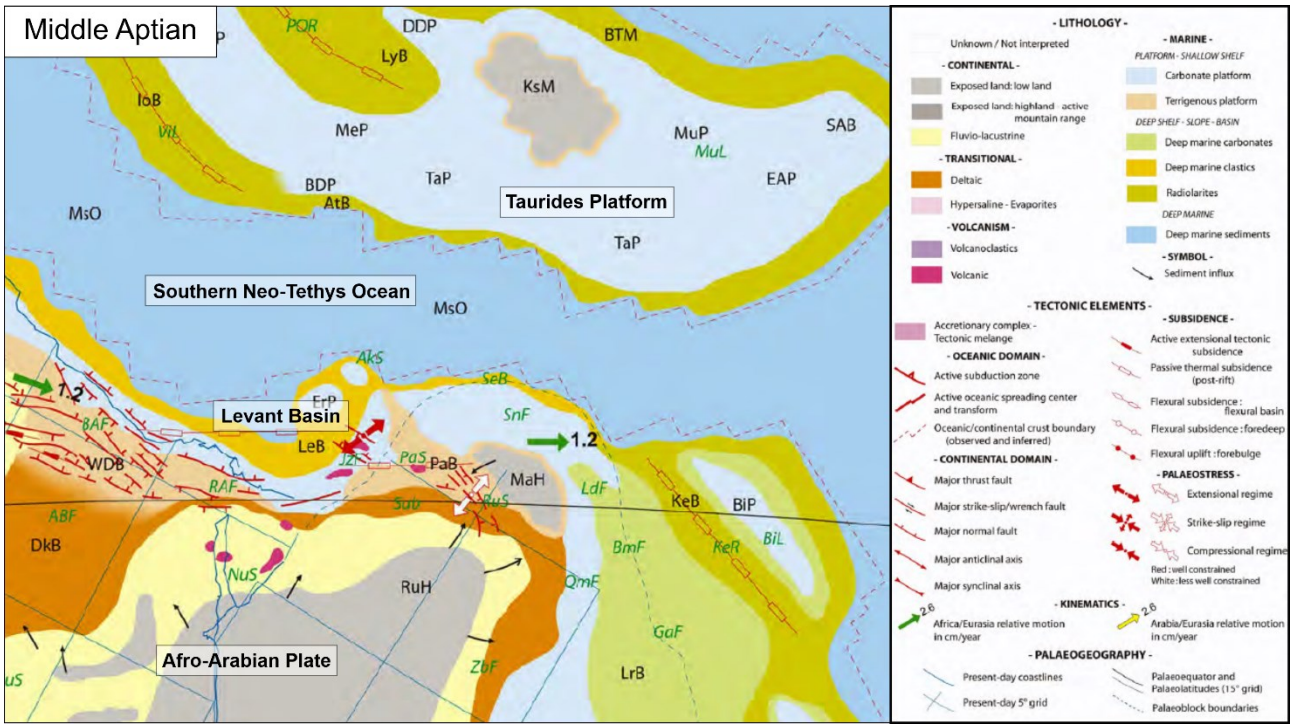

Figure 4: Paleotectonic reconstruction of the study area with the lithological distribution and their relative sedimentary environments in the Middle Aptian (~119 Ma) modified from Barrier & Vrielynck (2008).

Differential cooling led to the formation of a deep-water basin bounded by a shallow-marine shelf (Grafunkel, 1998). In fact, the Levant Basin is overlain by ~12-14 km of sediments dating from the Triassic-Jurassic to the present (Ben-Avraham et al., 2002; Vidal et al., 2000; Montadert et al., 2014). During the passive margin phase, recurrent marine transgression and regression cycles were characterized by onlaps, unconformities, stacking carbonate platforms, and turbidite deposition (Hawie et al., 2013).

Deposition associated with post-rifting subsidence begins in the Middle Jurassic with a thick carbonate platform and develops into a carbonate platform and pelagic carbonates in the Late Jurassic. As the basin continued to subside (Fig.4), the Lower Cretaceous rocks consist of pelagic carbonates with intercalated shales and sands in the Levant Basin (Hawie et al., 2013). In the intervening period, the margin was further uplifted, and the carbonate platform shows signs of erosion and karstification (Collin et al., 2010).

2.2.2 - Convergence phase (Upper Cretaceous – Paleogene)

During the middle Cretaceous, regional stresses changed to compressional stresses (Fig.5). The African plate shifted northwards relative to the Eurasian plate and the region experienced the onset of convergent tectonics. The previously formed NE-SW faults were inverted, and the oceanic crust of the Southern Neo-Tethys Ocean began to subduct beneath the Hellenic Arc to the west and beneath the Cyprus Arc to the east (Vidal et al., 2000; Netzeband et al., 2006; Segev et al., 2018; Van Hinsbergen et al. 2020). In the Late Maastrichtian, oceanic closure led to the obduction of ophiolites with a geochemical supra-subduction signature (Maffione et al., 2017). This type of ophiolite is widespread in the eastern Mediterranean and Middle East countries, forming an elongated belt extending from the Dinarides to Turkey, Cyprus, Syria, and Oman. Furthermore, the ongoing collision of the "Arabian promontory" triggered a 90° counterclockwise rotation of the Troodos Massif (i.e., the ophiolitic complex in Cyprus - Morris & Maffione, 2016; Maffione et al., 2017). As a result, the Troodos Massif was tilted to the south, creating a palaeoslope that influenced and controlled the deposition of lower Cenozoic carbonates and calciturbidites (Robertson, 1976).

Upper Cretaceous and Paleocene rocks in the Levant Basin are pelagic chalk, shale and turbidite deposits that are evidence of a deep-water environment (Fig.5 - Hawie et al., 2013; Papadimitriou et al., 2018).

This phase of convergence is also visible on seismic lines as an unconformity, indicated in the literature as Senonian Unconformity (Robertson, 1998b; Symeou et al., 2018).

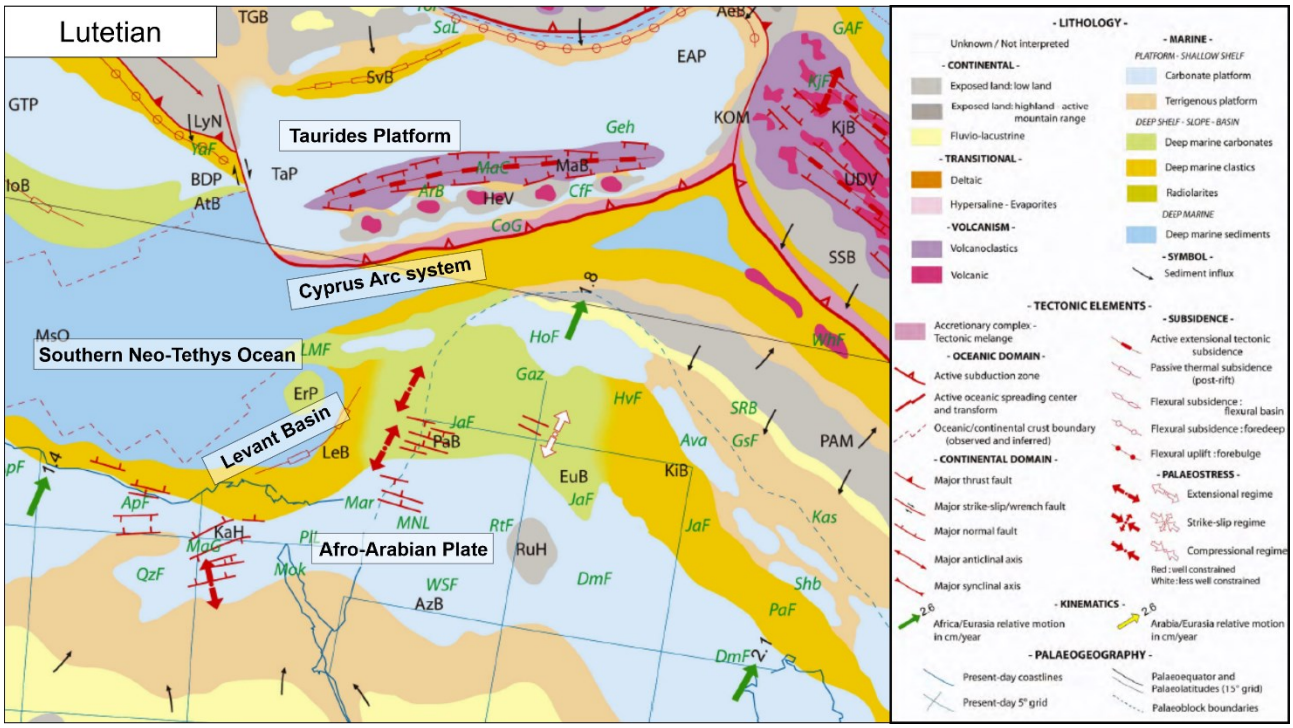

Figure 5: Paleotectonic reconstruction of the study area with the lithological distribution and their relative sedimentary environments in the Lutetian (~45 Ma) modified from Barrier & Vrielynck (2008).

At the end of the Paleogene, the Red Sea began to open, and the subsequent propagation of the Dead Sea Transform Fault Zone led to the separation between the African and Arabian plates (Hempton, 1987; Montadert et al. 2014). Brew et al. (2001) linked Eocene compression to the deformation of the Syrian Arc and the closure of the South Tauride Basin, a subduction zone north of Kyrenia. Indeed, sedimentation along the southern margin of the Taurides ceased at this time, while the Syrian Coastal Range still records deep-water sedimentation (Fig.5 - Bowman, 2011).

2.2.3 - Escape tectonic phase (Neogene – Recent)

During the Oligo-Miocene, extension continued in the Red Sea and the Dead Sea Transform Fault spreads northward. The northern margin of the Arabian plate initiated the phase of continental collision as the remaining oceanic crust was consumed (Fig.6). The faster movement of Arabia relative to Africa triggered a diachronous collision from east to west (Agard et al., 2011; Darin & Umhoefer, 2022). The Levant margin was further uplifted, and a thick sedimentary sequence was deposited in the deep-water Levant Basin (Fig.6). The Miocene sedimentary sequence is explained by a mixture of detrital material from the Proto-Nile to the south (Steinberg et al., 2011) and eroded

material from the Levant margins that entered the deep Levant Basin via canyon incisions (Ghalayini et al., 2018).

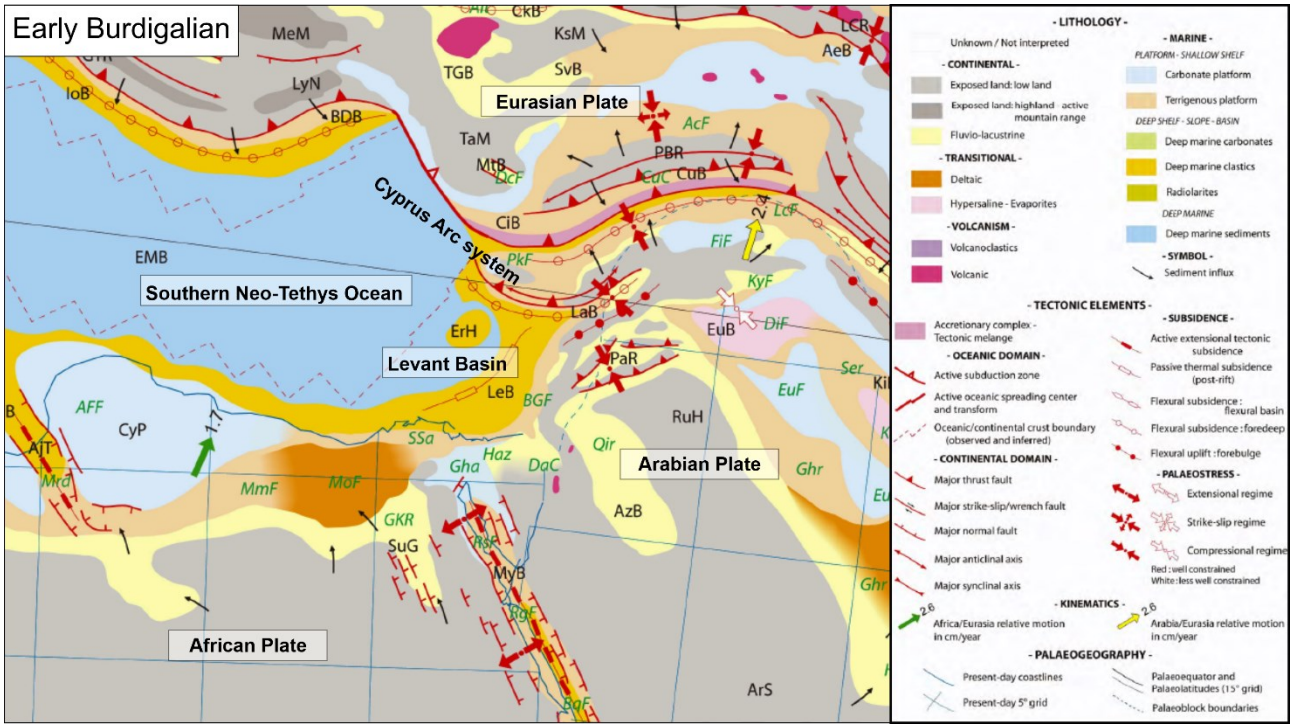

Figure 6: Paleotectonic reconstruction of the study area with the lithological distribution and their relative sedimentary environments in the Early Burdigalian (~20 Ma) modified from Barrier & Vrielynck (2008).

During the latest Miocene, the entire Mediterranean region experienced a drastic drop in sea level caused by the closure of the marine gateway between the Atlantic and the Mediterranean. This event is known as the Messinian Salinity Crisis (Hsü et al., 1978). The drop in sea level led to the precipitation of a thick layer of evaporites in the deep basins and erosion at the margins and structural highs. In general, evaporitic deposits in the Mediterranean are often associated with other sedimentary deposits. In general, the Messinian deposits can be subdivided into three units: the Upper Unit, which is mainly composed of gypsum; the Mobile Unit halite; and the Lower Unit, which is a mixture of gypsum and clastic deposits (these evaporites have never been investigated by direct drilling - Lofi et al., 2011). This subdivision is generally used for the Western Mediterranean and the Ionian Basin. The association of these three units is known as the "Messinian Trilogy" (Lofi et al., 2011). Loncke et al. (2010) stated that there is no clear evidence for the complete Messinian Trilogy in the eastern Mediterranean. They noted that in the Antalya Basin the existence of the Lower Unit and the Upper Unit is uncertain and that only the Mobile Unit is clearly visible. Instead,

in the Levant Basin a thick evaporitic succession precipitated while, at the same time, the margin continued to be eroded, and the sediments were transported into the basin along deeply incised canyons (Druckman et al., 1995), resulting in an alternation of pure halite, anhydrite and shale layers (Gvirtzman et al., 2017).

Different scenarios have been postulated to explain the Neogene evolution of the northeastern Mediterranean. Calon et al. 2005 proposed that subduction ceased during the Eocene and that subsequent deformation was related to suture tightening. Harrison (2004 and 2008) suggested that the Neogene basins' formation was controlled by diffuse sinistral strike-slip. Robertson (2002) proposed a northward dipping subduction zone south of Cyprus from the late Oligocene to early Miocene and recent uplift and plate reconfiguration due to collision with the Eratosthenes Seamount that inhibited the subduction. Other authors (Symeou et al., 2018; Reiche et al., 2016; Robertson et al., 2012) invoked a model of the forward propagation of the thrust belt suggesting successive compressional pulses since the early Miocene and a switch to strike-slip in the early Pliocene and/or early Pleistocene due to a westward movement of the Anatolian microplate (Fig. 7).

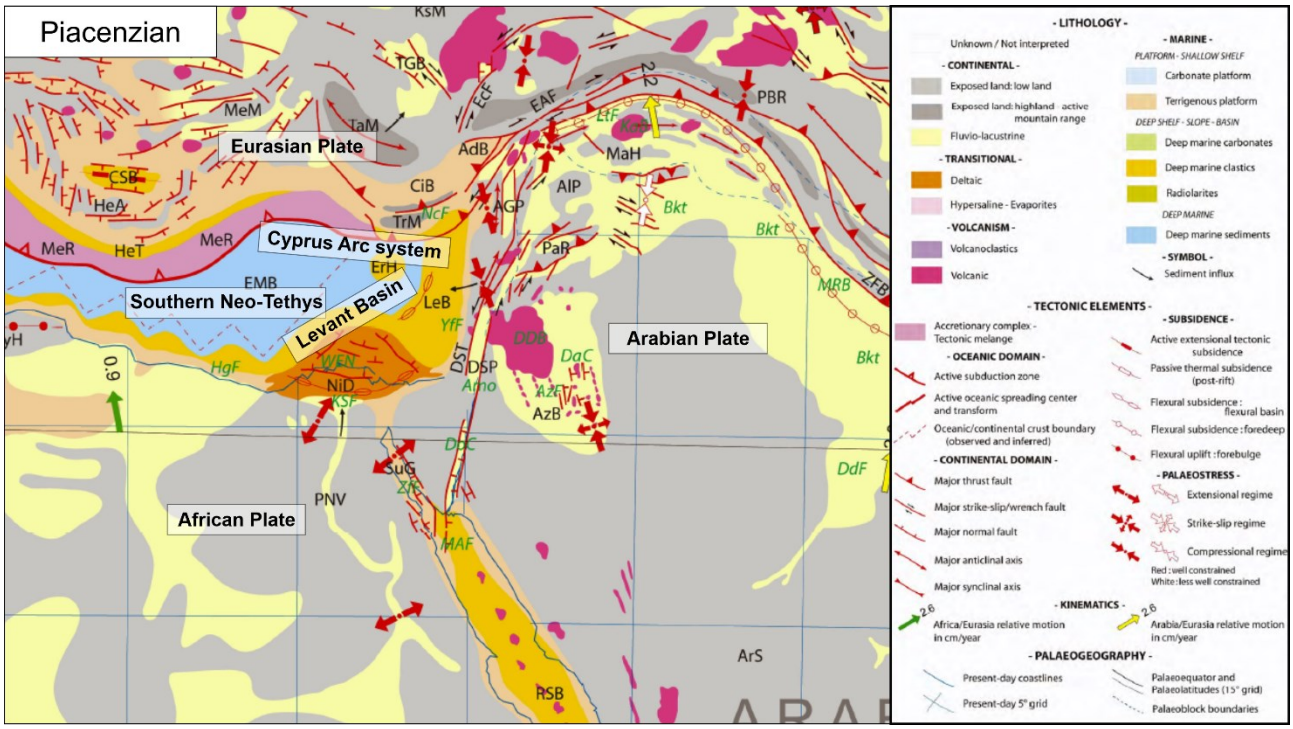

Figure 7: Paleotectonic reconstruction of the study area with the lithological distribution and their relative sedimentary environments in the Piacenzian (~3.5 Ma) modified from Barrier & Vrielynck (2008).

McClusky et al. (2000) use the GPS's velocities, to show a counterclockwise rotation centered approximately around Cyprus (Fig.8).

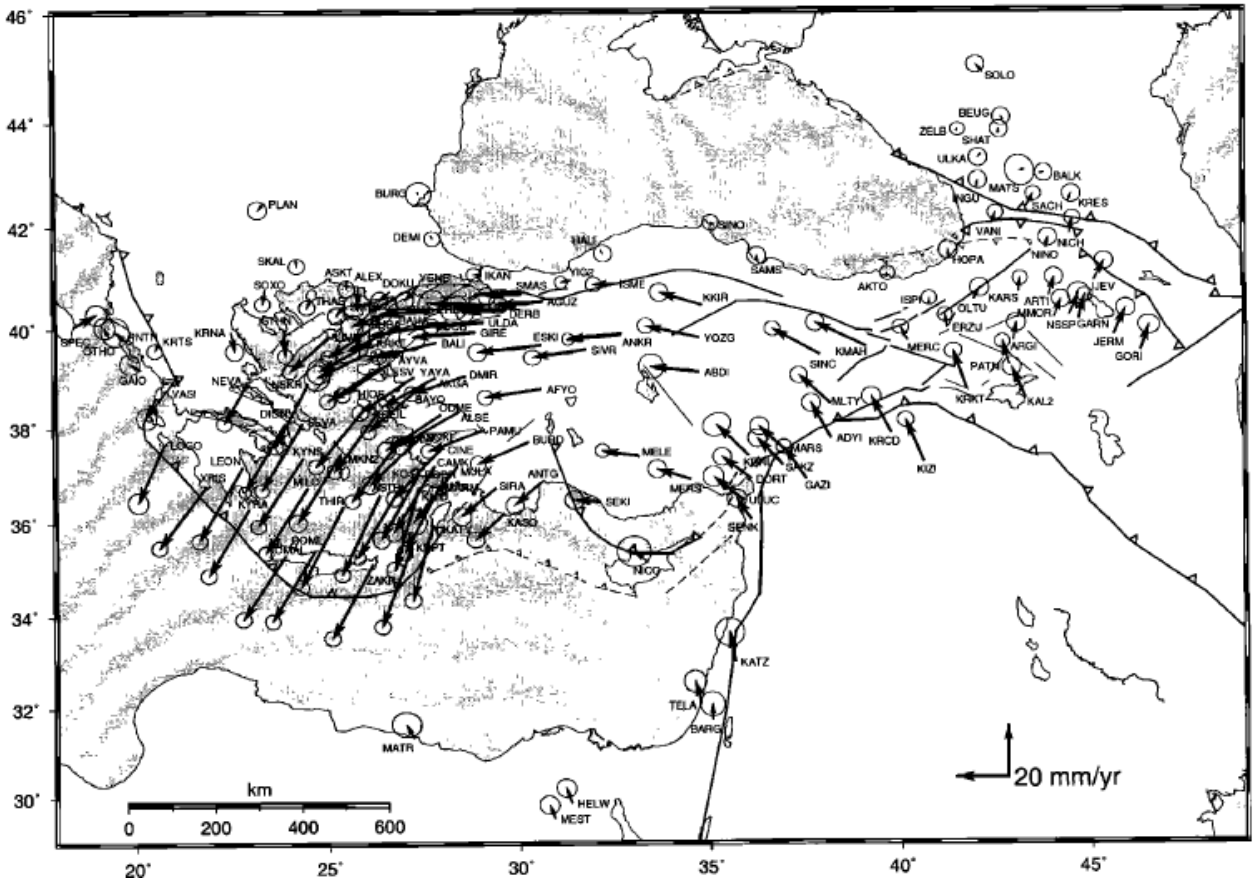

Figure 8: GPS velocity vectors with Africa as the fixed point. The vectors of the Hellenic Arc point SSW with the greatest intensity in this area. The tectonic escape of Anatolia is visible in the vectors running W in Turkey. The vectors turn from N to NW where the Dead Sea Transform Fault meets the East Anatolian Fault. The northern African margin moves slowly to the NW. In general, the velocity vectors of GPS show a counterclockwise rotation roughly centred around the Eratosthenes Seamount. Figure from McClusky et al. (2000).

A combination of factors could explain this eddy motion: the northward pushing of the Dead Sea Transform Fault, the westward suction deriving from the Aegean subduction, the rolling back of the subducting plate and the corresponding asthenospheric flow (Schildgen et al., 2014). The westward escape of the Anatolian microplate is thus mainly controlled by the North Anatolian Fault (right-lateral strike-slip), the East Anatolian Fault (left-lateral strike-slip) and the extension of the Aegean back-arc domain. In this complex plate configuration, the northeastern Mediterranean remains

squeezed near a triple junction where the Eastern Anatolian Fault, the Dead Sea Transform Fault and the Latakia Ridge (eastern termination of the Cyprus Arc system) meet (Fig.8).

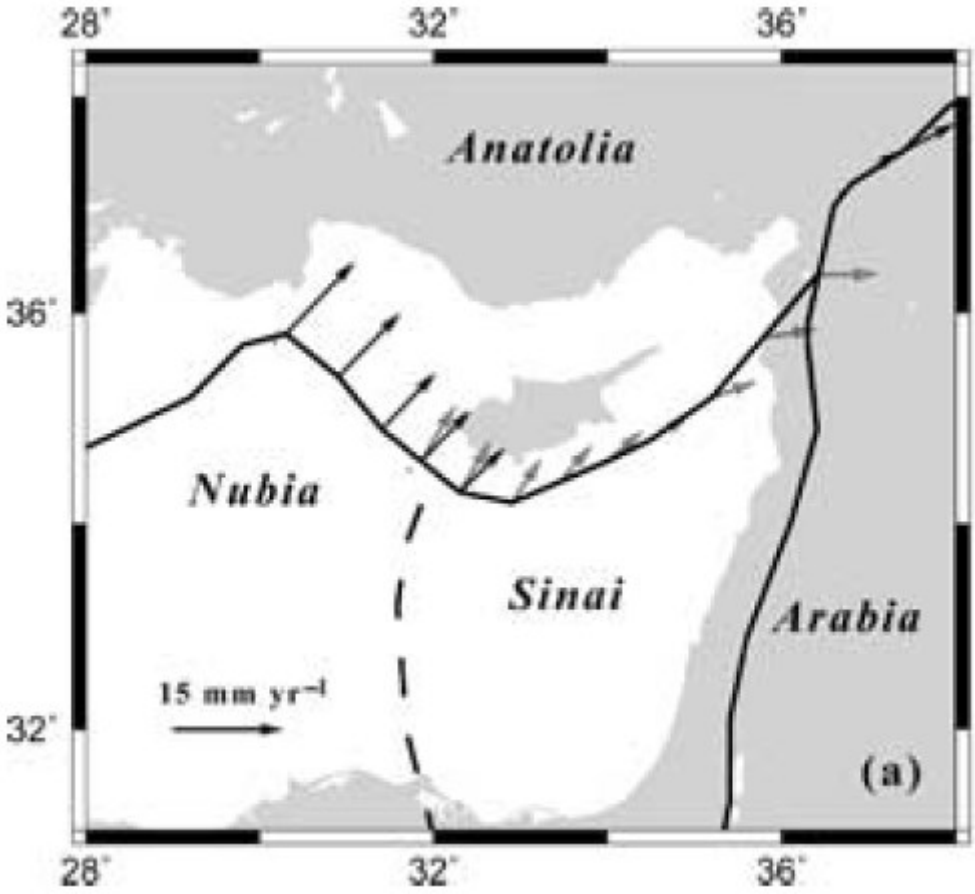

Figure 9: Predicted movement along the Cyprus Arc system. Note the difference in intensity and direction of the vectors moving along the Cyprus Arc system. The western part of this convergent boundary moves faster than the central and eastern parts. The vectors in the western region are orthogonal to the deformation front, while they turn to the east and run parallel and with lower intensity in the area of Latakia Ridge. This distribution of velocity vectors shows a change from active subduction beneath Florence Rise and a transition to strike-slip kinematics towards the east. Figure from Wdowinski et al. (2006).

By analyzing the GPS's velocities and the seismicity of the northeastern Mediterranean, Wdowinski et al. (2006) show how the direction and intensity of the vectors change along the Cyprus Arc system, which allows its subdivision into three segments with characteristic features: the Florence Rise, the Cyprus Arc and the Latakia Ridge (Fig.9).

CHAPTER 3: DATA & METHODS

3.1 – Data

We used several vintage multichannel seismic reflection profiles to investigate the geological structures beneath the northeastern Mediterranean Sea. Our dataset consists of two multi-channel seismic reflection surveys carried out in the 1970s: the MS (Mediterranean Sea) and the Strakhov-5 surveys. We have also integrated them by using almost all published information on the study area. All sections, maps, and interpretations available in the literature were georeferenced with the MOVE software and integrated with the seismic sections in the SEG -Y format of the MS and Strakhov-5 surveys.

3.1.1 – Mediterranean Sea project – multichannel seismic reflection dataset

The MS (Mediterranean Sea) project was a pioneering geophysical investigation carried out in the 1970s as part of a collaboration between the CNR (National Research Council of Italy), the OGS (National Institute of Oceanography and Applied Geophysics) and various scientists from several countries (Italy, France, UK, USA, Russia). In the 1960s, the Mediterranean Sea was almost entirely unexplored. Therefore, the extensive geophysical exploration carried out by the MS campaign was crucial to reveal the basic features of the Mediterranean, its tectono-stratigraphy, and the recognition of the different crustal domains (Finetti and Morelli, 1973; Finetti et al., 2005). This project is still the only scientific seismic network covering the whole Mediterranean area (Fig.10). In the following decade, the Black Sea was also explored by continuing this scientific project.

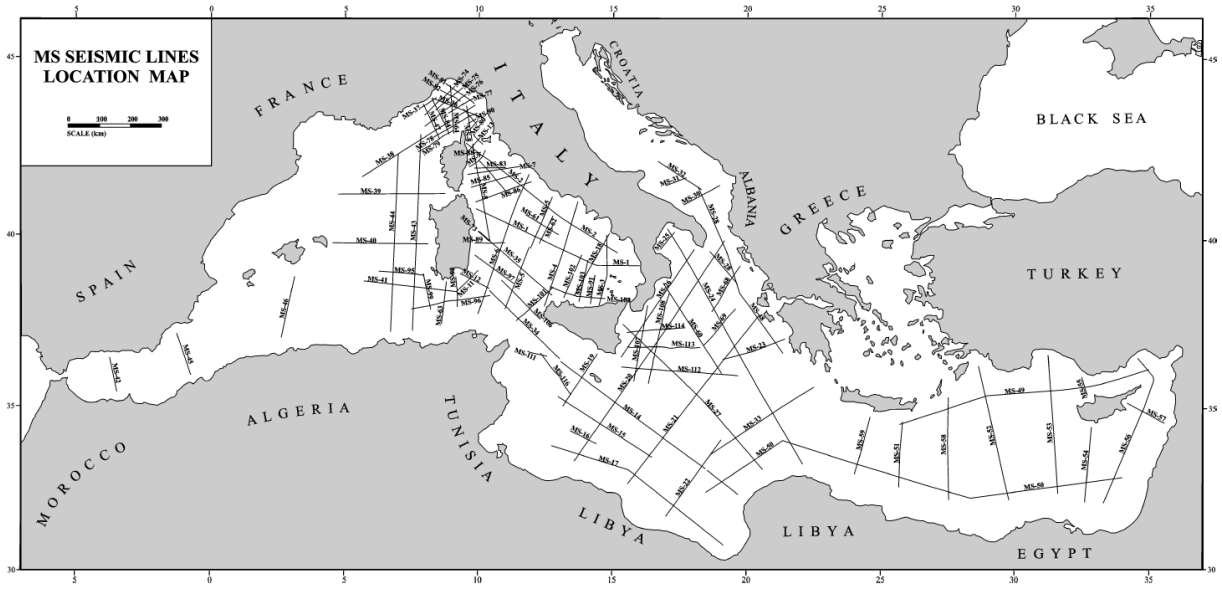

Figure 10: Location of the MS (Mediterranean Sea) multichannel seismic reflection profiles acquired by the R/V Marsili. Figure from Finetti et al. (2005).

Despite the coverage (Fig.10), the novelty of the MS project was also the acquisition technique. At that time, multifold digital seismic reflection technology was just being used industrially, so the OGS pioneered the acquisition of a large number of seismic lines using modern acquisition techniques (Tab.1). From 1969 to 1973, the CNR research vessel "Marsili" was equipped with a neutrally buoyant streamer with 24 channels at 100 m intervals. Then in 1982, a streamer with 48 channels spaced every 50 m was used. Dynamite energization was used with two Flexotir guns firing every 200 and 100 m, respectively, so these profiles had 6 or 12 fold coverage. The average length of the recorded seismic traces is 10 seconds (Tab.1).

Table 1: Acquisition parameters of the MS53 and MS56 seismic lines.

Seismic line	MS53 / MS56
Recording year	1973
Line length	~ 324 km / ~ 571 km
Streamer length	2400 m
Number of channels	24

Near offset	270 m
Group interval	100 m
Shot interval	100 m
Recording filters	10 – 72 Hz
Seismic source	Dynamite – Flexotir
Fold	1200 %
Record length	10 sec
Sampling interval	4 msec

The geophysical information obtained from this regional survey led to a wealth of scientific papers, proposals and hypotheses. The MS dataset is still important today as computer power and seismic processing algorithms have increased. Therefore, re-evaluating this vintage data with modern techniques is crucial (Brancatelli et al., 2022; Civile et al., 2021; Camerlenghi et al., 2020), as it is difficult to obtain new data from the oil and gas industry.

For this study, we focused on two MS lines: the MS56 and the MS53. The MS56 is located east of Cyprus and runs from the southern Turkish coast to the south of the Levant Basin. The MS53 traverses the western Cypriot offshore from Turkey to the south of the Herodotus Basin.

An advanced broadband processing technique was applied to these profiles to improve seismic imaging. Coherent and incoherent noises were attenuated to enhance the signal-to-noise ratio. Multiple attenuation was performed using the Surface-Related-Multiple-Elimination by Verschuur et al. (1992) and the Wave Equation Multiple Attenuation by Wiggins (1988). The frequency spectrum was broadened by deghosting and predictive multichannel deconvolution steps. Pre-stack Kirchhoff time migration was applied while the velocity field was iteratively updated. Each iteration had a quality control procedure based on a common distance stack. Finally, to increase the lateral continuity of the reflectors, FX deconvolution was applied to the Pre-Stack Time Migrated section, followed by a time-variant filter and amplitude equalisation of the trace. FX Deconvolution was used to attenuate the noise and improve the continuity of the signal.

The re-processing allowed obtaining important improvement in seismic data (Fig.11):

- better characterization of seismic facies
- more reliable imaging of subsurface features
- greater capacity of detection and interpretation of fluid related amplitude anomalies
- improved resolution

The vintage data were reprocessed as best as possible despite their low fold, the noisy appearance of the shot point gathers and the lost records during the tape transcription process to get the best out of this valuable data.

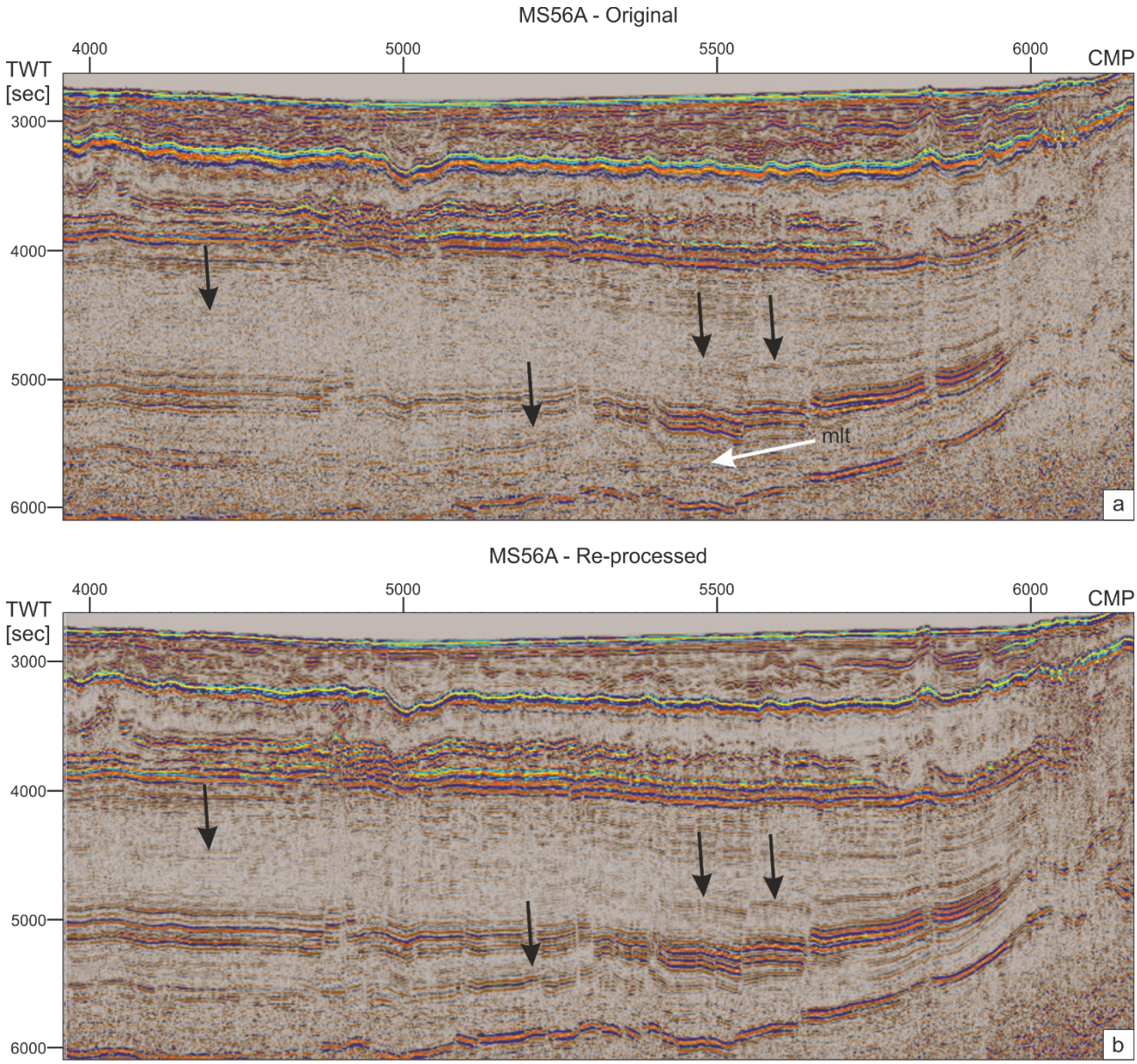

Figure 11: a) MS56A original vintage data. b) MS56A reprocessed data. The signals continuity and the imaging were improved by the modern broadband reprocessing techniques (black arrows) and the multiple reflections (mlt - white arrow) have been attenuated too.

3.1.2 – Strakhov-5 cruise – multichannel seismic reflection dataset

In 1987, GEOMAR (i.e., the Helmholtz Center for Ocean Research Kiel) collaborated with the Russian Academy of Sciences to acquire 1700 km of multichannel seismic reflection data across the Cyprus Arc system, from the Florence Rise to the Syrian coast during the 5th cruise of the research vessel Akademik Nikolay Strakhov. This was the first comprehensive geophysical data acquisition around the Cyprus Arc system and more generally in the northern Levant Basin (Fig.12). As with the MS survey, the Strakhov-5 dataset has contributed to the publication of numerous articles and the understanding of offshore geology.

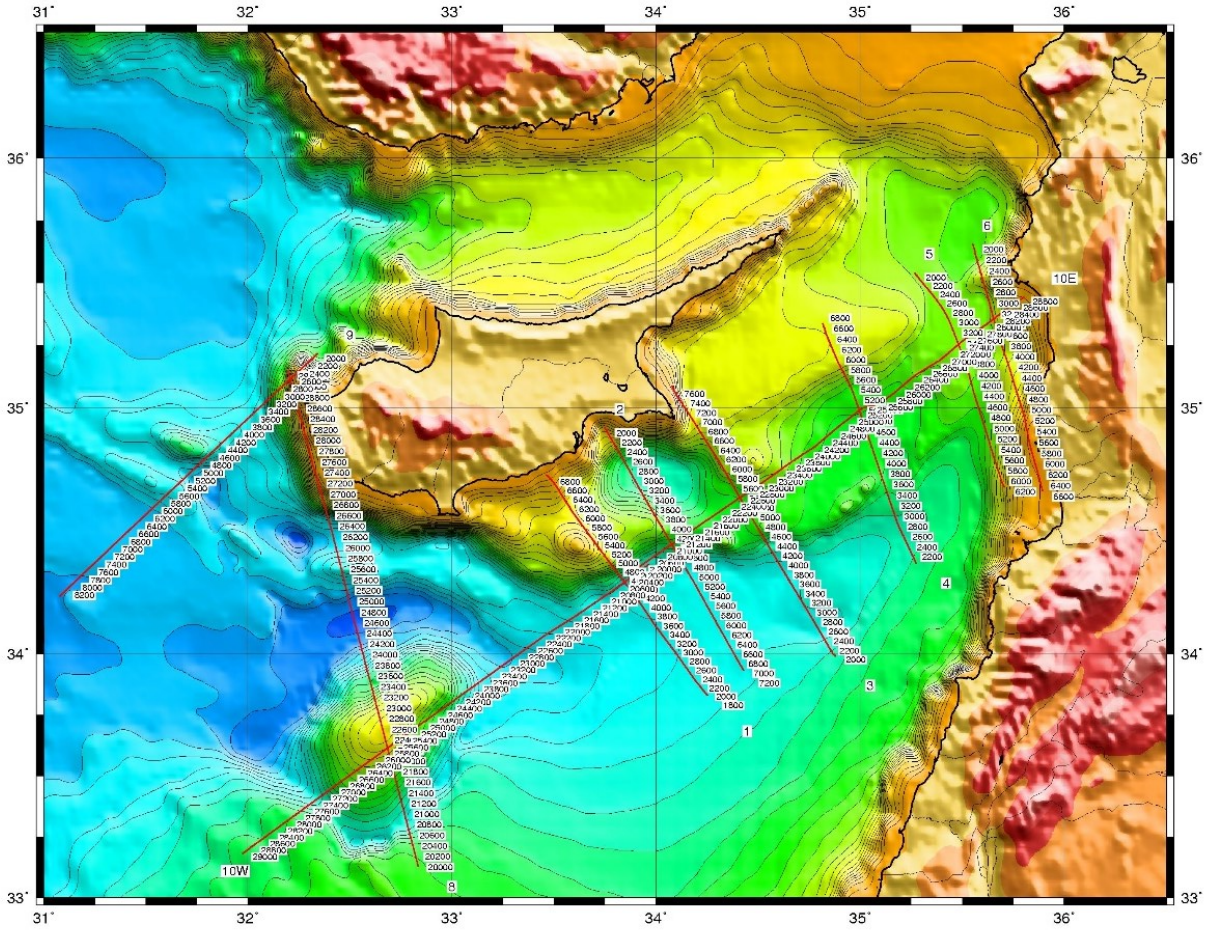

Figure 12: Location of the Strakhov-5 cruise multichannel seismic reflection profiles acquired by the R/V Akademik Nikolay Strakhov. Figure modified from Hall et al. (2005)c.

These seismic lines were also reprocessed to get the best out of these old data using new processing techniques (Klaeschen et al., 2005). For the seismic acquisition, a 12-litre airgun array sound source with a chamber pressure of 15 MPa was used and towed to a depth of 12 m below sea level. The

hydrophone array consisted of 48 channels spaced 50 meters apart and shot every 100 meters. The sampling rate was 4 milliseconds, and the total recording time was 12 seconds.

GEOMAR provided us with the stack, the pre-stack depth-migrated versions, and the velocity analysis to gain insight into the velocity of each interpreted seismic package.

3.1.3 - Data retrieval from available literature

3.1.3.1 - Georeferenced seismic sections

The MS and Strakhov-5 datasets consist of regional and deep multichannel seismic reflection profiles, but these sections are sparse within basins. Therefore, to increase spatial coverage, we also take advantage from the literature. During the literature review, seismic reflection profiles, maps and boreholes that have been published were georeferenced and inserted into the software MOVE (Fig.13). In this way, our dataset was enriched with many georeferenced images that can be used for better seismic tying of the interpreted horizons along the basins as the number of intersections of the sections is increased.

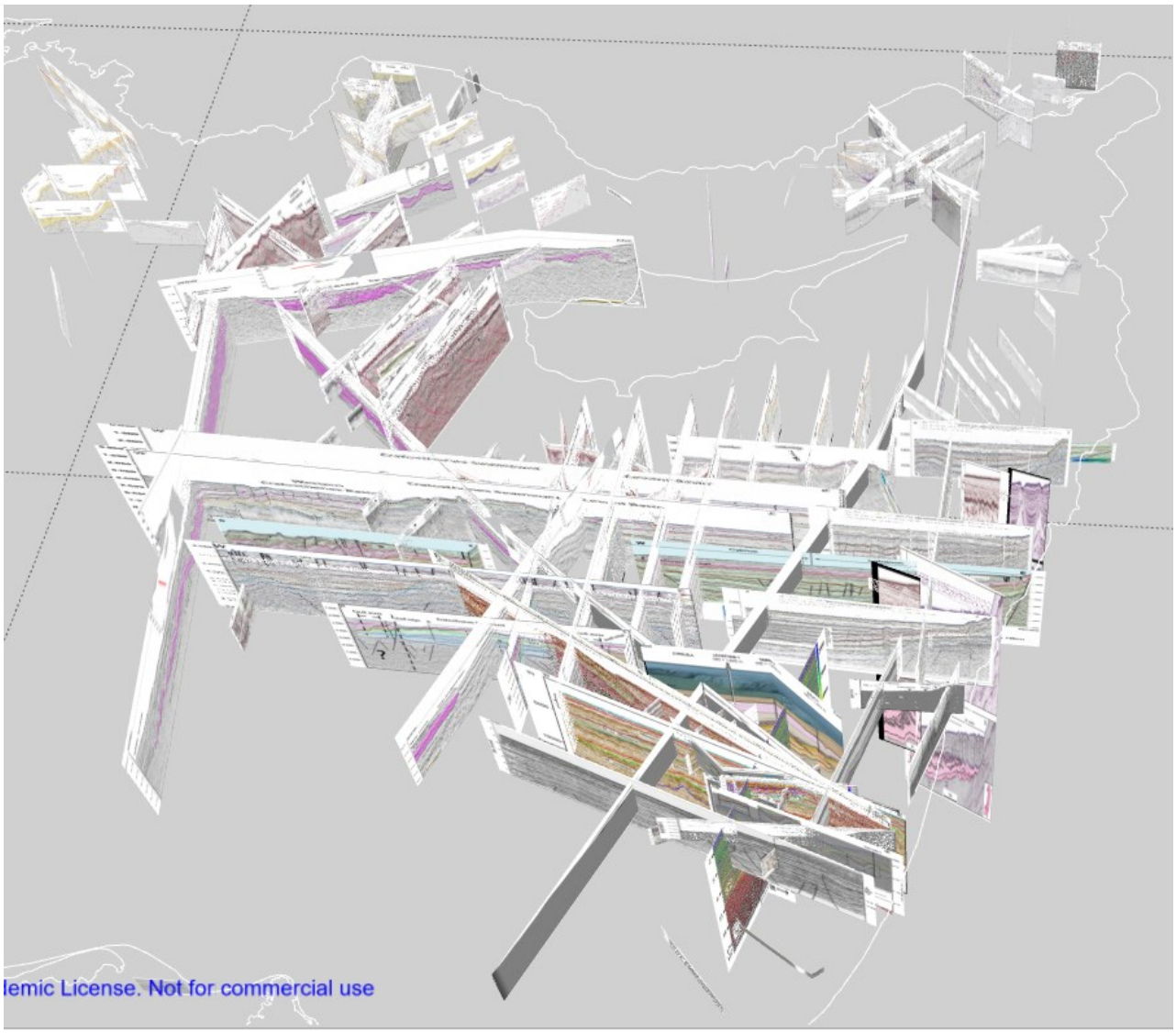

Figure 13: Location map of the seismic sections in PNG format geo-referenced in the MOVE software. Seismic lines are taken from the available literature: Brew et al. (2001); Bridge et al. (2005); Burton-Ferguson et al. (2005); Hall et al. (2005a/b); Isler et al. (2005); Ben-Avraham et al. (2006); Ozel et al. (2007); Güneş et al. (2009); Schattner (2010); Bowman (2011); Maillard et al. (2011); Sellier et al. (2012); Skiple et al. (2012); Hawie et al. (2013); Aksu et al. (2014); Ghalayini et al. (2014); Hall et al. (2014); Gorini et al. (2015); Sagy et al. (2015); Sahran (2015); Feng & Reshef (2016); Reiche et al. (2016); Gvirtzman et al. (2017); Aksu et al. (2018); Ghalayini et al. (2018); Güneş et al. (2018); Papadimitriou et al. (2018); Segev et al. (2018); Symeou et al. (2018); Haq et al. (2020); Evans & Jackson (2021).

Our multichannel seismic reflection profiles have a high depth of investigation, but to reconstruct the subduction boundary, since we are dealing with a subduction zone involving different crustal types, gravimetric and magnetic anomaly maps and the relocation of earthquake events are

valuable tools to underline the kinematics, basement structures and nature of this convergent boundary.

3.1.3.2 - Magnetic anomalies

Many magnetic maps have been proposed for the identification of magnetic anomalies in the study area (Makris et al., 1994; Ben-Avraham et al., 2002; Eppelbaum & Katz, 2015), but the most detailed is the analysis by Rybakov et al. (2011) (Fig.14). We have mainly used the latter to identify the different signals of the magnetic anomalies which are grouped into ophiolites and intrusive body-related anomalies. The magmatic intrusions are associated with the phases of rifting and crustal extension. Conversely, the ophiolite anomalies are associated with the supra-subduction ophiolites obducted during the convergence phase in the Upper Cretaceous.

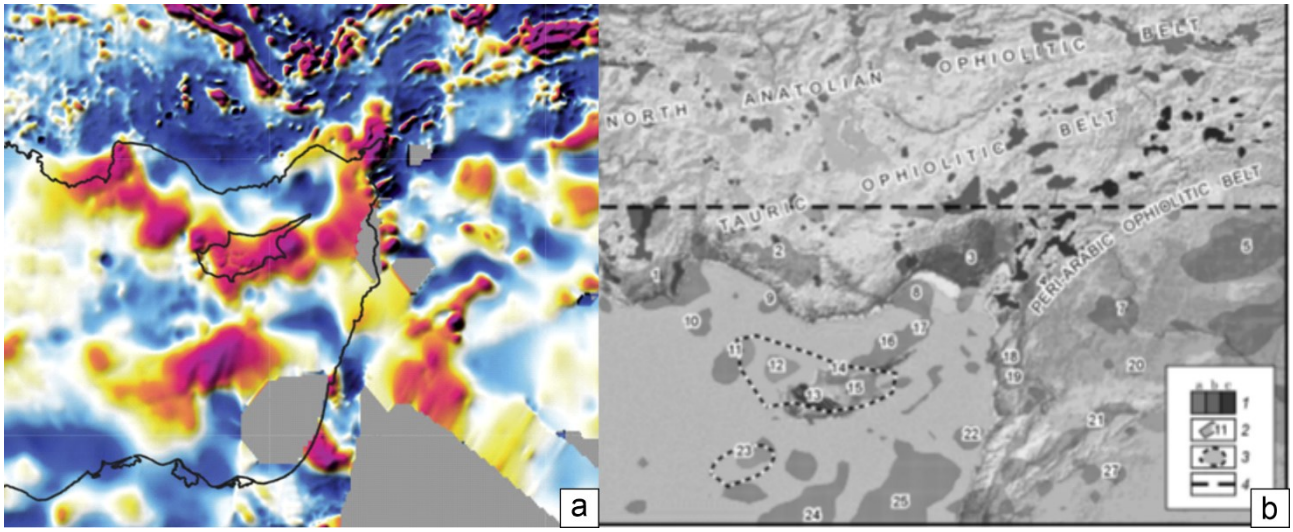

Figure 14: Comparison between a) the global model of magnetic anomalies EMAG2v3 and b) the model of magnetic anomalies in the eastern Mediterranean by Rybakov et al. (2011). a) Earth Magnetic Anomaly Grid with 2-arc-minute resolution from NOAA - National Centers for Environmental Information. The resolution of this model does not allow the accurate identification of individual anomalies. It is difficult to subdivide into smaller individual anomalies the big red/purple anomaly aligned along the Cyprus Arc system. b) The resolution of the model proposed by Rybakov et al. (2011) allows the identification of the individual sources for each anomaly. The authors have also grouped the magnetic anomalies into ophiolite and intrusive body anomalies: 1 - outcropped ophiolites; 2 - interpreted magnetic bodies and their numbers; 3 – contours of the unexposed Troodos and Niklas massifs as revealed by gravity data; 4 – northern boundary of the study region.

3.1.3.3 - Gravity anomalies

Further useful constraints on our seismic interpretation come from the gravimetric models available for the northeastern Mediterranean (Ergün et al., 2005). The gravity model proposed by Ergün et al. (2005) includes the presence of obducted ophiolites along the Cyprus Arc, which are associated with higher values of the Bouguer anomaly map (Fig.15). In their paper, they highlight the structures and composition of the plates involved in this convergent margin by presenting four cross sections: two on the western side of Cyprus, one to the south and across the island, and the last one crossing the eastern Cyprus offshore.

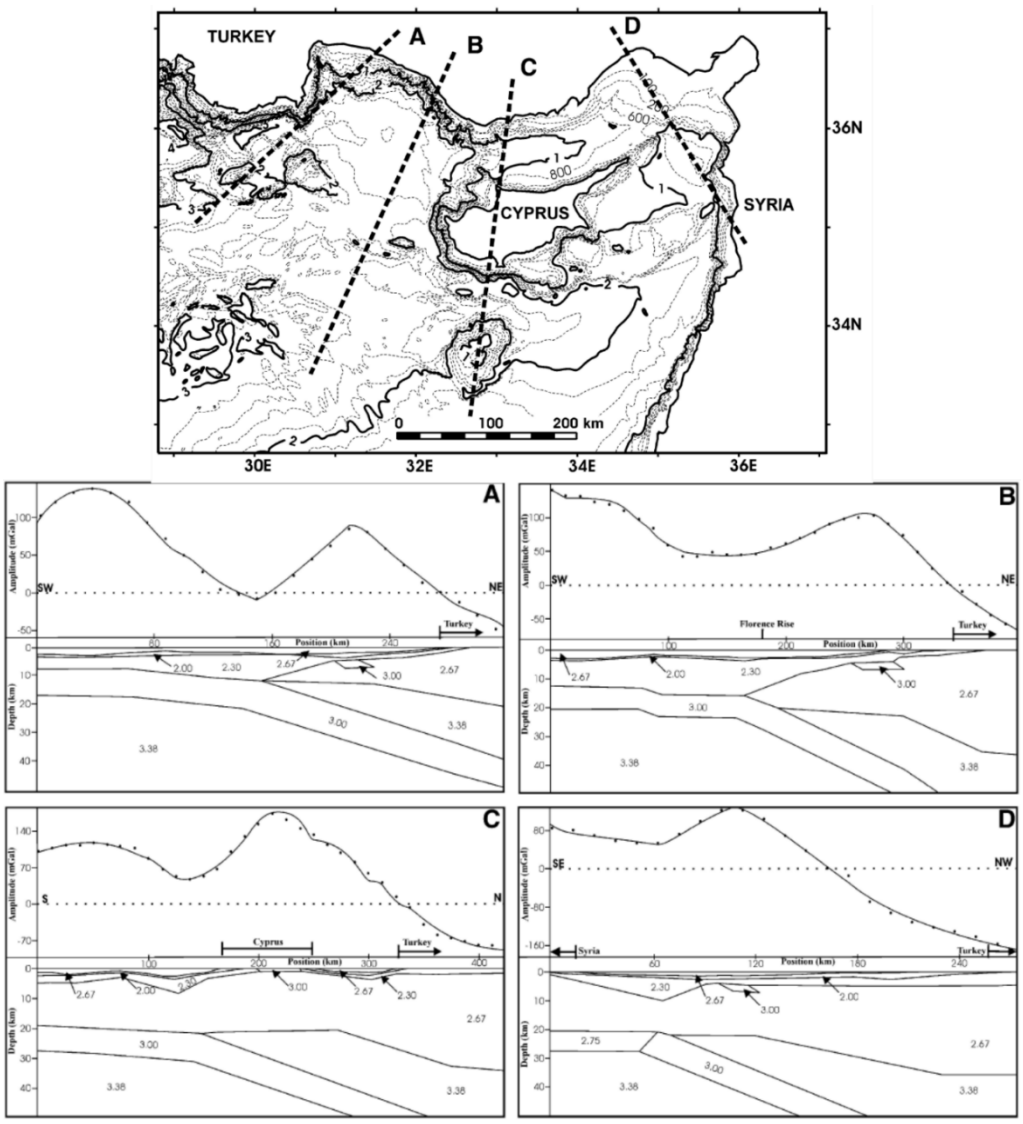

Figure 15: Location map of the gravity models proposed by Ergün et al., 2005 and the resulting sections. Insets A, B, C and D show the Bouguer gravity profiles and the 2D models. The dots are the observed gravity and the fitting curve. The modelled buried bodies' densities are given in mg/m^3. Figure modified from Ergün et al. (2005).

3.1.3.4 – Seismicity

Earthquake relocation is another powerful tool to constrain the deeper part of our seismic sections. The northeastern Mediterranean area is an active plate boundary and therefore, seismically active (Fig.16).

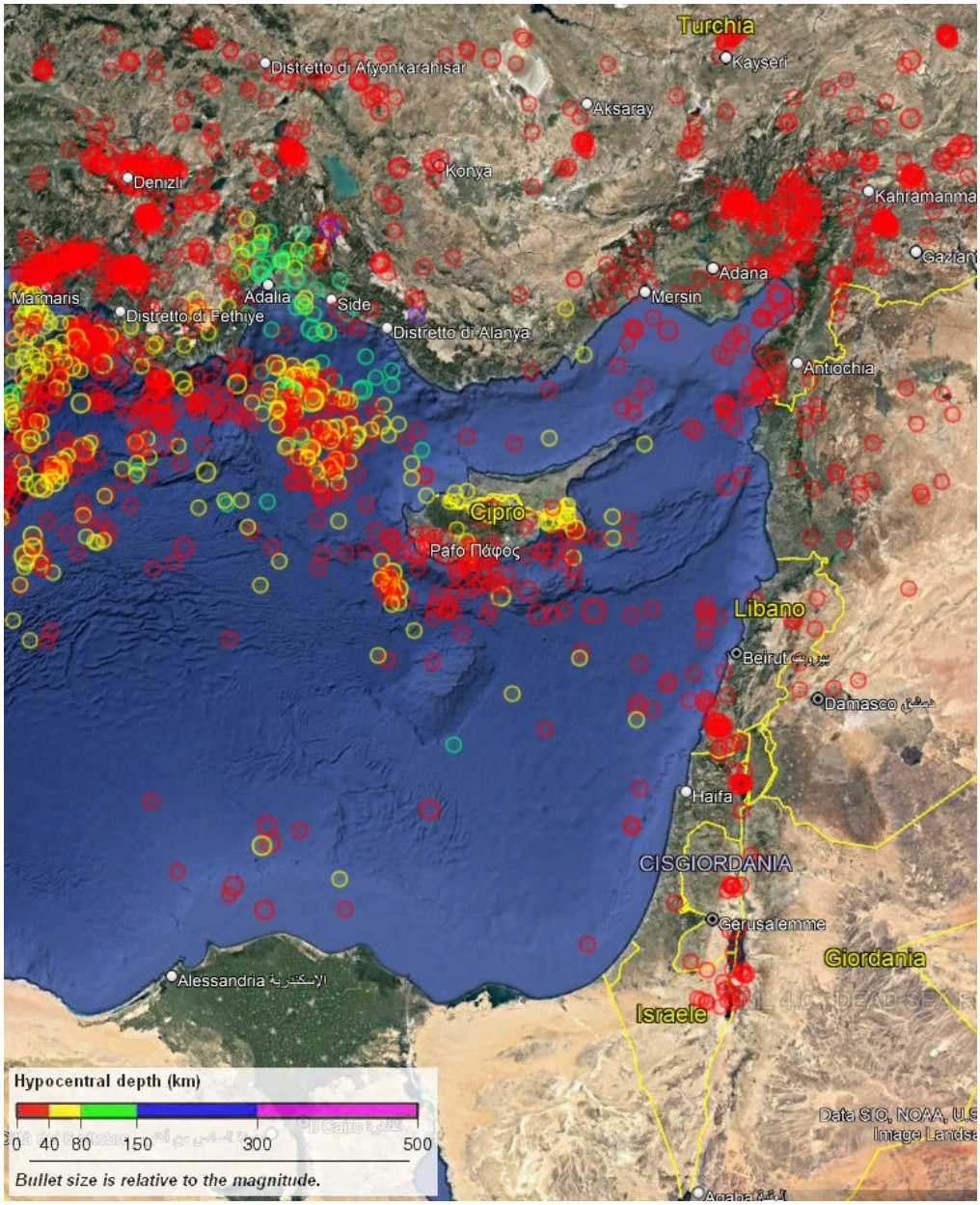

Figure 16: Google Earth overlay of magnitude > 3.5 earthquake events from 10.04.2004 to 12.09.2021 from the EMSC (Euro-Mediterranean Seismological Center) website. Note that offshore seismicity is concentrated below the Antalya Basin and south of Cyprus and becomes sparser towards the east. The color of the dots represents the hypocentral depth. In the Antalya Basin, the hypocentral depth of the seismic events indicates a north-deepening subduction plane, while it

becomes shallower towards the east. The diameter of the circles represents the magnitude of the events.

As can be seen in Figure 16, the western Cyprus offshore is seismically more active than the eastern part. Moreover, the seismicity becomes sparser and shallower from west to east. Güvercin et al. (2021) have relocated the earthquake events in the Antalya Basin and demonstrated an NNW-oriented slab beneath (Fig.17).

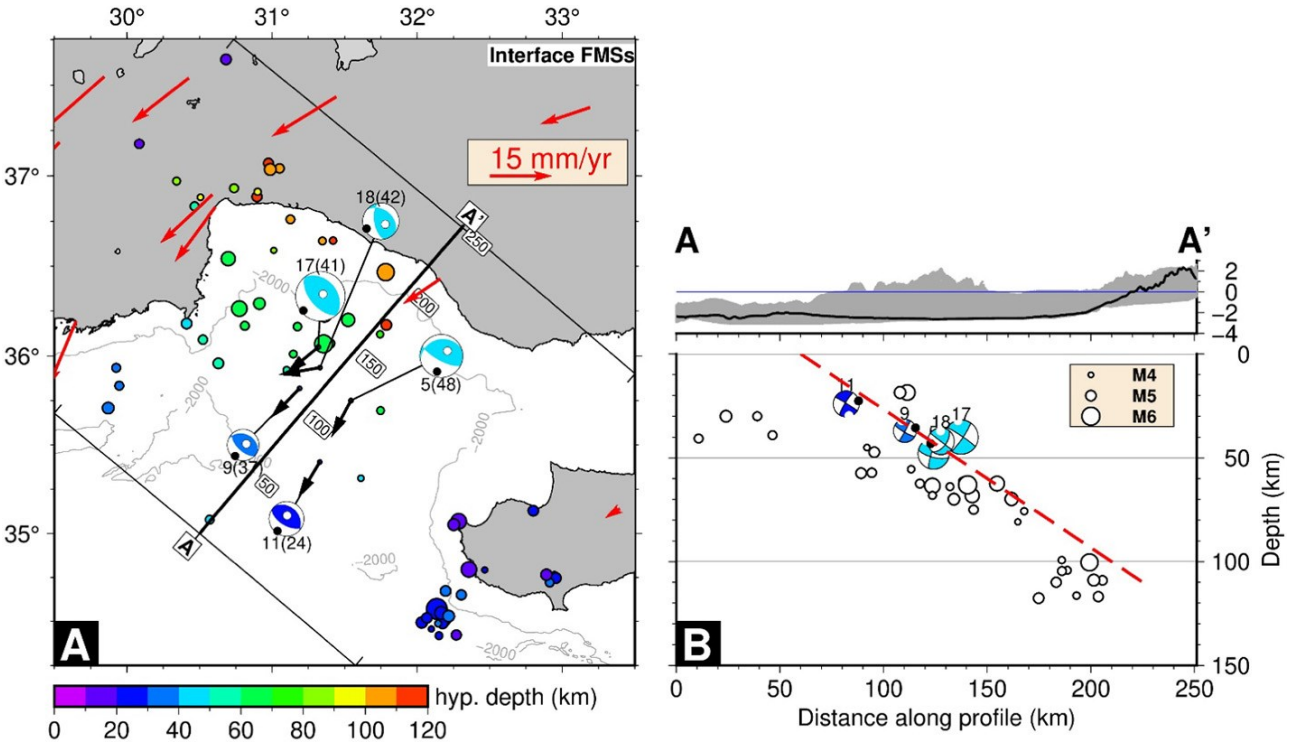

Figure 17: a) earthquake focal mechanisms accommodating the convergence between the African and Eurasian plates. The black and white-filled circles on the beach balls indicate the direction of the P and T axis respectively. The red arrows represent the GPS velocity vectors with respect to Africa and the black arrows show the slip vector of the seismic event with respect to the motion of the hanging wall. b) Cross-section oriented SW-NE along the northern Herodotus Basin and Antalya Basin. The grey-coloured area represents the thickness of the sediments in the basins. The red dashed line is the predicted slab interface obtained by fitting the hypocentres of the earthquakes. Figure from Güvercin et al. (2021).

3.1.3.5 – Boreholes

The available boreholes in the study area (Fig.18) fall into two main categories: the public wells and the oil and gas industry wells released in recent years.

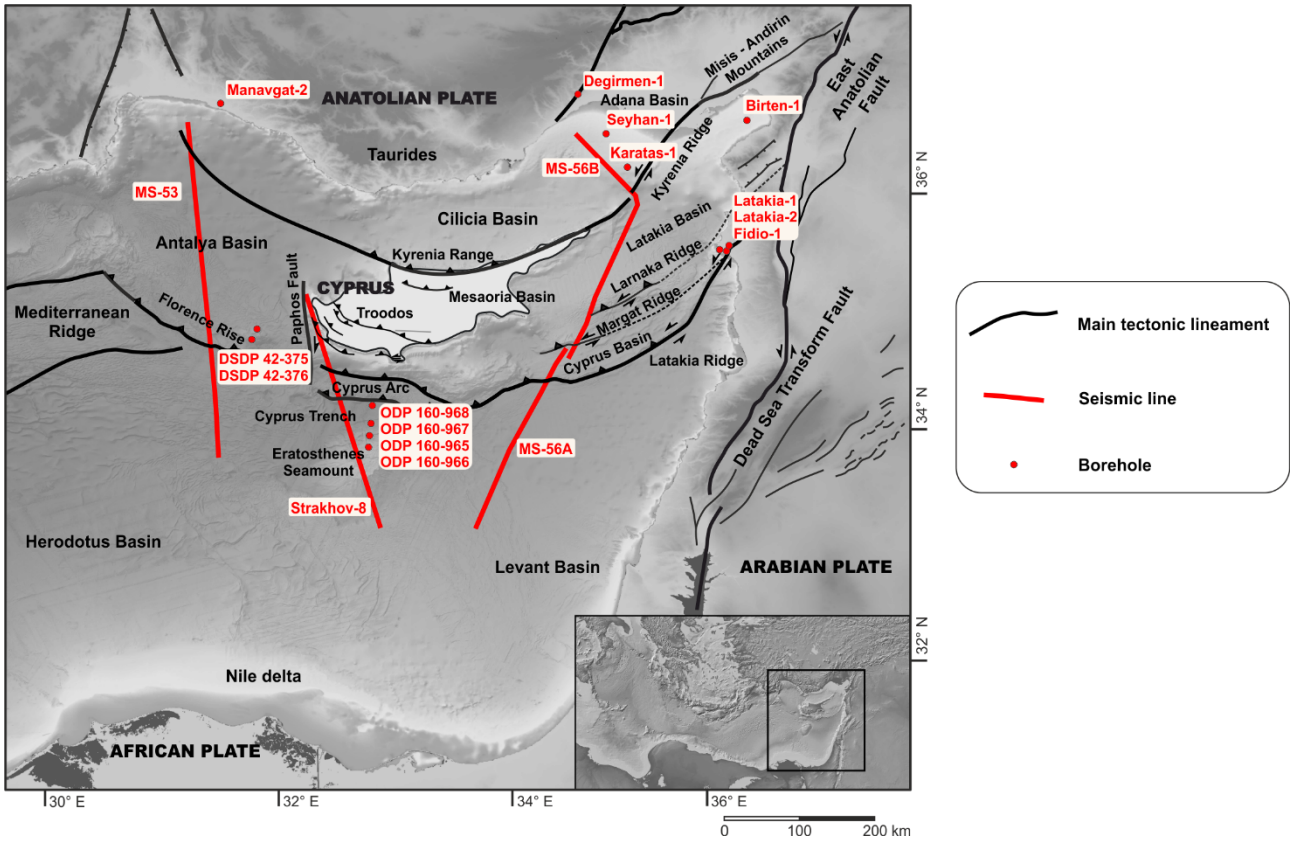

Figure 18: Tectonic map of the study area with the seismic lines and boreholes considered. Tectonic lineaments from Montadert et al. (2014); Longacre et al. (2007) and Mc Phee & van Hisbergen (2019). Bathymetry from EMODNet. Topography from GEBCO. Bottom right map inset from GeoMapApp.

The public boreholes, represented by the DSDP and ODP drillings, are in total 6 wells (Fig.19). 4 are located south of Cyprus: one on the accretionary prism (ODP 160-968), one in the Cyprus Trench (ODP 160-967) and two on the Eratosthenes Seamount (ODP 160-965, ODP 160-966). The other two are located on the Florence Rise (DSDP 42-375, DSDP 42-376).

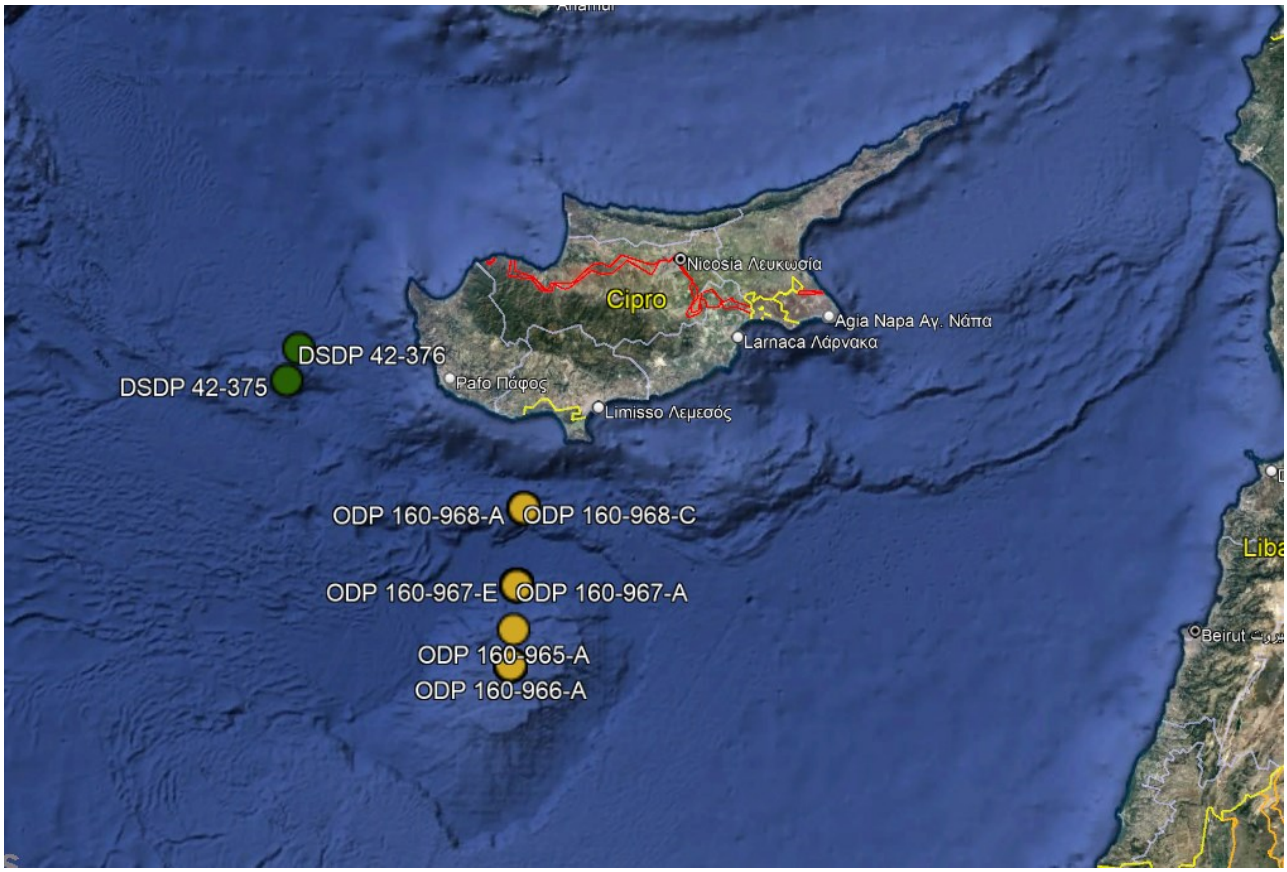

Figure 19: Google Earth showing the position of the DSDP (Deep Sea Drilling Project) and ODP (Ocean Drilling Project) boreholes around Cyprus. The two DSDP boreholes (DSDP 42-375 and DSDP 42-376) are located on top of Florence Rise. The four ODP boreholes (ODP 160-968, ODP 160-967, ODP 160-966 and ODP 160-965) were drilled along a north-south transect south of Cyprus. ODP 160-966 and ODP 160-965 are located on the Eratosthenes Seamount, ODP 160-967 in the Cyprus Trench and ODP 160-968 on the Cyprus Accretionary Prism. All IODP (International Ocean Discovery Program) boreholes are public and available on the IODP website (https://www.iodp.org/). DSDP, ODP and IODP are the same organization, which has changed its name over the last decades.

DSDP 42-375 is located near the top of Florence Rise (Fig.20) and reaches a depth of 821 meters. It has a sedimentary sequence from Burdigalian to Quaternary. DSDP 42-376 is located on the northern flank of Florence Rise (Fig.20) and reaches a depth of 216.5 meters. The age of the deposits ranges from Messinian to Holocene (Fig.20 - Hsü et al., 1978; Robertson, 1998). Eleven units were identified at Site 376: four units in the Early to Middle Miocene to pre-Tortonian sediments and one flysch unit in the Tortonian; two in the Late Miocene evaporite and post-evaporite successions and four in the pelagic Plio-Quaternary succession (Fig.20). Detailed descriptions of all units can be found in Hsü et al. (1978) and Robertson (1998). The Florence Rise is also characterized by thin deposits of

Messinian evaporites, which pinch out along the northern side of the underlying structural core ridge (Güneş, 2009).

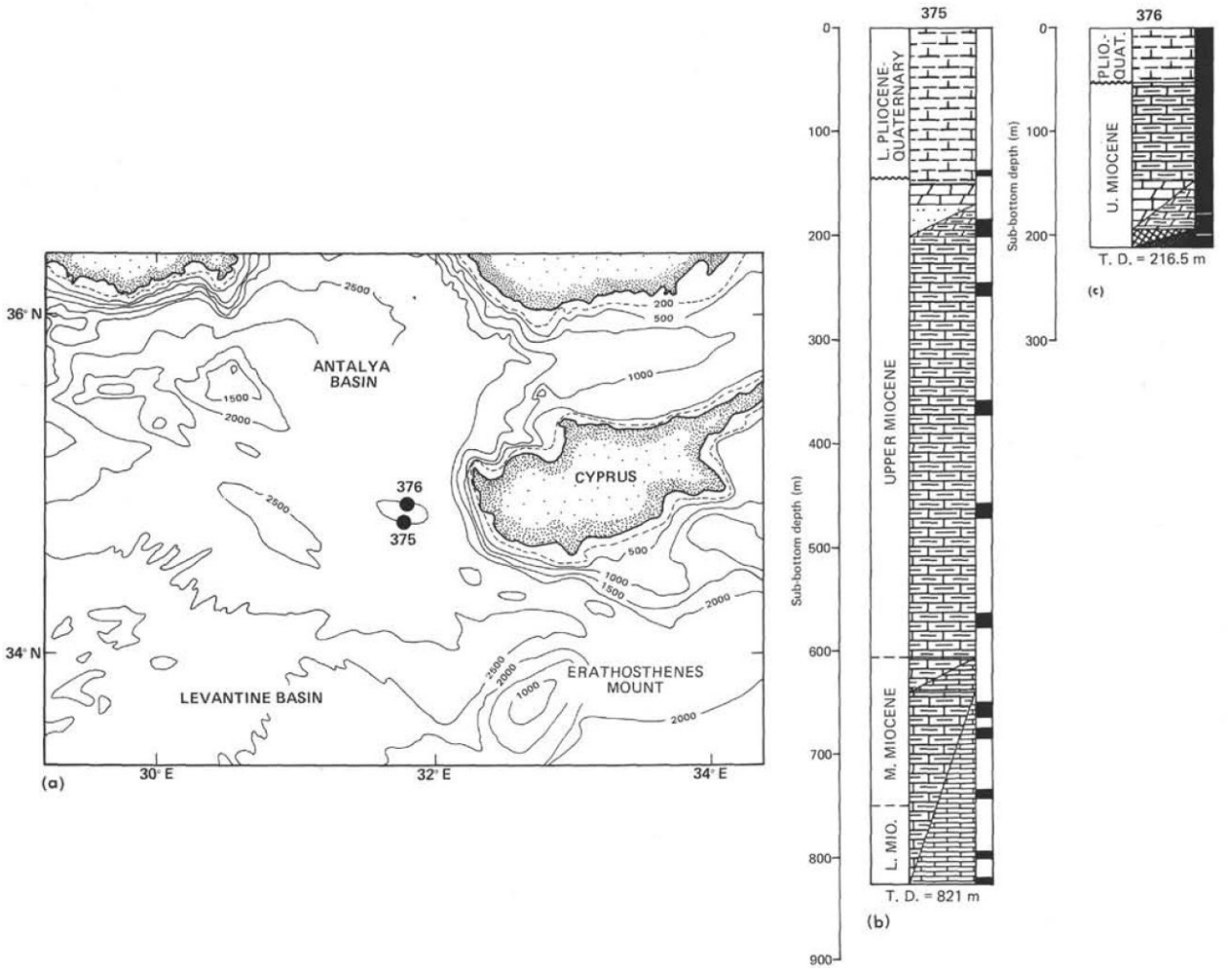

Figure 20: a) Location map of the DSDP boreholes; b) Lithostratigraphic column of the DSDP 42 Site 375; c) Lithostratigraphic column of the DSDP 42 Site 376. Figure modified from Hsü et al. (1978).

In the ODP boreholes (Fig.19 and Fig.21) the oldest recovered rocks are shallow marine carbonate platform with corals, calcareous red algae and foraminifera dated as Middle Cretaceous (ODP 160-967– Fig.21). Then, Late Cretaceous pelagic carbonates with chert (ODP 160-967– Fig.21) followed by Maastrichtian pelagic carbonates overlain by Paleogene chalk and Miocene shallow-water carbonates (ODP 160-967, ODP 160-966, ODP 160-965 – Fig.21). Messinian evaporites are absent or thin and hemipelagic marine sediments characterize the Plio-Quaternary (ODP 160-968, ODP 160-967, ODP 160-966, ODP 160-965– Fig.21). Detailed descriptions of the lithologies and associated tectonostratigraphic interpretation can be found in Robertson (1998) and Van Symaeys et al. (2019).

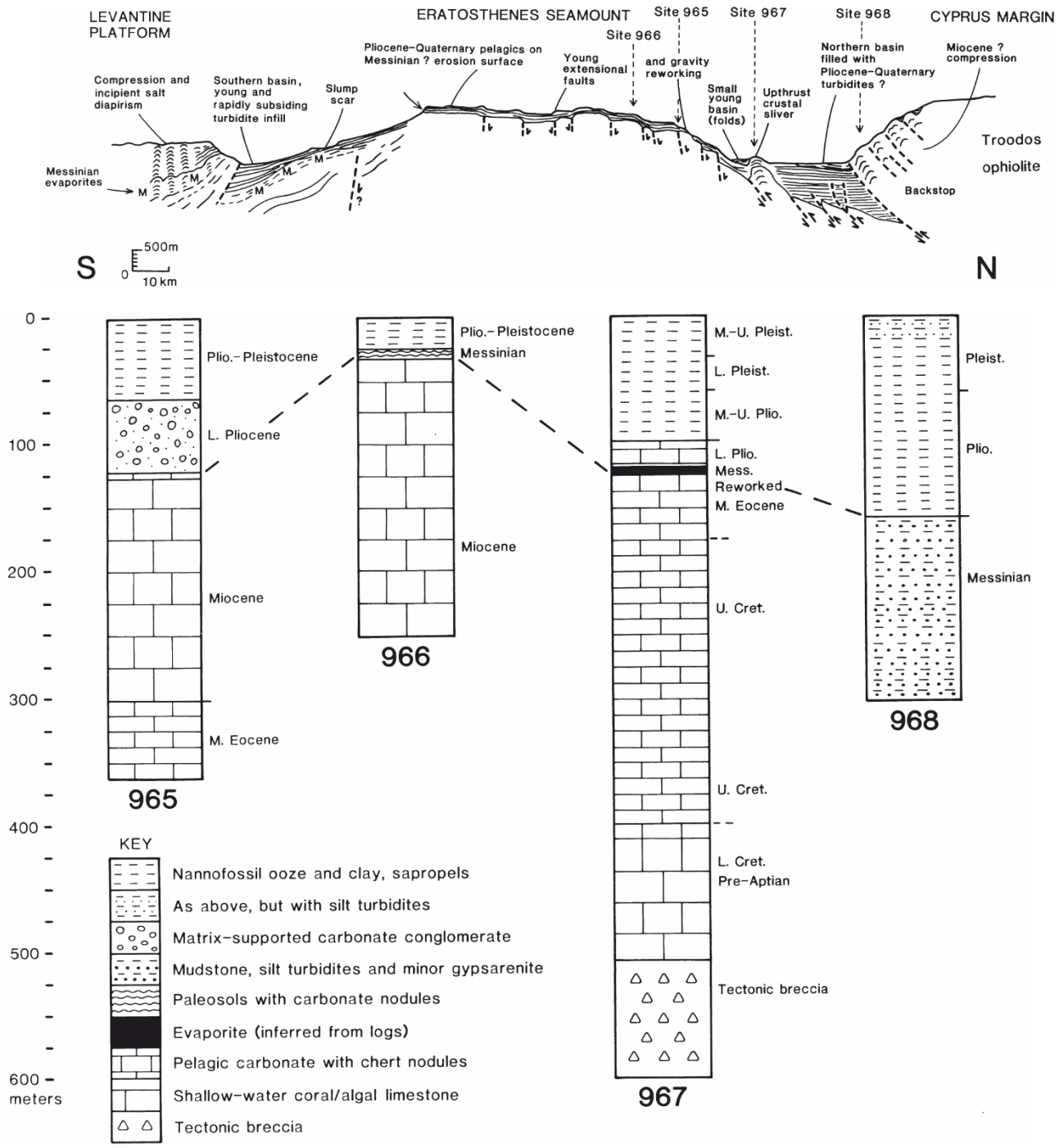

Figure 21: Upper panel: Tectonic interpretation of the Eratosthenes Seamount based on the seismic data obtained during the site survey cruise for the drilling of the ODP boreholes. Lower panel: summary and correlation of the lithostratigraphic columns of the ODP boreholes. Figure modified from Robertson et al. (1998).

Further borehole information comes from the TPAO (i.e., Turkish Oil Company) wells in southern Turkey.

The Manavgat-2 well is located in the Manavgat Basin, which lies north of the Antalya Basin and is considered its onshore continuation.

The Manavgat-2 well (Fig.22) reaches the base of the Aquitanian-Burdigalian formations (2246 m) and crosses 1750 meters of the pre-Messinian sediments (Fig.22 - Aksu et al., 2018). The Tortonian deposits consist of sandstones and siltstones with mudstones. The Serravallian deposits consist of siliciclastic rocks with minor limestones. The other formations, from the Langhian to the Aquitanian-Burdigalian, consist mainly of limestones. The pre-Messinian Miocene unit is tentatively associated with the deposits described in its surrounding areas. In the eastern part of the Antalya Basin, the pre-Messinian Miocene unit is associated with the formations outcropping in northern Cyprus (Bagnall, 1960; Follows and Robertson, 1990; Isler et al., 2005). These units are also associated with the predominantly siliciclastic successions of the Andirin Block and the Misis Mountains (Gökçen et al. 1988; Işler et al., 2005) and the similar formations of the Adana and Cilicia basins (Aksu et al., 2005). The Messinian succession consists of evaporites and interbedded siliciclastic layers. It consists of halite alternating with minor amounts of anhydrites and limestones. The Plio-Quaternary sediments consist of terrigenous siliciclastic deposits (Güneş et al., 2018).

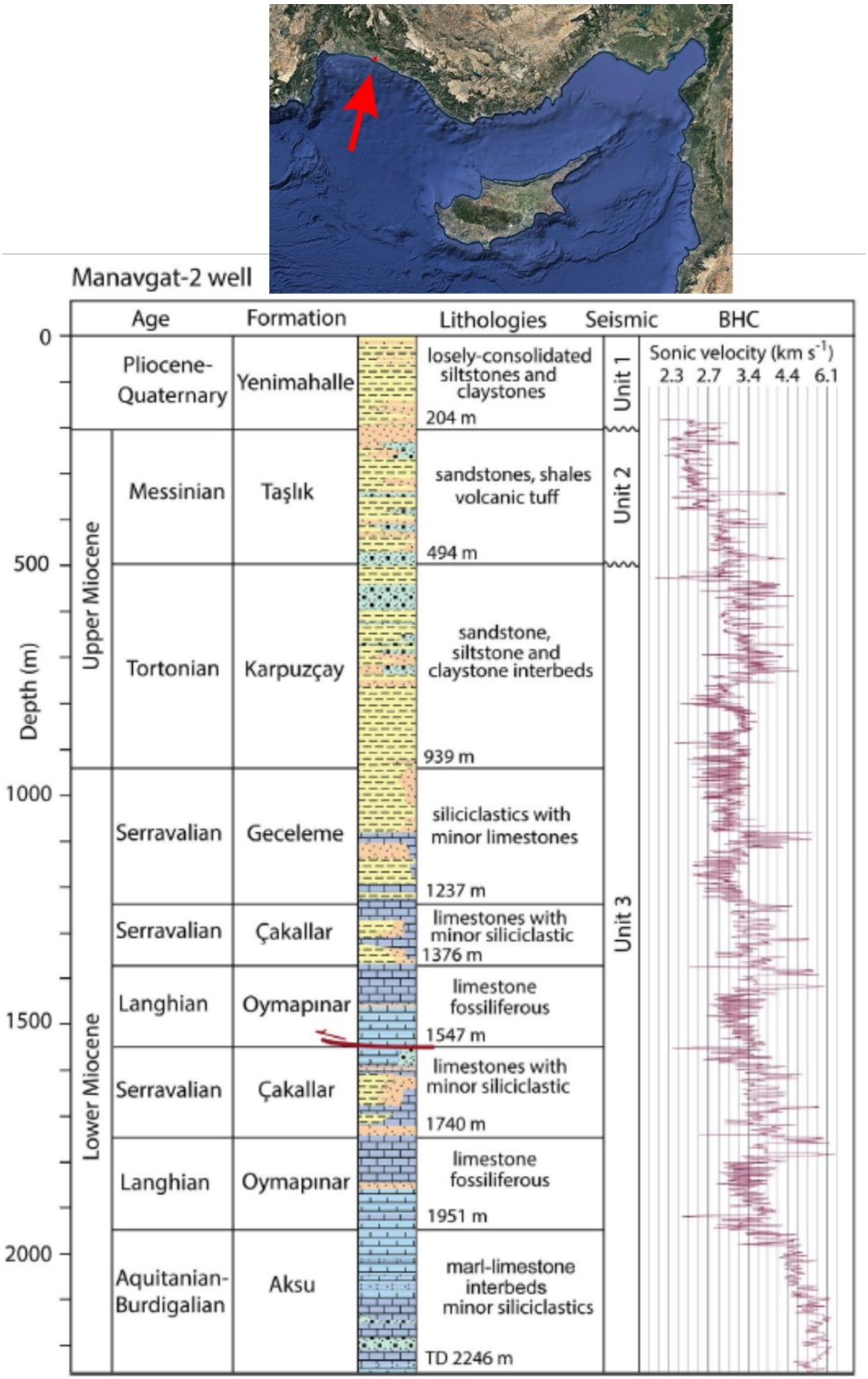

Figure 22: Location map of the Manavgat-2 borehole (drilled by TPAO), indicated by the red dot and the red arrow, and the borehole data. This borehole contains the lithostratigraphic column and the sonic compensated log, which is useful to know the sonic velocity of each drilled rock. The velocities

obtained from this sonic log are used as input parameters for the depth conversion of the MS53 seismic line. Note that the velocity generally increases with depth. This increase in velocity with depth is used to calculate the velocity gradient in Hz. Figure modified from Aksu et al. (2018).

There are three other wells in the Cilicia Basin published by Çiftçí et al. (2012): the Seyhan-1, the Karatas-1, and the Degirmen-1 (Fig.23).

The Paleogene period is represented by fluvial conglomerate and sandstone, transgressively overlain by the lower Miocene sequence composed of reefal limestones interfingered with pelagic marls and shales (Çiftçí et al. 2012). Then, the succession reflects the eustatic variations experienced by the Cilicia Basin evolving from lowstand incised valley conglomerates to middle slope fan sandstones, outer slope fan deposits represented by the alternation of sands and shales, capped by deep-marine sediments such as distal shales with sandstone intercalations. Instead, the Tortonian age was a regressive period depositing fluvial-deltaic clastic sediment. The lower Messinian comprises a thick sequence of sandstones, conglomerates, and some siltstones, representing a shallow marine or estuarine environment. The Messinian evaporites in the Cilicia Basin consist mainly of gypsum with minor sandstones and shales at the base, passing to dominant halite with anhydrite interbeds. The Messinian deposits are thicker in the basin centre and dramatically decrease toward the margins. The Plio-Quaternary sediments reflect the re-flooding of the Mediterranean Sea, starting with Pliocene conglomerates and sandstones passing into the Quaternary sequence composed of poorly consolidated clastics.

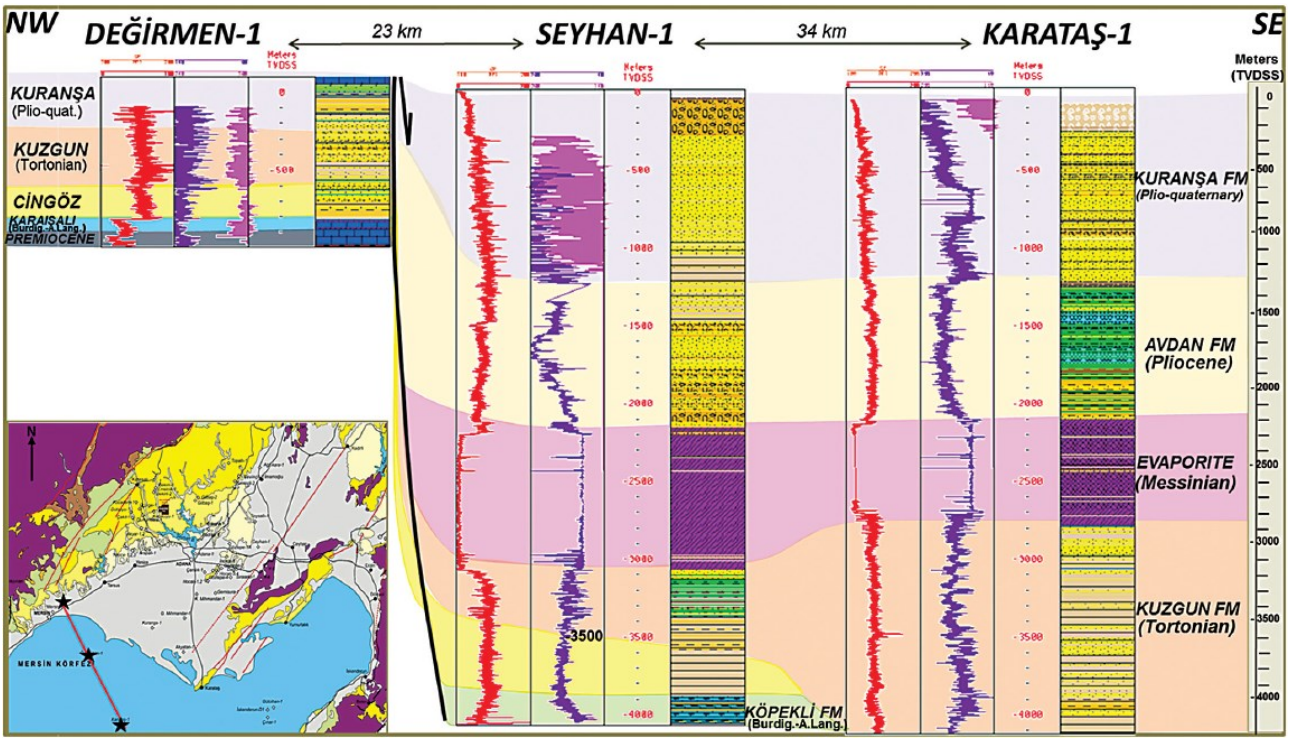

Figure 23: Bottom left: Location map of the boreholes in the Cilicia Basin. Three boreholes were drilled by TPAO along a NW-SE transect from the Adana Basin onshore to the Cilicia Basin nearshore and offshore. These boreholes are used to reconstruct the lithostratigraphy of the Cilicia Basin. Unfortunately, the sonic log values are not visible, so we cannot use them for the depth conversion of the MS56 seismic line. Figure from Çiftçí et al. (2012).

Further wells were drilled near the city of Latakia in Syria (Fig.24 - Latakia-1, Latakia-2 and Fidio-1 boreholes) and one near the coast offshore (Ayse-1 borehole), published by Bowman (2011).

In the onshore boreholes (Fig.24), the oldest rocks drilled are Triassic dolomite and limestone, followed by a thick carbonate succession of the Jurassic age. The Cretaceous and Paleogene successions consist of limestones and marls covered by an unconformity at the top. The Miocene succession continued with limestone, marl, and sandstone intercalations until the upper Miocene. In these boreholes, the Messinian deposits are a mixture of minor anhydrite, marl and shale overlain by the terrigenous Plio-Quaternary succession (Bowman, 2011).

The offshore Ayse-1 borehole ends with the Maastrichtian ophiolites at a depth of -1675 m. These ophiolites are in direct contact with the Miocene deposits, as the Paleogene is not present. The Miocene consists of carbonate overlain by terrigenous sediments and marls and capped by the

Messinian erosional surface. The uppermost part of the recovered rocks is the hemipelagic deposits of the Plio-Quaternary succession (Bowman, 2011).

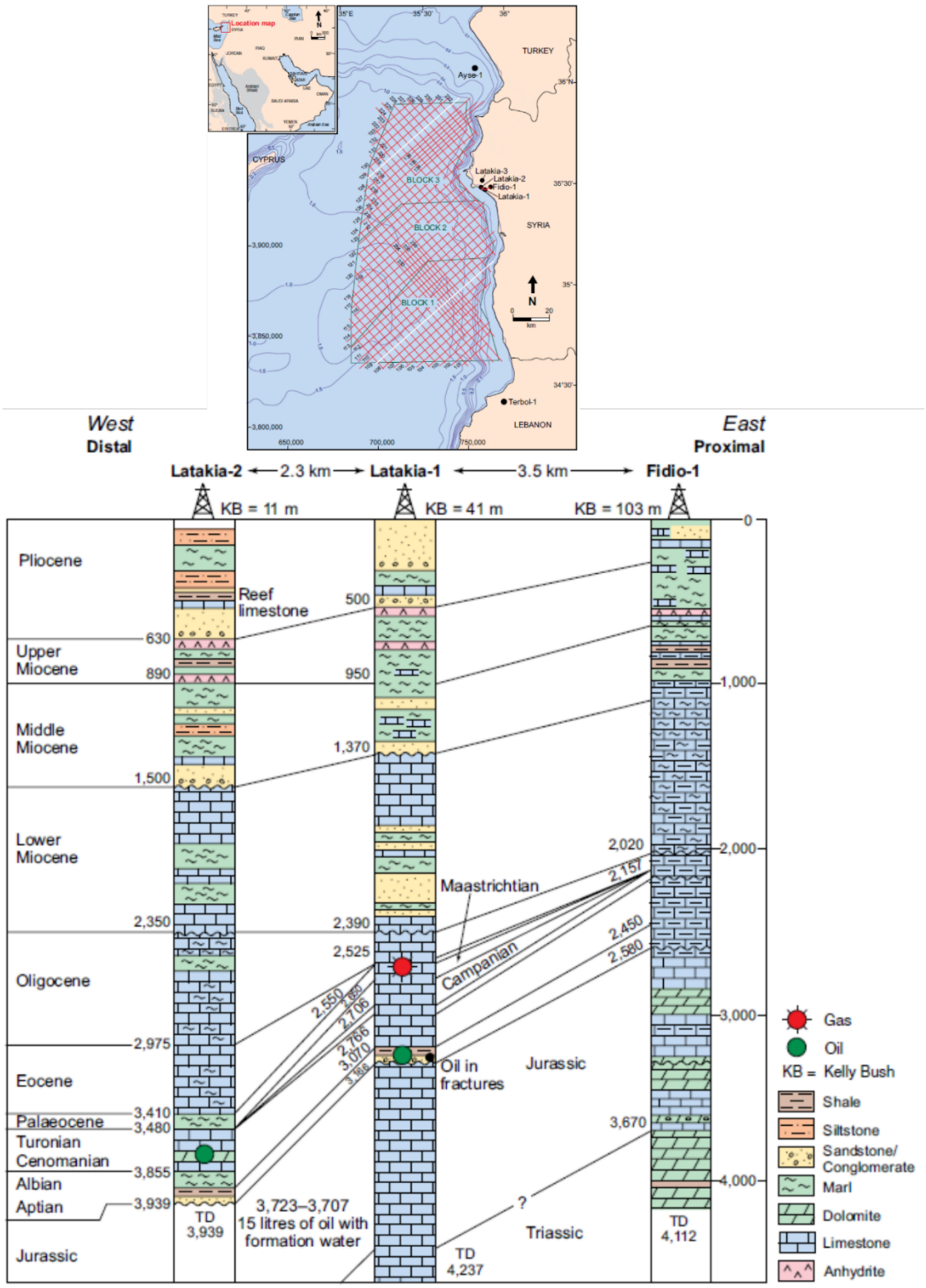

Figure 24: Upper panel: location map of the Syrian boreholes. Bottom panel: Lithostratigraphic columns and correlation between the three boreholes drilled near Latakia in Syria and offshore it.

These boreholes provide an approximate EW transect from the proximal to the distal setting. Figure modified from Bowman (2011).

The latest is the Birten-1 well (Fig.25), located in Iskenderun Bay, published by Bilim et al. (2017).

In the Birten-1 borehole, ophiolites from the Maastrichtian were encountered at a depth of -1306 m and the well was abandoned at a total depth (TD) of 3124 m while penetrating a thick basalt layer (1014 m). The Miocene sediments directly overlie the ophiolites and generally consist of shale-sandstone alternations. The Messinian erosional surface separates the Miocene succession from the Plio-Quaternary clastic deposits (Bilim et al., 2017).

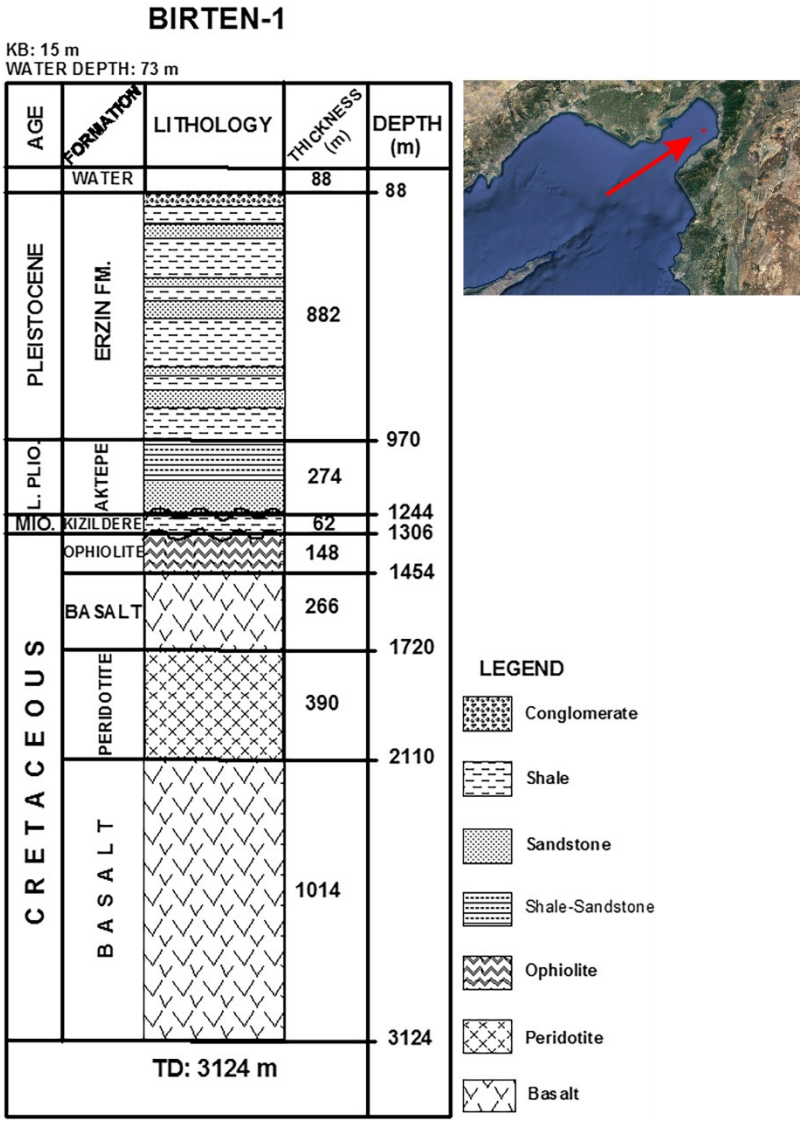

Figure 25: Location map and lithostratigraphic column of the Birten-1 borehole. Figure modified from Bilim et al. (2017).

3.2 – Methods

Since this work aims to describe the Cenozoic evolution of the Cyprus Arc system, we have selected three key transects that cross this convergent boundary. The Western Transect (i.e., MS53) extends from the Antalya Basin to the Herodotus Basin, crossing the Florence Rise (Fig.26). The Central Transect (i.e., Strakhov-8) extends from the western Cypriot nearshore to the south of the Eratosthenes Seamount, crossing the Cyprus Arc (Fig.26). The Eastern Transect (i.e., MS56) extends from the Cilicia Basin to the Levant Basin, crossing the Latakia Ridge (Fig.26). Thus, by analyzing these three sections, we focus on different segments of the Cyprus Arc system involving different plate's types, so that geometry and kinematics also change.

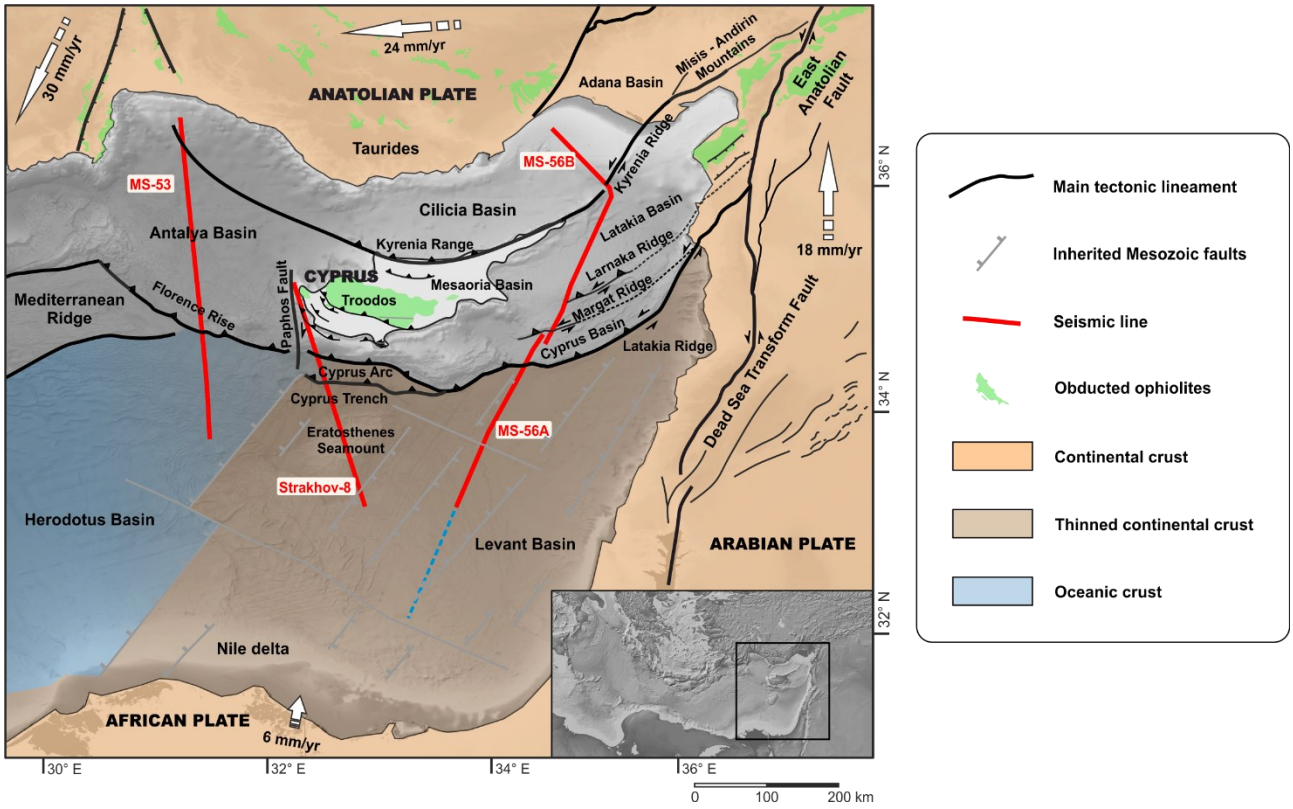

Figure 26: Tectonic map of the eastern Mediterranean. Red lines represent the interpreted seismic sections; the light blue dashed line represents the remaining part of seismic section MS56, which was not included in this study. Green spots are the obducted ophiolites from Mc Phee & van Hisbergen, 2019. Extensional faults in the Levant Basin are inherited from the Tethyan rifting phase. The white arrows show the GPS velocity of the plates from McClusky et al. (2000). Tectonic lineaments from Montadert et al. (2014); Longacre et al. (2007) and Mc Phee & van Hinsbergen (2019). The crustal domains beneath the Herodotus and Levant Basins are drawn from (Longacre et al., 2007; Granot,

2016). Bathymetry from EMODNet. Topography from GEBCO. Bottom right map inset from GeoMapApp.

The methodology can be summarized into four main steps:

- seismic interpretation;
- depth conversion of the interpreted time-migrated sections;
- structural modelling with the aid of other types of data and models or sequential restoration when other information is missing, and the seismic imaging permits it;
- validation of the geological model with the literature information and contextualization in the overall geodynamic picture.

3.2.1 - Seismic interpretation

The multichannel seismic reflection profiles interpretation consists in identifying the main seismic facies and assigning their tectonic-stratigraphic significance and their mutual relationships. As the available wells are located on the margin, on the structural high and south of Cyprus, it is difficult to correlate the seismic facies along all our seismic lines, as the signals and stratigraphic records are different in these areas. Therefore, we started by interpreting the most important horizons in the Levant Basin, which is the best explored among the others (i.e., Herodotus, Cyprus, Latakia, Antalya and Cilicia Basins), and then linked them along the whole seismic datasets. This process was facilitated by the use of the georeferenced seismic lines in PNG format (Calon et al., 2005; Bowman, 2011; Çíftçí et al., 2012; Hawie et al., 2013; Ghalayini et al., 2014; Symeou et al., 2018; among others), as the intersections of the lines were enlarged, thus facilitating the linkage between the datasets.

To minimize the interpretation uncertainties regarding the stratigraphic records, we also use the described stratigraphic columns of the surrounding countries. Our aim is to reconstruct the Cenozoic evolution of the northeastern Mediterranean. Therefore, we have interpreted only the main reflectors in the context of the main tectonic events. We have focused on the Cenozoic evolution because of the depth and resolution of our vintage datasets and because in the deformed basins to the north the deeper reflectors are attributed to the age of the Upper Cretaceous; below this reflector the signal-to-noise ratio deteriorates drastically.

3.2.2 - Depth conversion

The dataset MS is, as already mentioned, time-migrated. Therefore, depth conversion is mandatory to obtain a more realistic picture of the subsurface geometries and to correlate the horizons with

the Strakhov-5 dataset, which is depth-migrated. By applying an interval velocity to each interpreted seismic package, depth conversion transforms the scale of the seismic images and horizons from the two-way time domain to the depth domain.

After identifying the main seismo-stratigraphic units and the main tectonic lineaments, we depth-converted the MS53 and MS56 by assigning an interval velocity to each seismic package (Tab.2).

Table 2: Velocity [m/s] and gradient [Hz] values used for the depth conversion of the MS53 and MS56 seismic section.

Seismic package	MS53 velocity [m/s] / gradient [Hz]	MS56 velocity [m/s] and gradient [Hz]
Water	1520 / 0	1520 / 0
Plio-Quaternary	2000 / 0.2	2000 / 0.1
Messinian	4100 / 0	4100 / 0
Miocene + Paleogene	3150 / 0.2 (basin) – 3500 / 0.2 (Inner Deformation Zone)	3150 / 0.1
Acoustic Basement	5000 / 0.2	3500 / 0.2

We performed the depth conversion using the MOVE software, which allows polygons to be created with a characteristic velocity and gradient. To obtain the interval velocities we take advantage from the velocity analysis performed on the dataset of MS and Strakhov. We then calculated the mean and the variation with depth (gradient) for each interpreted seismic package to obtain the values for each MOVE polygon (Tab.2). Therefore, we created a polygon for each seismic package with its velocity and gradient values and then applied them to SEG -Y and to the line drawings in TWT to obtain the seismic depth section and horizons.

For the MS56 we used a set of interval velocities (Tab.2) derived from the velocity analysis of the seismic profile and previous work (Calon et al., 2005; Klaeschen et al., 2005).

For the MS53 we used the velocities (Tab.2) measured in the Manavgat-2 well and a velocity gradient for the deeper part that does not correlate with the drilled sequence.

3.2.3 – Sequential restoration

The sequential restoration of a geological section involves the removal of younger layers and deformations; it is a method used to determine the evolution of the structural geology of a particular area over time. The procedure starts with identifying a stratigraphic section of rock layers from the youngest to the oldest and calculating the subsidence rate of each layer by assuming a subsidence rate model or using subsidence data; we used the Sclater-Christie compaction curve to decompact each sedimentary package step-by-step. The next operation is to calculate the amount of shortening caused by the tectonic events on each layer by using structural data such as fault offset and fold vergence. Then by subtracting the calculated shortening of each layer, we can reconstruct the paleo-geometry and kinematics of the structures in each layer to understand the tectonic setting of the area at that time. The sequential restoration of a geological section is helpful in fields such as petroleum exploration, mineral exploration, and tectonics, providing insights into the tectonic history, kinematics, and dynamics of the area, and helping to understand the relationships between different structural events, as well as their timing, style, and magnitude.

CHAPTER 4: RESULTS

The Western and Central Transect allow us to describe the tectonic evolution of the area from the Messinian to the present day, as the base of the pre-Messinian succession is not imaged by seismic due to multiple reflections and the high absorption of seismic waves by the evaporites. Instead, the Eastern Transect has a higher resolution in depth, even in the deformation zone. Therefore, we use this profile to describe the Cenozoic evolution of this area, because in this section the deepest reflector is the boundary between Upper Cretaceous and Paleogene.

For the profiles of the MS survey, we describe the time-migrated version of the seismic profile, as depth conversion degrades imaging. In contrast, for the Strakhov-8 we describe the depth-migrated seismic profile, as it is better imaged than the stack version. The first step in seismic interpretation is the identification of the main seismic facies and the assignment of the corresponding lithologies.

The seismic units identified in this study comprise four/five seismic packages that are assumed to correspond to (from top to bottom): Plio-Quaternary, Messinian, Miocene, Paleogene, and the acoustic basement.

We have identified three main horizons on the Western and Central Transects: the seafloor, the Plio-Quaternary, and the Messinian base. Unfortunately, the boundary between Miocene and Paleogene is not easily discernible on these lines, but some deep reflections could be pointed out. Instead, the Eastern Transect has a higher resolution than the latter two, so we also subdivide the Miocene from the Paleogene on this profile, and its base is well identified along the seismic profile.

4.1 - Seismic facies interpretation

The seafloor and the Plio-Quaternary base reflectors bound the first seismic package. This seismic package is the Plio-Quaternary sequence. It generally consists of parallel and continuous high-frequency reflections with different amplitudes. The top and base reflectors are positive reflections with high amplitude, which means that the seismic impedance increases in depth and produces a positive signal. This sequence is ubiquitous in the study area and shows significant variations in thickness: it is thicker near the Turkish margin and in the Cyprus Trench than elsewhere. We have interpreted this first seismic package as terrigenous sequences from the Plio-Quaternary (Fig.27).

Two high-amplitude reflectors bound the second seismic package: the top is positive, and the base is negative. These reflectors delineate a seismically transparent sequence that we have interpreted

as Messinian units (Fig.27). There are some acoustically strong and continuous reflectors in this package, which we have interpreted as part of the Messinian Trilogy. These reflective signals are due to siliciclastic inputs that occurred during the precipitation of the evaporites. This seismic package is very thick in the Herodotus, Levant, and Antalya basins. In the Cyprus, Latakia and Cilicia basins, it reduces in thickness, and it is confined to local mini-basins becoming an erosional surface at the margin and on the structural highs.

The third seismic package is bounded above by the strong negative reflector of the Messinian base and below by another strong reflection, referred to in the literature as the Senonian unconformity. This seismic package represents the pre-Messinian Cenozoic succession. On the Western and Central transects it is a single package, while on the Eastern Transect it is subdivided into the Miocene and the Paleogene packages due to better seismic imaging (Fig.27).

Our seismic profile does not image the pre-Messinian successions in the Herodotus Basin because of the overlying thick Messinian units that inhibit and absorb the propagation of the seismic waves, so its base and the underlying package are not visible (Fig.27-1).

In the Antalya Basin, the pre-Messinian units in the southern part of the Antalya Basin generally consist of acoustically strong, low-amplitude and continuous reflectors that are parallel and continuous (Fig.27-2). Based on the bibliographic information and their seismic characteristics, they can be considered siliciclastic and basinal carbonate deposits. Unfortunately, due to the quality of the seismic section, the base of the succession cannot be identified (Fig.27-2).

In the Eratosthenes Seamount area, it has a maximum thickness of about 1000 m. The seismic facies consists of undulating, not very continuous reflectors with medium-high amplitude and medium-low frequencies (Fig.27-3), representing shallow-water carbonate.

Along the Eastern Transect, the pre-Messinian succession could be divided into the Miocene and Paleogene seismic packages (Fig.27). Below the Messinian deposits, continuous parallel reflections characterize the third seismic package, which is visible along the entire seismic section; however, it has different seismic facies along the section. In the Levant Basin, the package can be divided into two sub-facies: The upper and lower parts are represented by low to high amplitude undulating reflectors separated by a high amplitude parallel triplet and bounded at the base by a strong reflector. These triplets are key horizons that are clearly visible throughout the Levant Basin (Fig.27-

5). In the Cyprus and Latakia basins, the basal reflector is characterized by high amplitude and low frequencies and merges into a more transparent central part (Fig.27-6 and Fig.27-7). In the Cilicia Basin, this third package is composed of several chaotic and lenticular bodies that flow down from the Kyrenia Ridge and downlap onto the deeper package (Fig.27-8). This seismic package can be associated with the Miocene, which consists of deep marine sediments.

Below the Miocene deposits, the seismic facies in the Levant and Cilician basins are chaotic and not well resolved (Fig.27-5 and Fig.27-8). Nevertheless, some coherent signals with high amplitude and low frequencies can be detected. In the Cyprus and Latakia basins, the resolution of this part is higher, with facies from low to medium amplitude south of the Larnaka Ridge to higher amplitude north of it (Fig.27-6 and Fig.27-7). The entire sequence is an overlapping wedge with a visible and ubiquitous continuous basal reflector of high amplitude and low frequency. This final seismic package is associated with the Paleogene sequence, which consists mainly of chalk and marl. The basal reflector represents the boundary between the Paleogene succession and the Upper Cretaceous deposits, e.g., the Senonian unconformity as cited in the literature (Fig.27).

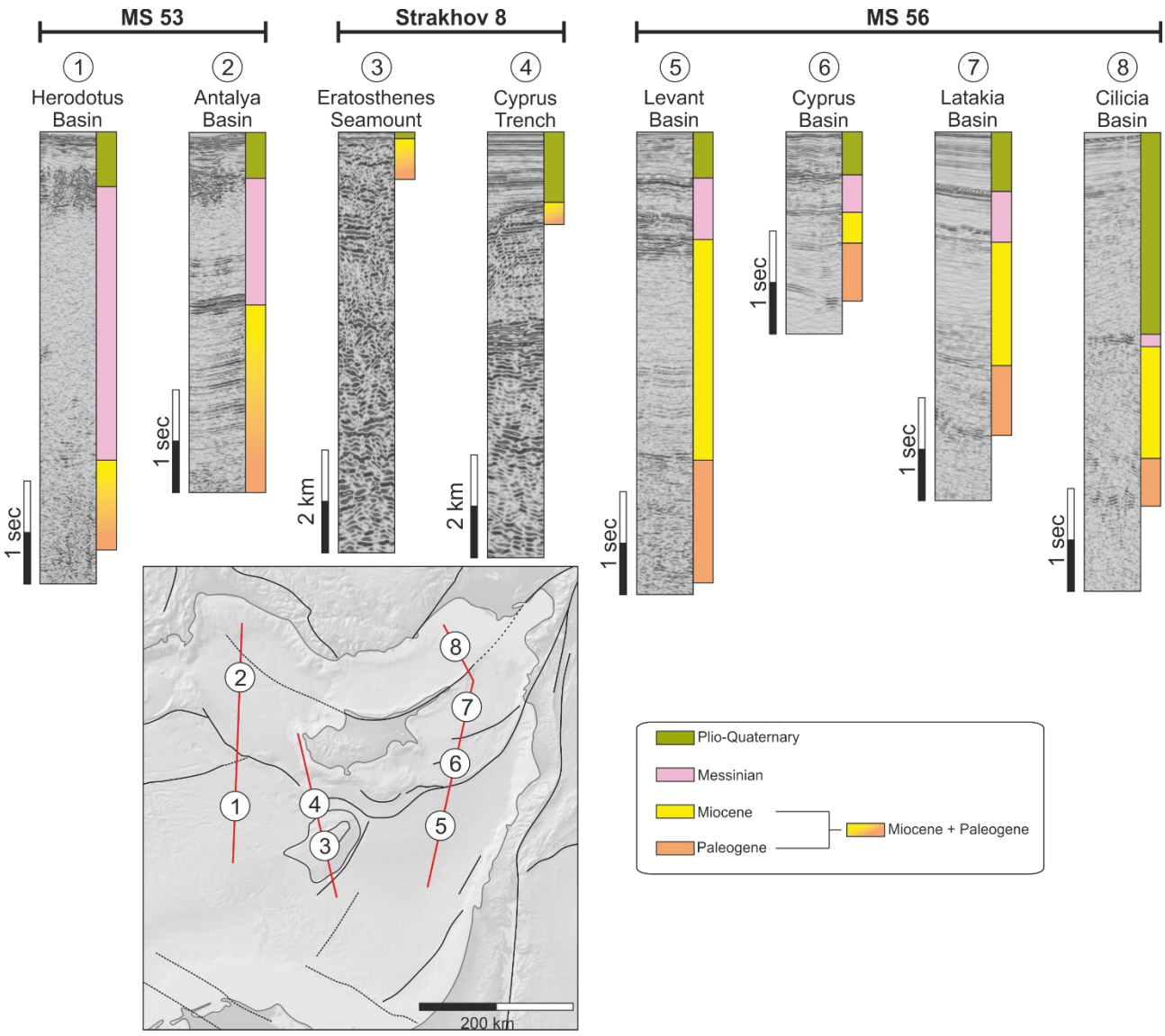

Figure 27: Seismic facies comparison of the three selected multichannel seismic reflection profiles for the making of this study. Seismic profiles MS53 and MS56 are time-migrated and the corresponding columns are shown with a vertical exaggeration x6. The Strakhov-8 seismic section is depth-migrated and its column is vertically exaggerated x2. The map below shows the position of the column shown in this figure: 1) Herodotus Basin, 2) Antalya Basin, 3) Eratosthenes Seamount, 4) Cyprus Trench, 5) Levant Basin, 6) Cyprus Basin, 7) Latakia Basin, 8) Cilicia Basin.

4.2 - Detailed interpretation of the tectonostratigraphic setting

Once the seismic facies have been identified and tied along the seismic dataset, the next step is to analyze their distribution along the basins and define their tectonostratigraphic relationships. In the following sections, the individual transects are discussed in detail from south to north, i.e., from the undeformed basin towards the deformation zone.

4.2.1 - Western Transect (MS53)

Figure 28 shows the MS53 time-migrated seismic section with vertical exaggeration x6 and the position of the details discussed in this paragraph.

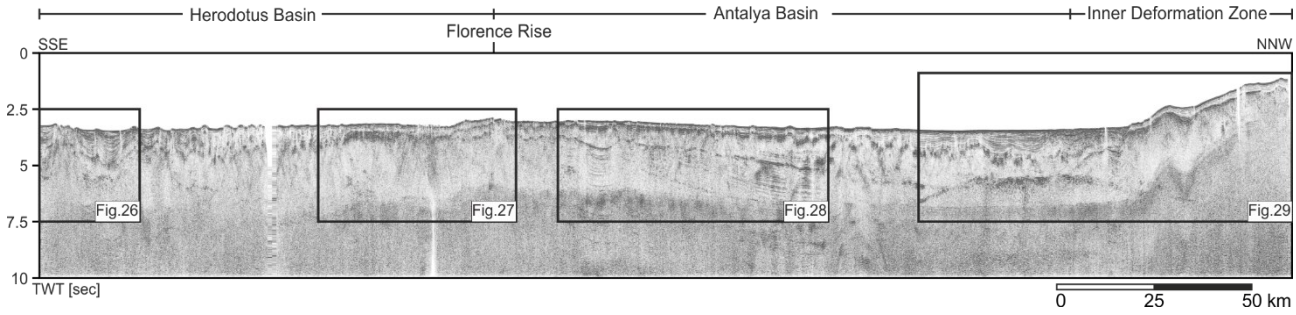

Figure 28: MS53 time-migrated seismic section with vertical exaggeration x6. The rectangles represent the detailed zooms discussed in the following paragraphs.

4.2.1.1 – Herodotus Basin

The seismic signal in the Herodotus Basin is good in the uppermost part of the seismic profile and deteriorates rapidly (Fig.29a). The Plio-Quaternary package has a maximum thickness of 1.5 seconds. It thins to about 0.5 seconds towards Florence Rise (Fig.28 and Fig.29). It is strongly deformed by the halokinetic movement of the underlying Messinian package, which is thicker here than elsewhere (slightly more than 2 seconds). However, this interpretation is speculative as the base is difficult to determine (Fig.29a/b). The uppermost Messinian reflector is clearly visible, but sparse hard signals and seismic attributes suggest its base. As the evaporites are known to be a high impedance medium, it is typical for the seismic signal to deteriorate quickly, and the base is not well imaged (Fig. 29a).

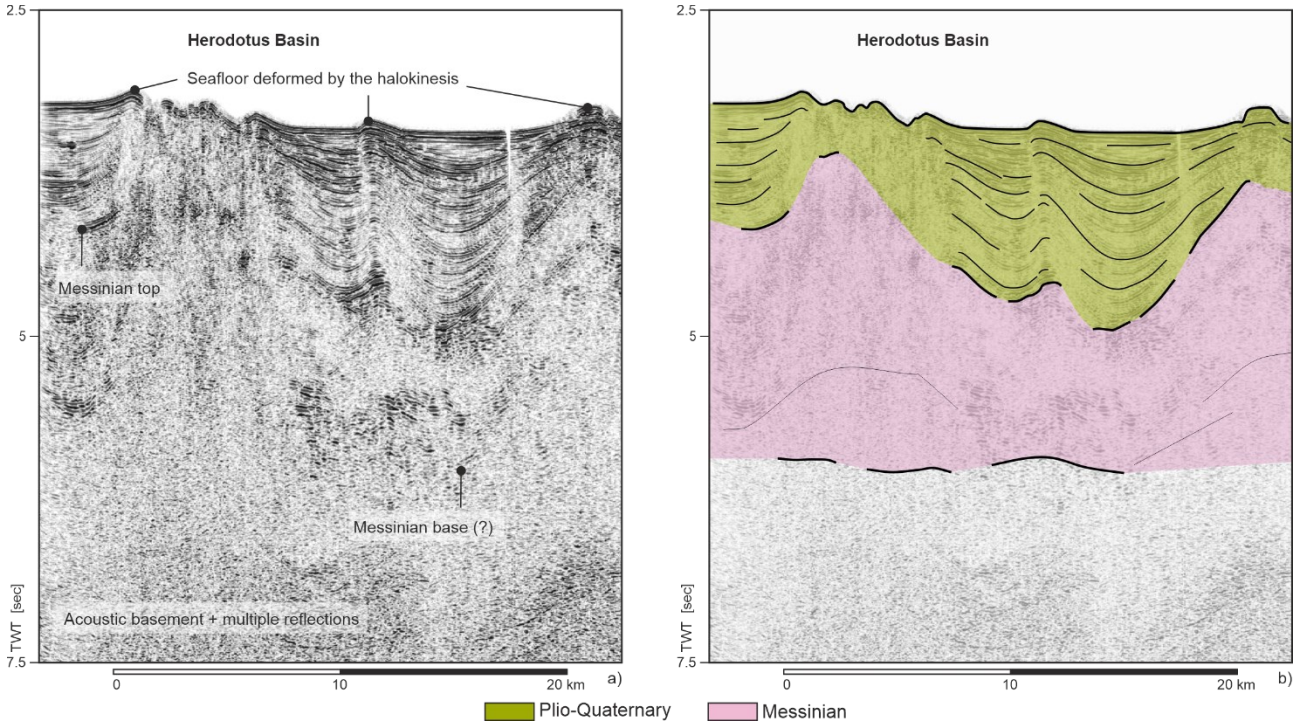

Figure 29: Zoom of the MS53 time-migrated seismic section in the Herodotus Basin. a) Part of the seismic section without interpretation highlighting the seafloor deformations and the main reflectors visible in this part of the basin. b) Same part of the seismic section of a) with the superimposed seismic packages and line drawing.

Therefore, we constrain its base by using some sparse signals, seismic attributes and by tying it along our "extended dataset" with georeferenced published profiles. This enormous thickness is difficult to explain by the autochthonous precipitation of evaporites. It is more likely that the evaporites accumulated in the northeastern Herodotus Basin by gliding northward, thus reaching this enormous thickness of allochthonous evaporites. The gliding of the evaporites to the north indicates that the pre-Messinian deposits must have been tilted to create a slope on which the evaporites could move.

4.2.1.2 – Florence Rise

The Florence Rise is a tectonic structure separating the undeformed Herodotus Basin in the south from the deformed Antalya Basin in the north. It is only slightly pronounced in bathymetry (300 m of seafloor step) and runs roughly east-west.

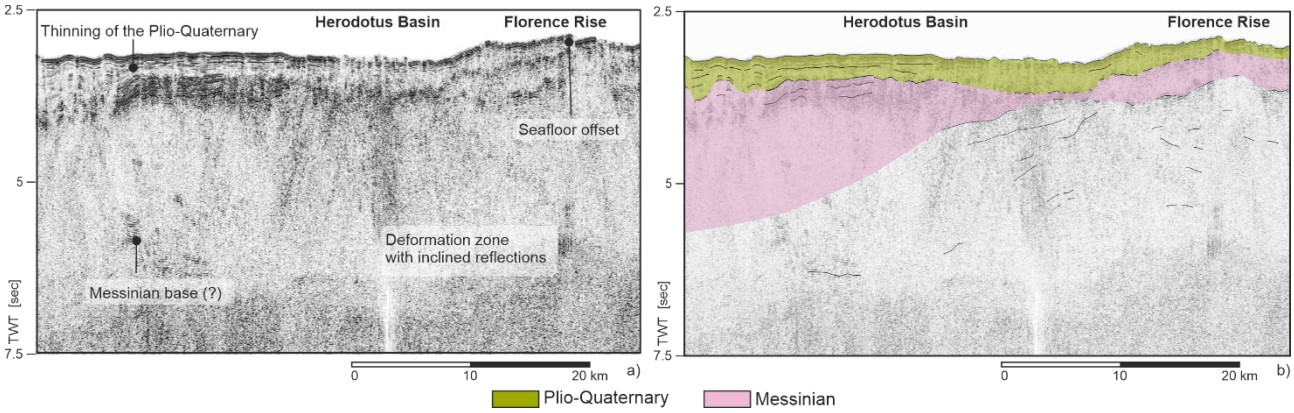

Figure 30: Zoom of the MS53 time-migrated seismic section in front of the Florence Rise. a) Part of the seismic section without interpretation highlights the thinning of the Plio-Quaternary seismic package, the offset on the seafloor on top of the Florence Rise, and the chaotic seismic facies in the deformation zone. b) Same part of the seismic section of a) with the superimposed seismic packages and line drawing.

In the Florence Rise area, both the Plio-Quaternary and Messinian packages are thinner than in the neighboring Herodotus and Antalya basins (Fig.30). As this area is a long-lived deformation zone, seismic imaging is not optimal, but some considerations can be made. The low thickness of the Plio-Quaternary and Messinian compared to the adjacent basin indicates an already active structure, which is considered a structural higher sector at least before the inception of the Messinian Salinity Crisis, as evidenced by the deformed Messinian base (Fig.30b).

The inferred thickness of the pre-Messinian seems to be greater in the Antalya Basin than in the Herodotus Basin, suggesting that the Florence Rise was already a barrier to the sediments that mainly invaded from the north and were deposited in greater quantity in the Antalya Basin.

Considering the features mentioned earlier and its position in the overall tectonic picture, it can be considered an accretionary prism.

4.2.1.3 – Antalya Basin

The seafloor in the Antalya Basin dips toward the north and shows slight deformations due to the halokinesis of the Messinian units (Fig.31). Naturally, the Plio-Quaternary package is also deformed by the movement of the underlying evaporitic succession. This seismic package has a wedge shape with a thickness of a few milliseconds near the Florence Rise and becomes more than 1 second thick in the northern Antalya Basin (Fig.31).

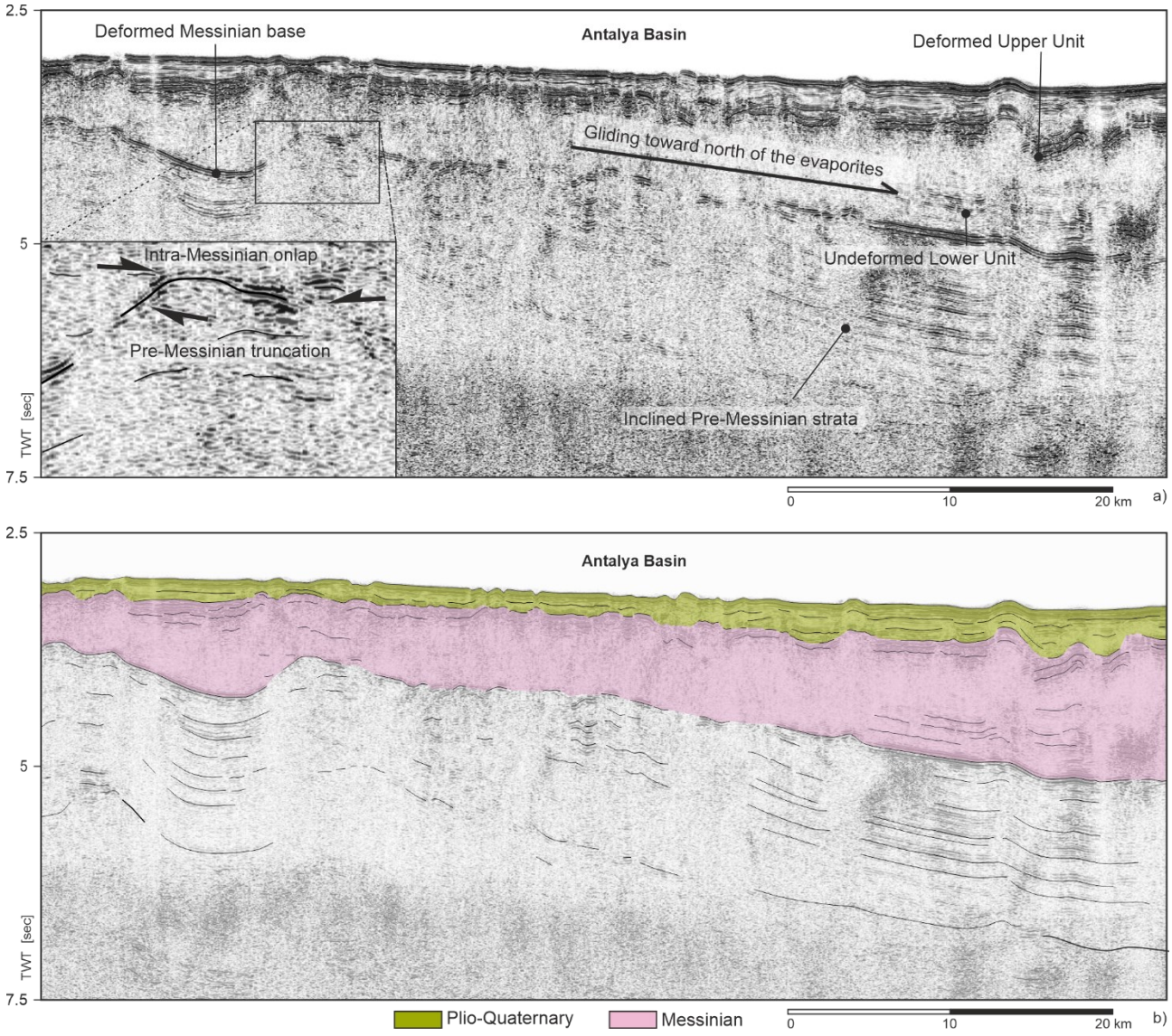

Figure 31: Zoom of the MS53 time-migrated seismic section in the Antalya Basin. a) Part of the seismic section without interpretation, highlighting the deformation on the Messinian base and top and the gliding of the evaporites toward the north. The inset in a) shows an erosional truncation on the buried anticline's apex and the intra-Messinian reflectors' onlap. b) Same part of the seismic section of a) with the superimposed seismic packages and line drawing.

The Messinian evaporites have the same wedge shape, thickening towards the north. Its top is deformed by halokinesis, while the base is deformed by active tectonics. As can be seen in Figure 31, the bottom of this package has two south-verging open folds and the whole basin is tilted towards the north. The pre-Messinian sequence is also tilted to the north and eroded in correspondence with the fold crests. In Figure 31a the inset highlights the pre-Messinian strata truncation at the fold apex and the onlap of the intra-Messinian reflectors onto the underlying

reflectors. This relationship of truncation and onlap proves that these tectonic structures were active before the onset of the Messinian Salinity Crisis.

The northward tilting of the Antalya Basin influences the movements of the evaporites, resulting in a northward gliding of this sequence (Fig.31a). In this area, the Messinian Trilogy is well visible and some intra-Messinian reflectors show internal deformation (Fig.31a). Because the evaporites are considered plastic and more prone to deformation than the surrounding rocks, they deform internally using different detachment levels, testify by the relatively undeformed Lower Unit and by the strongly deformed Upper Unit (Fig.31a).

4.2.1.4 – Inner Deformation Zone

The northernmost part of the Western Transect is occupied by the transition between the deep Antalya Basin and the Turkish slope. In this sector, the seafloor rises from about -2500 m water depth to the Turkish coast in about 120 km.

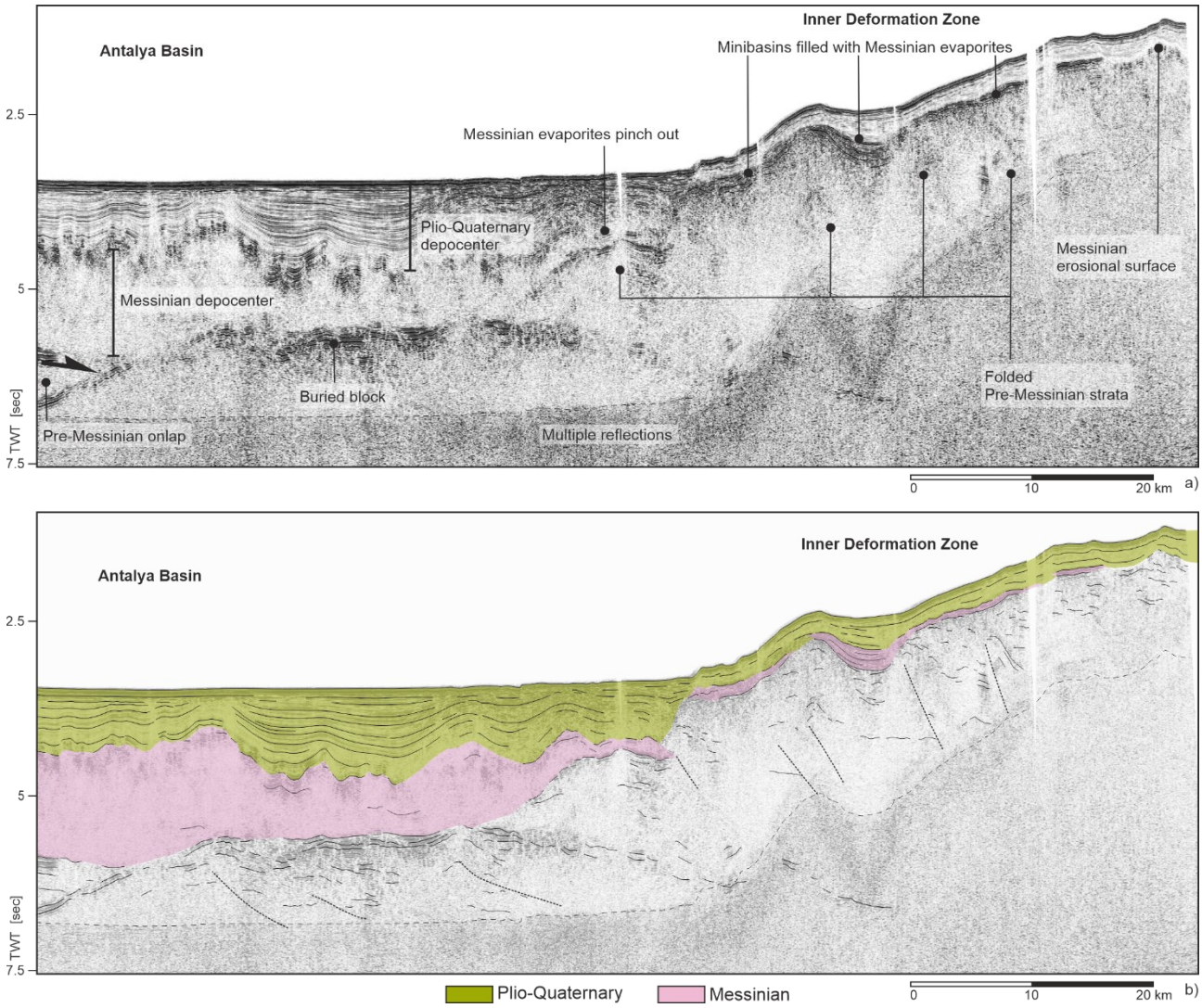

Figure 32: Zoom of the MS53 time-migrated seismic section in the northern Antalya Basin. a) Part of the seismic section without interpretation highlighting thinning of the Plio-Quaternary seismic package on the Inner Deformation Zone, the Messinian minibasins, the high seismic impedance buried block, and the folded pre-Messinian succession in the Inner Deformation Zone. The Messinian seismic package is thick in the Antalya Basin, thinner in the Inner Deformation Zone, and is figured as an erosional surface on the northernmost part of the section. b) Same part of the seismic section of a) with the superimposed seismic packages, some inferred faults, and line drawing. The light grey dashed line represents the seafloor's multiple reflections; the signal degrades quickly below it.

In this part of the basin, the Plio-Quaternary package is skinny and thickens towards the south, at the frontal zone of deformation (Fig.32).

The Messinian evaporites are present in local minibasins (synclines) with internal growth strata geometry. Elsewhere, the Messinian Salinity Crisis is an erosional surface that puts the Plio-Quaternary and pre-Messinian successions into direct contact (Fig.32b).

In general, the pre-Messinian package is chaotic and only some reflectors can be interpreted because multiple reflections degrade the seismic signals. In this seismic package, some dipping reflectors representing multiple folds could be identified (Fig.32a). There are no clear signs of faulting, but it can be inferred from the fold structures and seafloor deformations (Fig.32b). As this sector has a wedge-shaped and contractional structures (Fig.32), it is considered to be another accretionary prism located off the Tauride Mountains (on the Turkish coast).

The necking zone between the deep Antalya Basin and this deformation zone has the most significant thicknesses of Plio-Quaternary and Messinian, and the pre-Messinian strata onlap onto a high impedance contrast buried body (Fig.32a). This is further evidence of pre-Messinian Salinity Crisis structurization of this sector before the formation of this prism. This buried block also has fold structures, but they appear to be different from the rest of the prism. They have higher amplitude and lower frequencies than the northern part (e.g., greater impedance contrast).

4.2.2 - Central Transect (Strakhov-8)

Figure 33 shows the Strakhov-8 depth-migrated seismic section without vertical exaggeration and the position of the details discussed in this paragraph.

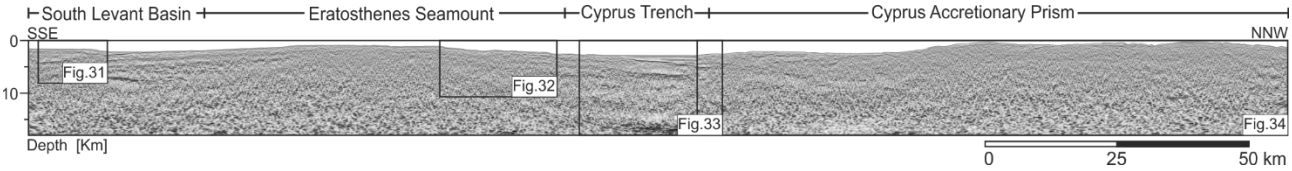

Figure 33: Strakhov-8 depth-migrated seismic section without vertical exaggeration. The rectangles represent the detailed zooms discussed in the following paragraphs.

4.2.2.1 – South Levant Basin and Eratosthenes Seamount

The Eratosthenes Seamount occupies the southern and central parts of the Central Transect. South of it, the Plio-Quaternary package reaches a maximum thickness of about 1000 m and rapidly thins on the seamount, reaching 200 m of thickness. In the southern part of the Eratosthenes Seamount, the Messinian evaporites are about 2000 m thick and pinch out towards the north (Fig.34). The Messinian top is quite flat, while the base is deformed by high-angle faults. The pre-Messinian

Cenozoic sequence is also cut by the same high-angle faults, which lower the basement to the south and represent a Mesozoic paleo-high with a lower sedimentary thickness on it and a greater thickness to the south and north (Fig.34). The thickness of the pre-Messinian package (Miocene + Paleogene) ranges from 1000 m south of the paleo-high to 500 m approximately on top of it (Fig.34 and Fig.35).

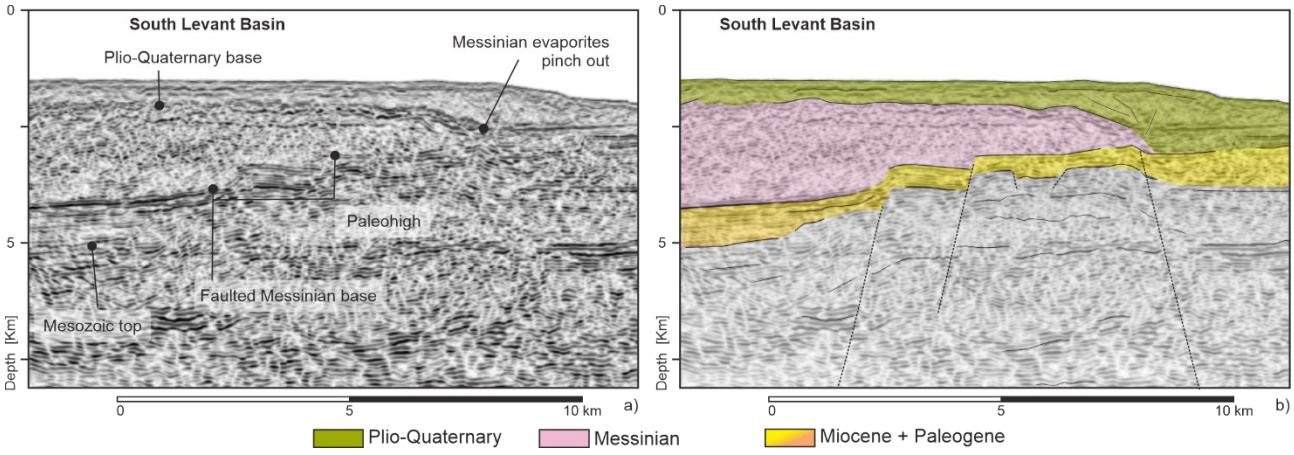

Figure 34: Zoom of the Strakhov-8 depth-migrated seismic section on the passage between the south Levant Basin and the southern flank of Eratosthenes. a) Part of the seismic section without interpretation highlighting the deformation on the Messinian base, the pinch-out of the evaporites on the southern flank of Eratosthenes Seamount and the paleohigh beneath the Messinian seismic package. b) Same part of the seismic section of a) with the superimposed seismic packages, some inferred faults and line drawing.

On the Mesozoic horst, the Messinian succession pinches out and north of it, on the Eratosthenes Seamount, this package is absent (Fig.34 and Fig.35); an erosional surface represents the Messinian Salinity Crisis.

In the Eratosthenes Seamount area, the Plio-Quaternary thus rests directly on the pre-Messinian sequence, which has a similar thickness to that measured at its southern end (Fig.34 and Fig.35).

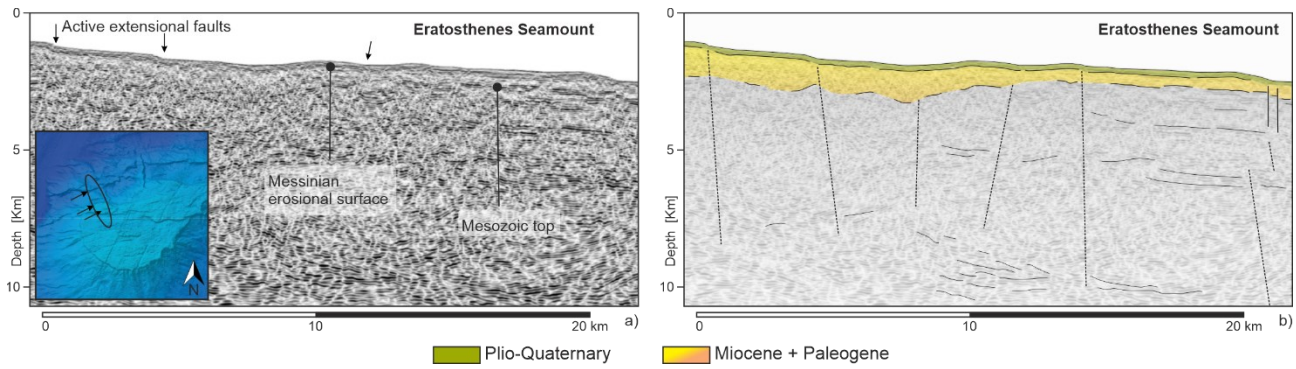

Figure 35: Zoom of the Strakhov-8 depth-migrated seismic section on the Eratosthenes Seamount. a) Part of the seismic section without interpretation highlighting the active faulting on the seafloor, also visible on the bathymetry (bottom left inset in a). b) Same part of the seismic section of a) with the superimposed seismic packages, some inferred faults and line drawing. The seismic facies degrade quickly in the Eratosthenes Seamount area.

Below it, the Mesozoic sequence is not easy to interpret and divide into sub-packages, as it mainly consists of carbonates, a medium of high impedance for seismic reflection methods. Some reflectors could be interpreted, and high-angle extensional faults can be inferred by the offset on the main reflectors and are also visible on the seafloor (Fig.35a). In Figure 35 some of these extensional faults are highlighted and linked to their bathymetric expression. ENE - WSW trending normal faults are visible on the Eratosthenes Seamount, dipping mainly to the north on the northern side and to the south on the opposite flank. These faults could be inherited by the rifting phase and are now reactivated by the flexure caused by the weight of the upper plate overriding it to the north.

4.2.2.2 – Cyprus Trench

The northern flank of the Eratosthenes Seamount is overlain by the Cyprus Trench, which is well identified on the seismic profile by the growth strata of the Plio-Quaternary sequence. In the Cyprus Trench, the Plio-Quaternary package has a maximum thickness of 2000 m and a wedge shape with onlapping reflector to the south on the Messinian erosional surface. This wedge is characterized by growth strata that flatten in the uppermost part (Fig.36a). In addition, the trench is affected by flexural faults crossing the entire sequence almost to the seafloor (Fig.36b).

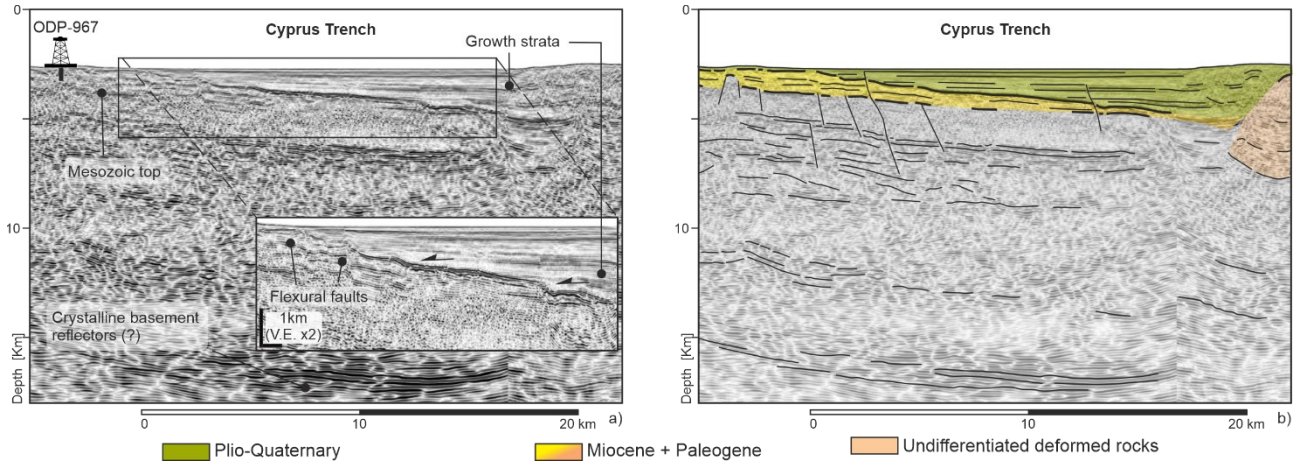

Figure 36: Zoom of the Strakhov-8 depth-migrated seismic section in the Cyprus Trench. a) Part of the seismic section without interpretation highlighting the growth strata in the trench (see the inset for more with higher resolution). The ODP 160-967 is close to our section, so we projected it and used it to constrain the upper reflectors' seismic tying. The deeper set of reflectors can be associated with the top of the crystalline basement due to their high amplitude and low frequencies. b) Same part of the seismic section of a) with the superimposed seismic packages, some inferred faults, and line drawing. Notice that some extensional faults almost reach the seafloor also in this sector.

The pre-Messinian succession is about 200 m thick; below it, some high amplitude low-frequency signals are visible in the Mesozoic succession. These reflectors are inclined and have an extensional offset toward the north. The deepest (about 16 km) series of reflectors could be attributed to the top of the crystalline basement (Fig.36a).

4.2.2.3 – Cyprus Accretionary Prism

The northern limit of the Cyprus Trench is the associated accretionary prism, where the seafloor rises from -700 m to -200 m in about 100 km. The seafloor is deformed, offset, and incised by canyons (Fig.37a). Some large steps in the seafloor can be associated with active thrusts breaching through it.

The Plio-Quaternary is very thin, albeit in local synclines and near the coast of Cyprus, where it is a maximum of 400 m thick. It is directly underlain by the deformed Cenozoic sediments, except for a local minibasin in the frontal part of the prism, which hosts 500 m of (syn-tectonic) evaporites; elsewhere the Messinian Salinity Crisis is figured as an erosional surface (Fig.37).

Below the Messinian erosional surface, it is challenging to interpret due to the intense deformation of the area. Some dipping reflectors could be picked but they are not continuous and well resolved by seismic. Several fold structures are highlighted in Figure 37. The link between folds and seafloor offset can help identify the ensuing faults (Fig.37b).

There are also some aligned deep reflections. These signals are tilted to the north, have a high amplitude and a low frequency, and appear to flatten towards the north. In addition, reflectors with similar seismic facies are visible at the base of the wedge in the central part of Figure 37b and also beneath the Cyprus Trench in Figure 36. Should they be associated with the subduction boundary or with the underthrusting of the African plate? In the following chapter, these issues will be addressed in light of the other models and data types available.

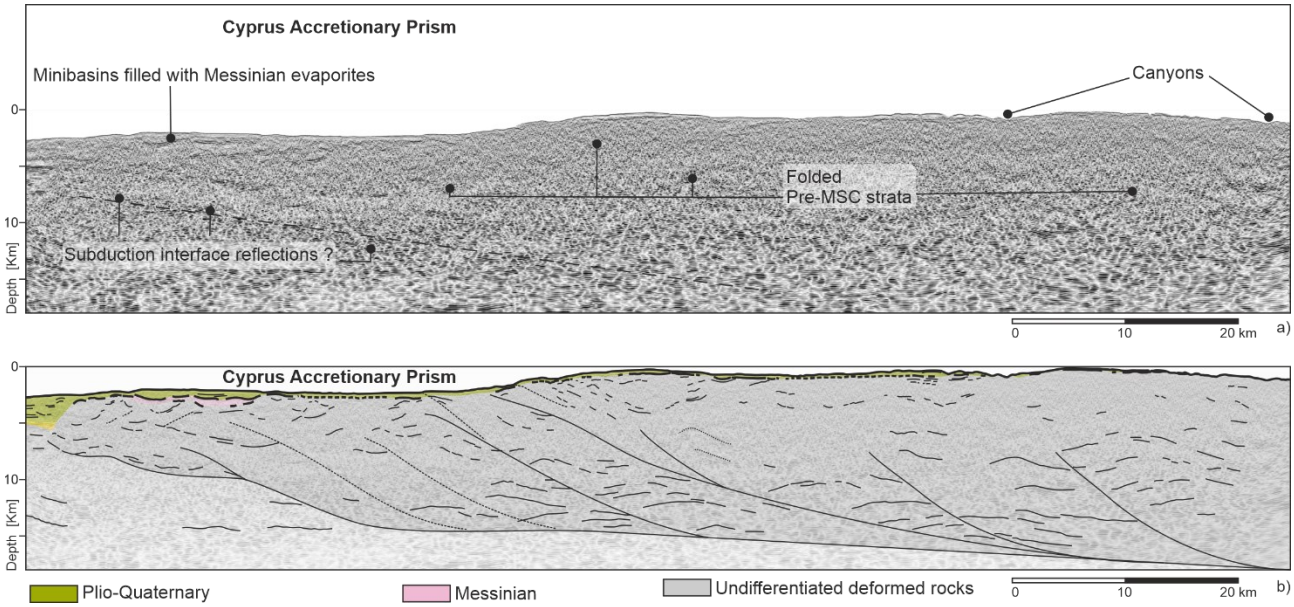

Figure 37: Zoom of the Strakhov-8 depth-migrated seismic section in the Cyprus Accretionary Prism. a) Part of the seismic section without interpretation, highlighting the folded reflections in the wedge, the canyon incisions to the north, and the possible reflections associated with the subduction interface. b) Same part of the seismic section of a) with the superimposed seismic packages, the inferred faults, and subduction interface and line drawing. Notice the folded reflections at the base of the wedge; these reflectors have high amplitude and low frequencies. This set of reflectors is important and discussed later during the geological model building paragraph as they can be associated with crustal accretion, reflecting from the underthrusting African crust.

4.2.3 - Eastern Transect (MS56)

Figure 38 shows the MS56 time-migrated seismic section with vertical exaggeration x6 and the position of the details discussed in this paragraph. The MS56 is composed of two seismic lines, the southern MS56A and the northern MS56B. These two profiles have 8 km of overlap in the Cyprus Basin.

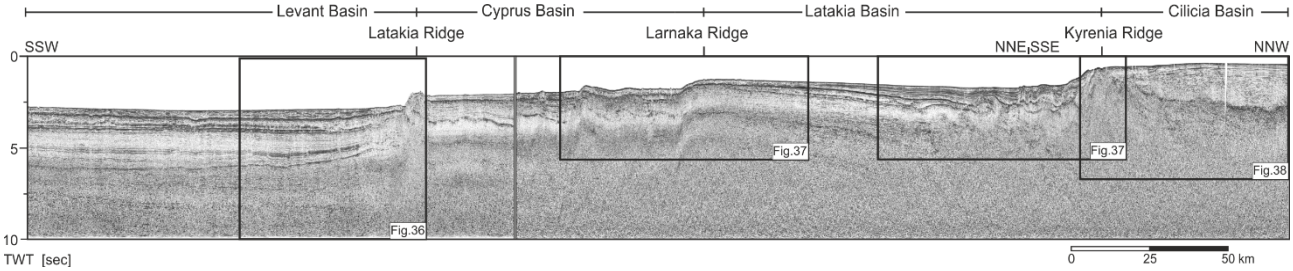

Figure 38: MS56 time-migrated seismic section with vertical exaggeration x6. The rectangles represent the detailed zooms discussed in the following paragraphs.

4.2.3.1 – Levant Basin

In the Levant Basin, the Plio-Quaternary deposits have a slightly constant thickness in the southern zone and become thinner near the Latakia Ridge. The seismic facies changes from the south-central sector to the northern one. This seismic package can be interpreted as hemipelagic and pelagic deposits in the south-central sector. In the northern sector, near the Latakia Ridge, the chaotic seismic facies indicates erosion and re-deposition of the deposits from the ridge. Although the resolution of the seismic data in the Latakia Ridge is low, the partial erosion of its Plio-Quaternary deposits is confirmed by their reduced thickness in the southern part of the section and testifies to the recent activity of the structure (Fig.39). This tectonic activity is led by the two high-angle faults that border the ridge both to the north and to the south.

A thick sequence of Messinian evaporites is visible beneath the Plio-Quaternary deposits. In the Levant Basin, the evaporites show internal reflections due to the intercalation of some shaly layers, resulting in an alternation between salt (transparent facies) and salt mixed with clastic deposits (reflective layers; Fig.39a). This alternation influences the rheological behaviour and leads to several internal detachment levels, as afore described for the Antalya Basin. In the southern sector of the Levant Basin, the Messinian deposits form smooth diapirs. In the central sector, a gravity wedge can be seen in Figure 39a, with detachment at the base of the evaporites of the Messinian deposits. A thrust system at its southern end and extensional faults at its northern margin (Fig.39b). These intra-

evaporites deformations related to the tilting of the Messinian base induced by the action of reverse faults associated with the uplift of the Latakia Ridge (Fig.39). The Messinian deposits are not visible on the Latakia Ridge because this area already was a structural high at that time.

Moving to the Miocene deposits, they appear as parallel and continuous reflectors in the seismic section, which we have interpreted as hemipelagic deposits. In the middle of this package, a high amplitude triplet is visible, associated with turbidite deposits. This easily recognizable triplet, together with the high impedance Miocene base, allows the interpretation of various high-angle extensional faults. As with the Plio-Quaternary and Messinian deposits, the Miocene sequence also becomes thinner near the Latakia Ridge. This variation in thickness, visible south of the Latakia Ridge, is controlled by reverse faulting.

The seismic signals of the Paleogene package are compromised due to their depth and are sometimes distorted by multiple reflections. However, some reflections can be representative of their structures. The change in thickness of the Paleogene deposits testifies to the activity of these overthrusts at this time. In particular, we recognize two unconformities (Fig.39a): the shallower one as the Eocene unconformity and the deeper unconformity as the Senonian unconformity. A deeper reflector was interpreted as Upper Jurassic. These two unconformities are intersected by thrust faults near the Latakia Ridge. Note that we identified the Upper Cretaceous (or Senionian unconformity) reflector in the core of the Latakia Ridge 2-3 seconds (TWT) higher. This means that the Latakia Ridge has been a structural high since, at least, the Paleogene. Therefore, the greater thickness of the Paleogene package in front of the Latakia Ridge could represent the paleotrench, developed before the inception of the strike-slip phase.

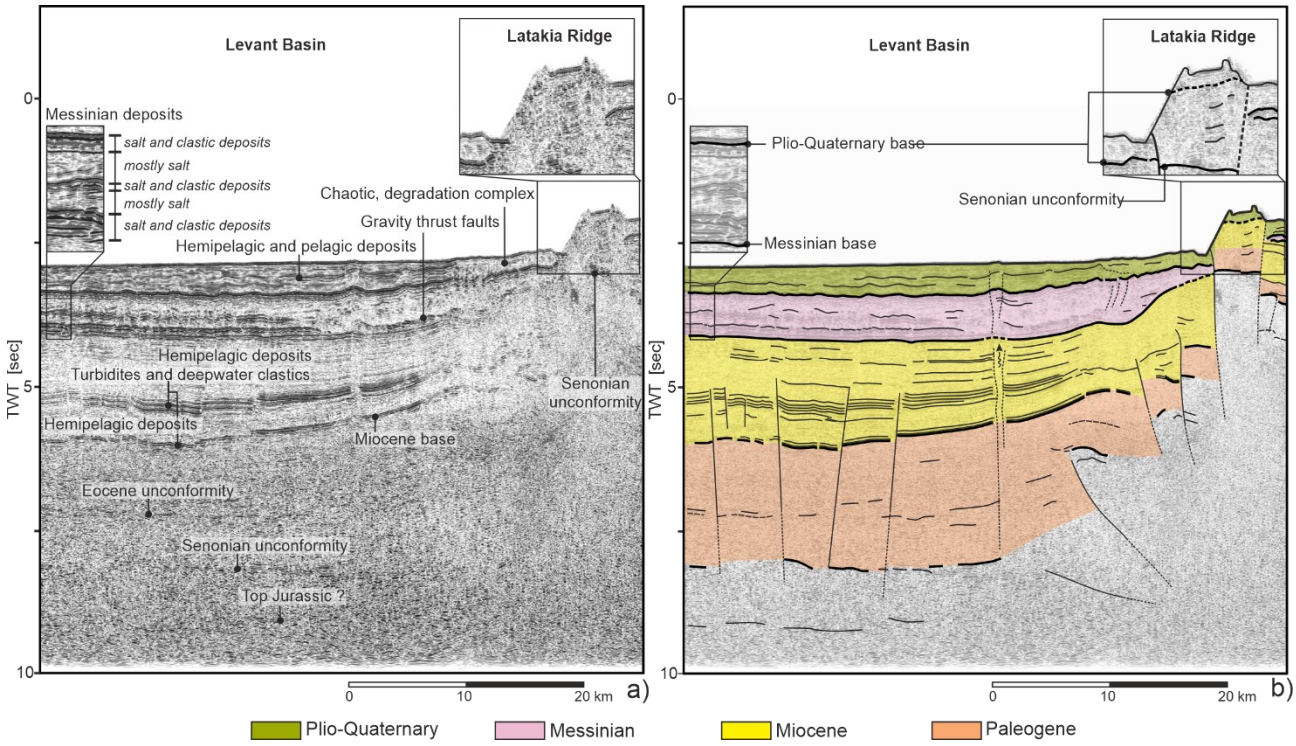

Figure 39: Zoom of the MS56 time-migrated seismic section in front of the Latakia Ridge. a) Part of the seismic section without interpretation highlighting the main horizons. The left inset shows the Messinian package's internal stratification in the Levant Basin. The right inset shows a detail of the Latakia Ridge. b) Same part of the seismic section of a) with the superimposed seismic packages, faults, and line drawing.

4.2.3.2 – Cyprus and Latakia Basins

In the central sector of the seismic section, i.e., in the Cyprus and Latakia basins, the Plio-Quaternary deposits thicken towards the north, especially in front of the Kyrenia Ridge. In the Cyprus Basin, it has a relatively constant thickness; in the Latakia Basin, instead, it is wedge-shaped and thins towards the south, reaching a minimum value on the Larnaka Ridge (Fig.40a and Fig.40b). At the top of the Larnaka Ridge, the Plio-Quaternary deposits appear to be thinner due to the extension caused by the gliding of the Messinian evaporites (Fig.40a and Fig.40b). South of the Kyrenia Ridge, the Plio-Quaternary deposits show growth strata and crestal extensional faults coincident with prominent contractional folds (Figs.40c and Fig.40d). At the top of the ridge, the thickness of the Plio-Quaternary deposits is less, indicating recent tectonic uplift.

Below the Plio-Quaternary package, the Messinian deposits are discontinuous: evaporite precipitation took place in the local minibasins and erosion affected the structural highs. In the center of the two depressions, its transparent seismic facies suggests halite precipitation while the

chaotic facies at their margins are associated with redeposited sediments resulting from the erosion of the Messinian structural highs (Fig.40a). On the top of the Larnaka Ridge, the Messinian package appears to have been thinned by salt gliding to the south, where an isolated Messinian basin has internal contractional systems due to the gilded materials coming from the north (Figs.40a and Fig.40b). South of the Kyrenia Ridge, in the most prominent contractional fold, Messinian deposits are absent due to uplift of this structure at this time.

The thickness of the Messinian deposits decreases at the top of the fold south of the previous structure, indicating their Messinian activity (Figs.40c and Fig.40d).

The Miocene deposits are thinner in the Cyprus Basin than in the Latakia Basin, with an abrupt change across the Larnaka Ridge (Fig.40a and Fig.40b); therefore, the Miocene deposits on this ridge have an inverse thickness relationship with respect to the Messinian and the Plio-Quaternary ones. This can be related to the shift in the kinematics of the Larnaka Ridge over time. During the Miocene, this ridge coincided with an extensional fault system that created a larger accommodation space in the northern sector. The thinning of the Plio-Quaternary deposits and the gliding of the Messinian evaporites mark an inversion of a Miocene basin during the Messinian and the Plio-Quaternary tectonic phases (Fig.40). In the Latakia Basin, the Miocene thickness does not show abrupt changes and the reflectors are quite parallel and continuous.

The Paleogene sedimentary wedge thickens from south to north and onlaps the Senonian unconformity. In the Cyprus and Latakia basins, the top of the acoustic basement is shallower than in the other basins so some reflectors can be interpreted also below it. For example, some isolated carbonate build-ups and aggradations were interpreted in the Larnaka Ridge area (Fig.40a and Fig.40b). The interpretation of the top of the acoustic basement reflector also allows us to identify the deeper roots of the faults and, together with the observations in the shallower packages, can provide insights into the kinematic history of the main tectonic structures. In the Latakia Basin, the top of the acoustic basement reflector indicates extensional faults that were active during the deposition of the Paleogene package. These extensional faults were reactivated during the recent tectonic phase as transpressive structures in the Larnaka Ridge sector. Transpressive kinematics is appropriate to interpret the structures visible on the Kyrenia Ridge too. The transpressive activity of the Kyrenia Ridge has triggered the development of the contractional structures detected south of it, representing an extensive positive flower structure active since the Messinian.

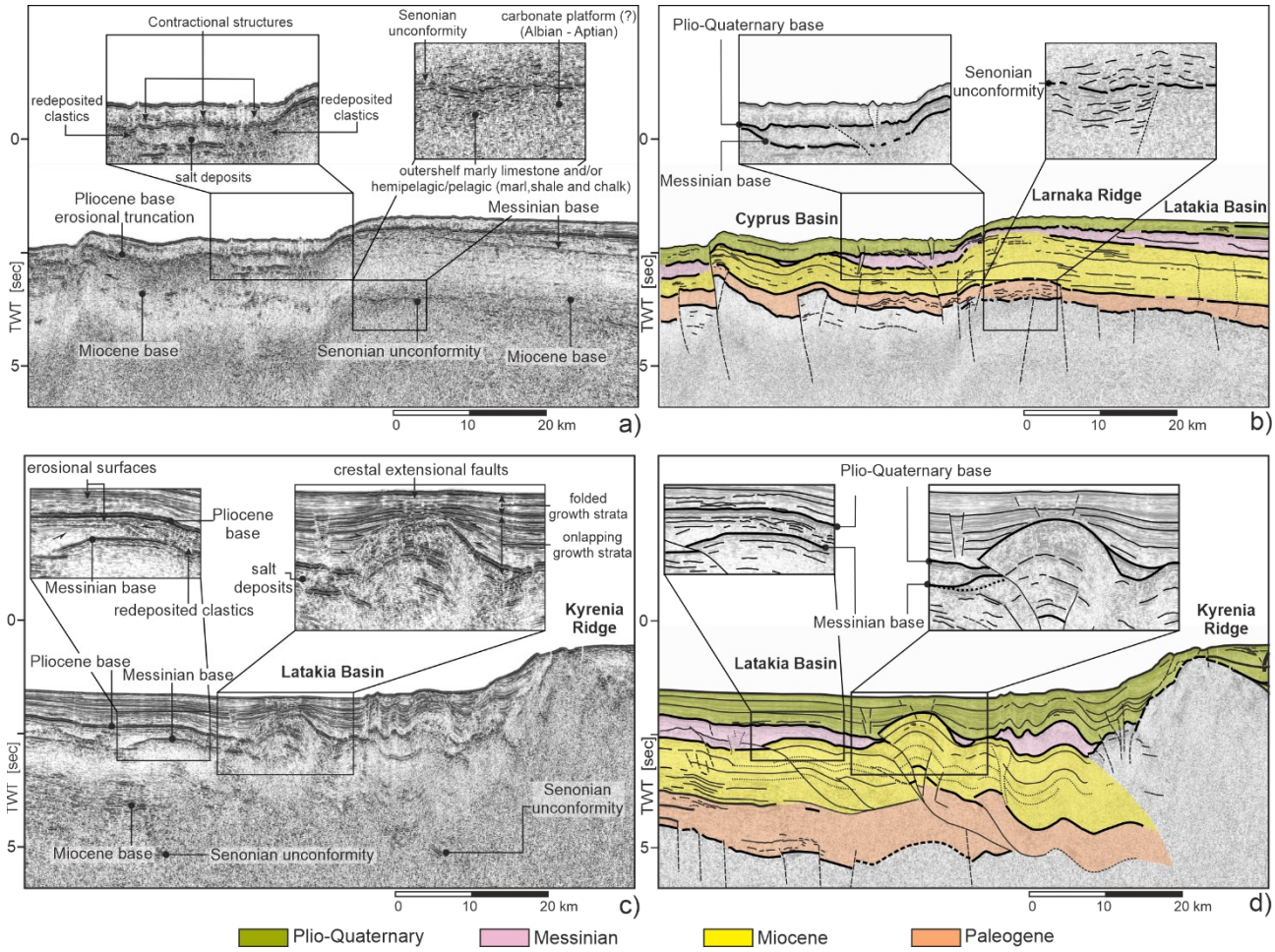

Figure 40: Zoom of the MS56 time-migrated seismic section. a) Part of the seismic section in the Cyprus Basin across the Larnaka Ridge without interpretation highlighting the main horizons. The left inset shows the Messinian minibasin with contractional structures due to salt gliding from the Larnaka Ridge. The facies change in this minibasin, composed of redeposited clastics at the margins and salt in the centre. b) Same part of the seismic section of a) with the superimposed seismic packages, faults, and line drawing. c) Part of the seismic section in the Latakia Basin in front of the Kyrenia Ridge without interpretation highlighting the main horizons and structures. The left inset shows syntectonic evaporite precipitation, testified by the intra-Messinian onlap on the fold and by the redeposited clastics in its northern part, coming from the other fold structure to the north. The right inset shows the main fold of this thrust system in front of the Kyrenia Ridge. It began its activity before the inception of the Messinian Salinity Crisis, and it is still active since the seafloor is deformed and the crest of the anticline is affected by extensional faulting. d) Same part of the seismic section of c) with the superimposed seismic packages, faults, and line drawing.

4.2.3.3 – Cilicia Basin

In the Cilicia Basin, the Plio-Quaternary deposits reach their maximum thickness in the study area. The Plio-Quaternary and Messinian bases are the only identifiable key reflectors in this area. Below the Messinian seismic package, the signal deteriorates due to multiple reflections, which are numerous because of the shallow water depth. For this reason, the location of the other two key reflectors can only be inferred (Fig.41a). The arrangement of the Plio-Quaternary horizons and the displacement of the Plio-Quaternary and Messinian bases and seafloor suggest a still active extensional phase. The geometry of the Plio-Quaternary sediments shows two roll-over anticlines with their main antithetic faults rooted beneath the Messinian base and separated by a halokinetic structure of Messinian evaporites due to the accumulation of salt glided from the margins of the basin (Fig.41). The Plio-Quaternary overburden, more deformed in its lower and middle parts, is almost undeformed in its upper part, indicating minor halokinesis during the Late Quaternary.

Mapping the internal structure of the Kyrenia Ridge is difficult due to the resolution of the data. On the laterally buried side of this ridge, the Miocene deposits are onlapping, tilted and partially eroded, testifying to a relative uplift before the Messinian.

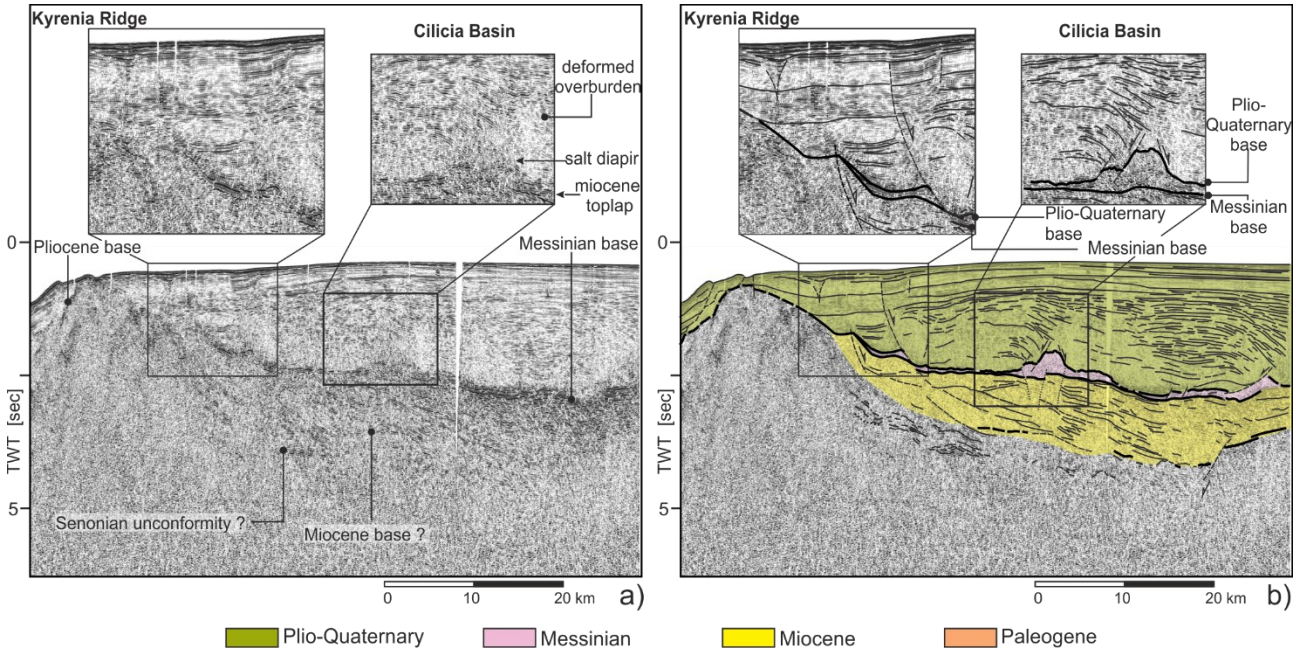

Figure 41: Zoom of the MS56 time-migrated seismic section in the Cilicia Basin. a) Part of the seismic section without interpretation highlighting the main horizons. The left inset shows an extensional fault that facilitates salt movements toward the basin centre. The right inset shows a turtle-back structure due to the halokinesis of the underlying evaporites, which create accommodation space

for the Plio-Quaternary to be deformed. b) Same part of the seismic section of a) with the superimposed seismic packages and line drawing.

4.3 - Depth Conversion

Seismic depth conversion is the process of converting the depth, expressed in two-way-travel time, of subsurface geological features as shown on a seismic survey to their actual depth below the earth's surface. It is important to note that seismic depth conversion is not an exact reconstruction of the actual depth features, as the resulting depth estimates are often subject to some uncertainty due to the assumed velocities. Factors such as variations in subsurface velocity and the complexity of the subsurface structure can introduce errors into the depth conversion process. For this purpose, we use the velocity analysis of the MS and Strakhov datasets and the published velocity models of the area (Tab.2). We performed the depth conversion using the software MOVE, which can be used to create polygons with a characteristic velocity and gradient. To obtain the interval velocities, we use the velocity analysis performed with the dataset from MS and Strakhov. We then calculated the mean and the variation with depth (gradient) for each interpreted seismic package to obtain the values for each MOVE polygon. Therefore, for each seismic package, we created a polygon with its velocity and gradient values and then applied them to SEG -Y and to the line drawings in TWT to obtain the seismic depth section and horizons.

4.3.1 - Western Transect (MS53)

To convert the MS53 seismic section to depth (Fig.42), we divided the different deposits into five packages: the Plio-Quaternary, the Messinian, the Pre-Messinian Deformed, the Pre-Messinian in the basins and the acoustic basement. The water column was added to these five packages.

Different approaches were used to determine the velocity values for the seismic packages. For the water, we chose an average value of 1520 m/s. For the Plio-Quaternary sediments, an average value of 2000 m/s was assumed. For the Messinian evaporite sequence, a velocity of 4100 m/s was given, considering an average of the values proposed by Feng and Reshef (2016) and the values of the velocity analysis from the Strakhov seismic lines (Klaeschen et al., 2005). The pre-Messinian sequence was divided into two seismic packages: the pre-Messinian in the basins and the deformed pre-Messinian in the Inner Deformation Zone, representing the deformed northern part of the Antalya Basin. For the first, an average value (equal to 3150 m/s) was taken from the velocity analysis of the Strakhov-8 and Strakhov-9 seismic lines. For the second, the borehole compensated

sonic log data from the Manavgat-2 well was used (Fig.22) and a value of 3500 m/s was set. The last value considered was the acoustic basement one, which was set at 5000 m/s according to the sonic log from the Manavgat-2 well (Fig.22). Knowing the lithology of each seismic package also allows the determination of the gradient (k), expressed in Hz (s^{-1}). The gradient is the rate of change of velocity with depth. For evaporites and water, a value of k equal to 0 Hz was assumed because they are incompressible. A k value of 0.1 Hz was chosen for the pre-Messinian unit and 0.2 Hz for the Plio-Quaternary and acoustic basement (Fig.42a).

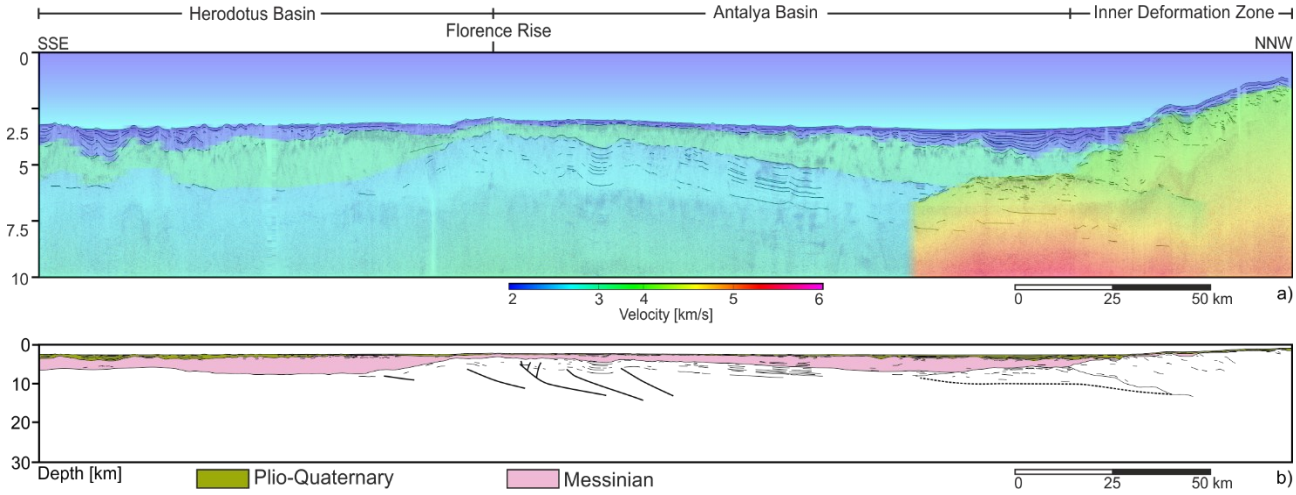

Figure 42: a) MS53 TWT seismic section with line-drawing of the main reflectors and velocity field used for depth conversion (vertical exaggeration x6). b) Interpreted depth section. Note that a velocity gradient is applied from approximately 6 sec to the bottom, but multiple reflections corrupt the deeper part. Therefore, deeper sectors are reconstructed in the following paragraphs.

The depth-converted MS53 seismic section could only be interpreted for the first 9-10 km depth. Multiple signals obscure the actual signals in deeper areas, except for some acoustically strong reflectors.

4.3.2 - Eastern Transect (MS56)

To convert the MS56 seismic section to depth (Fig.43), we divided the different deposits into four packages: the Plio-Quaternary, the Messinian, the Miocene and the Paleogene packages were considered as a single package and the acoustic basement. The water column was added to these four packages. Therefore, an interval velocity was assigned to each interpreted seismic package. We used the interval velocities derived from the root-mean-square velocities obtained from the velocity analysis of seismic profile MS56 and previous works (Calon et al., 2005; Klaeschen et al., 2005).

Knowledge of the lithology of the individual seismic packages also allows speculation on the velocity gradient (k), expressed in Hz (s^{-1}), associated with the compaction of the rock at depth. 0 Hz thus represents a constant velocity value that does not increase with depth due to the incompressibility of the considered medium.

For the water column, we chose an average value of 1520 m/s and 0 Hz, 2000 m/s and 0.10 Hz for the Plio-Quaternary package, 4100 m/s and 0 Hz for the Messinian package, 3150 m/s and 0.10 Hz for the Miocene/Paleogene package and 3500 m/s and 0.2 Hz for the acoustic basement (Fig.43a).

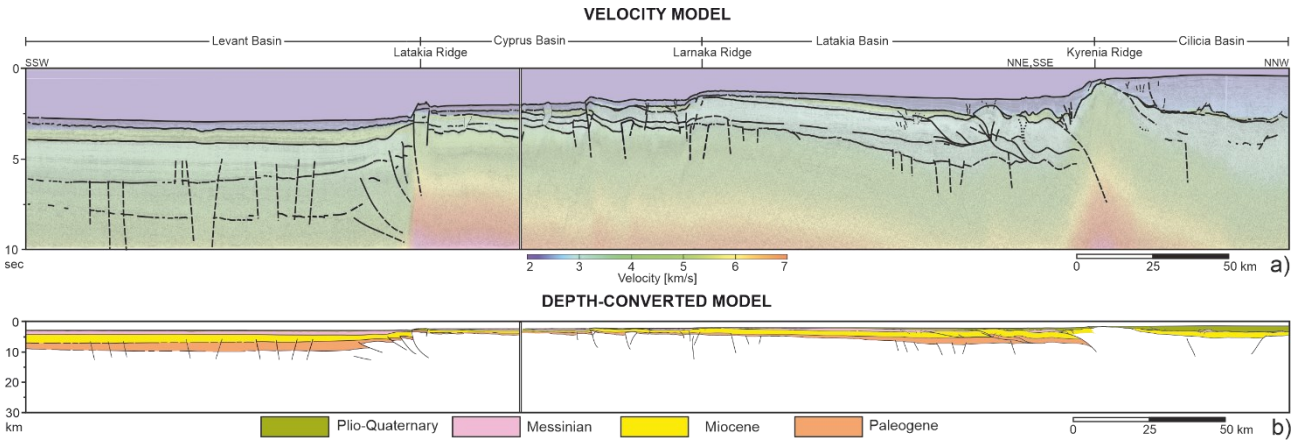

Figure 43: a) MS56 TWT seismic section with line-drawing of the main reflectors and velocity field used for depth conversion (vertical exaggeration x6). b) Interpreted depth section. Note that a velocity gradient is applied from approximately 7.5 sec to the bottom of the Levant Basin and from 5 sec to the base for the deformed northern basins. Still, multiple reflections corrupt the deeper part. Therefore, deeper sectors will be reconstructed in the following paragraphs.

The depth-converted MS56 seismic section could only be interpreted for the first 10 km in the Levant Basin and about 7 km in the deformed northern basins. Multiple signals obscure the actual signals in deeper areas, except for some acoustically strong reflectors.

CHAPTER 5: DISCUSSION

5.1 - Geological models building

The interpretation of the time-migrated sections allowed us to identify the main tectonostratigraphic features of the study area. In addition, several key sectors provided insights into the kinematic evolution of the main structures. As a first step towards creating a viable geological model, we converted our interpretations of the time-migrated version to depth in meters. The in-depth outcomes are now ready to be the basis for structural modelling and discussions.

5.1.1 Western Transect geological model

To reconstruct the deeper part of the Western Transect (Fig.44), the first constraint comes from a study of gravity anomalies along the Cyprus Arc system (Ergün et al., 2005). This gravimetric model predicts the presence of oceanic lithosphere beneath the Herodotus Basin at a depth of about 10-12 km, deepening to about 15 km beneath the Florence Rise and then dipping northwards to reach a depth of 40 km in the northern Antalya Basin. The boundary between the crust and the mantle is placed at a depth of about 20 km beneath the Inner Deformation Zone. The gravity anomaly data show that the continental crust is thinned in the area of the Turkish slope. The projection of the modelled geometries by Ergün et al. (2005) on MS53 allows the subducting oceanic crust to be delineated along the profile (Fig.44a).

Further input to determine the subducting plate's location is taken from the distribution of seismicity in the area. From the ISC Bulletin catalogue (2000-2020), Güvercin et al. (2021) extracted the focal mechanism of the main seismic events and precisely located their hypocentral depths, visualizing a north-dipping slab. Based on these data, subduction is still active. Therefore, the Florence Rise represents the accretionary prism of an active subduction system (Güvercin et al., 2021). The slab is oriented to the north-northeast, so it is not parallel to seismic section MS53. The reconstructed subducting plane have been projected on the Western Transect to display what the subduction interface looks like along our section (Fig.44a). In the European Database of Seismogenic Faults (EDSF – Basili et al., 2013) 3D grid of the subduction interface geometry can be downloaded and also the Slab2 model proposed by Hayes et al. (2018) can be download in 3D grid too. Hence, we also plotted this 3D models on our section. These four projections provide information on the position and dip of the oceanic crust and the general trend of the slab. The projection of the modelled sub-surface geometries based on gravity anomalies (Ergün et al., 2005) and the projection of the model of subduction interface based on earthquake locations (Güvercin et al., 2020) fits well

with the interpretation of the shallower part made on the seismic section (Fig.44a). Once the entire section was delineated using the seismic interpretation for the shallow part (about 10 km depth) and the data from other studies for the deepest part, a complete tectonic model of the area could be created (Fig.44b). Note that the location of the subduction inferred from both the seismicity and gravity data is consistent with the basin architecture and tectonic structures we interpreted in the seismic section. Therefore, we can suggest that the Florence Rise is the accretionary wedge of an active subduction system, the Antalya Basin is the corresponding forearc basin, and the Herodotus Basin is the foreland basin above a subducting plate, as suggested by other authors (e.g., Hall et al., 2014). The stress is partitioned between the Inner Deformation Zone and the Florence Rise as both structures are still active in fact, the European Database of Seismogenic Faults proposed 7.5 as expected maximum magnitude.

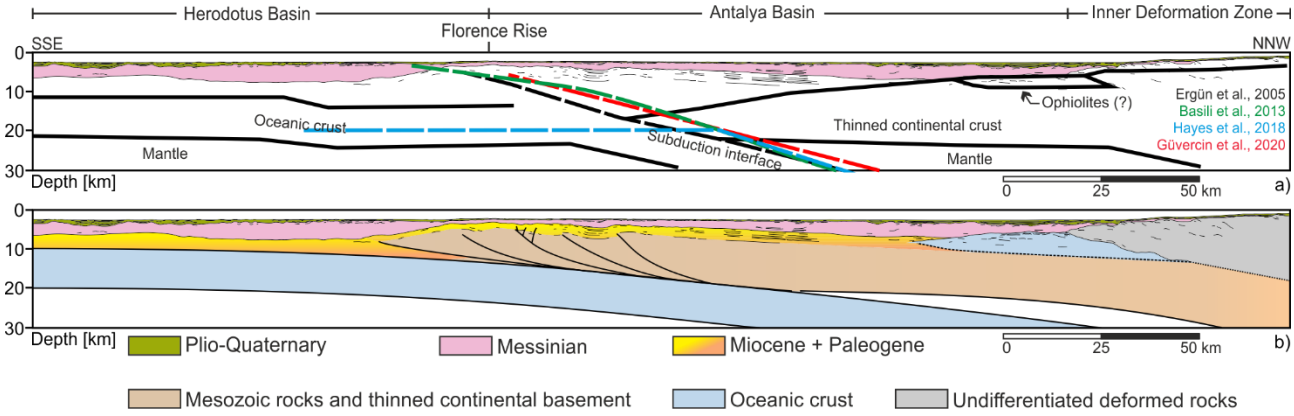

Figure 44: a) Depth converted MS53 seismic section with overlain the projected models: black lines from Ergün et al. (2005) represent the top and base of the oceanic crust, the subduction interface and the obducted ophiolites in the northern part, coincident with the "buried block anomaly" obtained by gravimetric modeling. The red line from Güvercin et al. (2020) represents the subduction interface obtained by the relocation of earthquake events in depth. The green line from Basili et al. (2013) represents the subduction interface proposed by the European Database of Seismogenic Faults (EDSF) / Project SHARE. The light blue line represents the subduction interface modeled by Hayes et al. (2018) for their Slab2 model. b) Western Transect geological section compiled after the projection of the models above.

5.1.2 - Central Transect geological model

The reconstruction of the deeper part of the Central Transect was facilitated by the fact that it was already depth migrated and by the high depth of investigation, which made it possible to visualize

some deep reflections that can be associated with the subduction boundary (Fig.34). As a step forward to better constrain our geological model, we used the available literature and other data in the area (Fig.45a).

The first step is the comparison with previously published geological depth sections by Fernández-Blanco et al. (2021) and McPhee et al. (2022) (Fig.45a). The depth and dip of the subduction interface is in good agreement with our interpretation. We also used a model based on the seismic refraction method (Feld et al., 2017), which also fits well with our results, of both the trench and subduction boundary geometries. In addition, the model proposed by Feld et al. (2017) also showed the base of the lower plate, which is consistent with the deepest set of reflectors seen on the seismic section (i.e., the reflections of the crystalline basement top – Fig.45a). Finally, we have also projected the Merry et al. (2022) relocation of the earthquake events. Again, the subduction interface is similar to that interpreted in the seismic profile (Fig.45a).

Moreover, some qualitative considerations can be made about the shape of the accretionary prism as the Coulomb critical wedge theory predicts the stability of an accretionary prism (Davis et al., 1983; Dahlen et al., 1984; Noda, 2016). It is based on the principle that the stability of a wedge depends on the balance between the forces that hold it in place and the forces that destabilize it. This theory predicts that the sum of the topographic angle (α) and the basal detachment dip (β) should be kept constant, among other parameters such as internal friction, basal friction, and pore fluid pressure. When something destabilizes the wedge, it reacts to adjust this balance. Based on this concept, the topographic angle of the Cyprus accretionary prism can be divided into different values. The frontal part has a lower α-value than the inner sector. Therefore, β must be lowered at the transition from the frontal to the inner part of the prism in order to keep their sum constant. For this reason, we have interpreted the subduction interface in the inner part as flattened compared to the frontal zone.

Therefore, the base of the Cyprus accretionary prism has been delineated as well as the thickness of the subducting plate (Fig.45b). Our interpretation is viable as it is consistent with models obtained from different types of data.

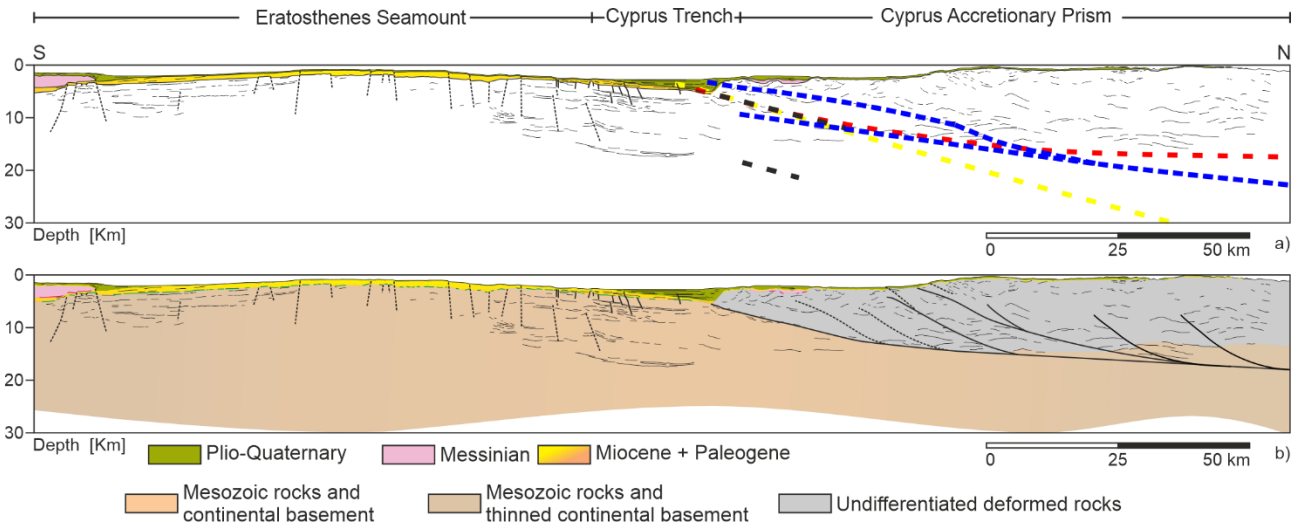

Figure 45: a) Strakhov-8 with overlain the projected models: blue lines from Fernández -Blanco et al. (2019), the yellow line from Merry et al. (2022), black lines from Feld et al. (2017), the red line from McPhee et al. (2022), the crust-mantle boundary from Smaily (2017). b) Central Transect geological section compiled after the projection of the models above.

5.1.3 - Eastern Transect geological model

The MS56 seismic profile is divided into two lines overlapping 8 km. We first joined the two segments into one continuous seismic section to create a geological section by removing the overlapping sectors. In addition, since we aim to describe the deformation front, we do not consider part of the central undeformed Levant Basin but only its northern part near the Latakia Ridge (Fig.46a).

Then, to build a viable structural model, we must first interpret the regional detachment. We could not visualize the regional detachment, or a preserved fold and-thrust system originating from the Cretaceous compressional phase with our seismic data. However, we can use indirect observations. The first observation is the considerable thickness of the Paleogene deposits in the Levant Basin and their thinning near the Latakia Ridge. These data suggest that this area was the foreland basin of an accretionary system that was active until the Paleogene time. Within this framework, the blind reverse faults south of the Latakia Ridge represent the outer thrusts of an accretionary prism associated with a deeper detachment. We located the regional detachment in the Triassic evaporites calibrated in the northern Levant Basin (Ghalayini et al., 2018). We also considered previously published crustal models based on gravity modelling (Ergün et al., 2005), seismic refraction data (Feld et al., 2017) and a crustal geological section (Fernández-Blanco et al., 2019).

Another feasible assumption helpful in reconstructing the subduction interface in the innermost sector is the increase of the basal dip moving toward the hinterland suggested by Noda (2016) and Fuller et al. (2006). As afore mentioned, the Coulomb critical taper theory states that topographic and basal detachment angles are interdependent, i.e., their sum should be kept constant. Therefore, a negative topographic angle (i.e., a landward dipping forearc basin) is associated with an increasing dip of the basal detachment (Fuller et al., 2006), so a change in its dip was assumed in the transition zone between the outer and inner wedge (Fig.46).

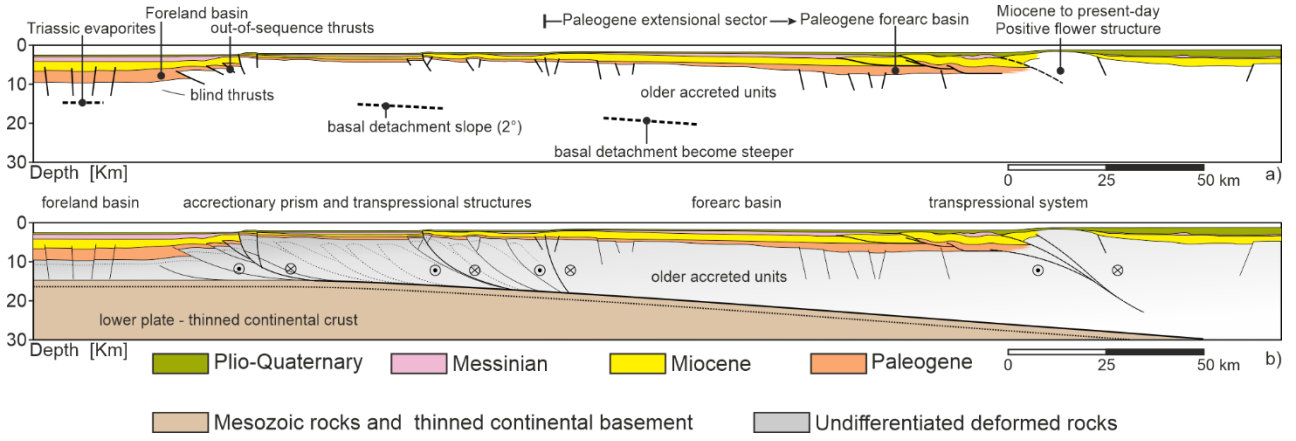

Figure 46: a) Shallow structural model and corresponding detachment slope. b) Eastern Transect geological section with deeper parts compiled using structural model and information from Ergün et al. (2005); Feld et al. (2017); Fernández-Blanco et al. (2019). See also Figure Supplementary Material 3 for bigger image.

5.2 – Geological models discussion

5.2.1 - Western Transect

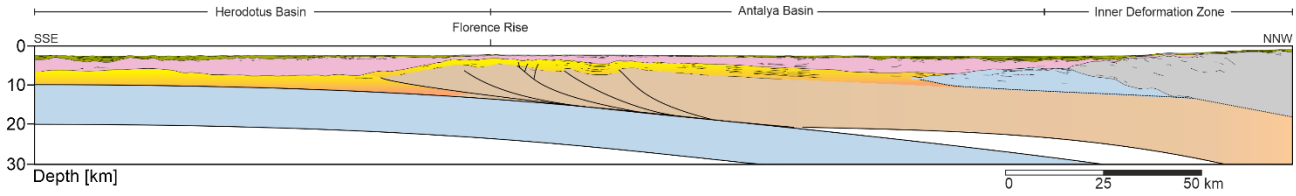

Figure 47: Geological model of the Western Transect created after interpreting the time-migrated seismic section, its depth conversion, and then projecting the gravity model from Ergün et al. (2005) and the seismological model from Güvercin et al. (2021). See also Figure Supplementary Material 1 for bigger image.

From the previous paragraphs, a detailed description of the Western Transect has been produced by comparing our model with those proposed by other authors (Fig.47). The northern part of the

section, after adding the deepest part according to the models proposed by Ergün et al. (2005) and Güvercin et al. (2021), does not change what has already been said about this area. A comparison with the models of Hall et al. (2014) and Güneş et al. (2018), confirms that several thrusts indicate a compressional style of deformation. For this reason, the inner sector can be considered a contractional wedge (Inner Deformation Zone) due to its characteristic shape and reverse faults. At the same time, the Florence Rise is the accretionary outer-wedge of the subduction system (Fig.47). The base of the Inner Deformation Zone reaches a depth of about 15-18 km at its thickest sector. Its southern part acts as a rigid buttress for the Messinian succession of the Antalya Basin, which is gliding northward. The thrusts mentioned above produce fold structures which isolated Messinian mini-basins on the Inner Deformation Zone. These mini-basins are probably filled with Messinian gypsum, the first lithology deposited in an evaporitic succession (Nichols, 2009). The model proposed by Ergün et al. (2005) has made it possible to define the boundary between the continental crust and the lithospheric mantle (northern part of the section – Fig.47), giving a complete picture of the northern part of the Antalya Basin. The thickness of the continental crust in this area is about 20 km and represents thinned crust. The gravity model is also consistent with the seismic interpretation of the acoustic basement we made in the northern part of the Antalya Basin. It consists of different regional lithostratigraphic units, probably ranging from Mesozoic to Paleogene, although no calibration is available (Aksu et al., 2018). A study based on the gravity anomalies of the Cyprus Arc (Ergün et al., 2005) analyzed the correspondence of the buried block in the northern Antalya Basin with a high value of the Bouguer gravity anomaly. The authors modelled its density (3.0 mg/m^3) and proposed an ophiolitic composition, hence they proposed a supra-subduction ophiolite obducted during the Upper Cretaceous as in Cyprus, Syria, Turkey and the peri-Arabic ophiolitic belt.

The association of the Antalya Basin with the forearc basin of the system suggests that the pre-Messinian sediments in the centre of the Antalya Basin are probably marly turbidites with turbiditic distal facies. The depocenter of the forearc (i.e., Antalya Basin) has migrated during its evolution: during the Miocene (Fig.47a), the depocenter was probably located where the pre-Messinian deposits are thicker, in front of the “buried block”. The depocenter migrated successively northwards and was located where the Messinian sequence is thicker, on top of the toe of the “buried block”. It, again, migrated northwards and now it is located in the thicker part of the Plio-Quaternary sequence, above the “buried block” (Fig.47). The landward migration of the depocenter of the forearc basin indicates that the accretionary prism has evolved from the pre-Messinian to

Plio-Quaternary. A complete overview of the system also allows the landward tilting of the forearc basin to be justified but, it is necessary to focus on the area around the Florence Rise to better explain it.

The Florence Rise is considered an accretionary prism in our interpretive model. The movement of the African Plate's oceanic crust under the Eurasian Plate's continental crust created the accretionary prism formed by the accretion of sediments scraped from the subducting plate. The development of an accretionary prism can be complex: its shape results from a balance between contractional stresses, the rheology of the rocks involved, and the mechanical property of the main detachment levels and several other factors. As a wedge is the typical shape of contractional systems, any factors that change this shape force the system to re-equilibrate the wedge (Davis et al., 1983; Dahlen et al., 1984; Noda, 2016). The main factor that can change its shape can be erosional phases or the change in rheology during the involvement of new rocks in the deformation zone. The ways in which a wedge can regain its original shape are thrusting and folding. In the case of convergence between plates, this equilibrium is broken by the strength of push and compressive resistance. Two angles usually describe the wedge shape: β is the inclination of the main basal detachment, and α is the topographic angle (Davis et al., 1983; Dahlen et al., 1984; Noda, 2016; Fuller et al., 2006).

In our case, the α-angle of the Florence Rise wedge was certainly subject to a change in its shape due to erosional processes, as interpreted on the seismic section. However, the most important factor that changed the shape of the accretionary wedge occurred during the deposition of the Messinian evaporitic succession in the Herodotus Basin. In a first phase, the wedge tried to propagate forward, producing minor external thrusting (Fig. 47). This means that the sedimentation rate at the beginning of Messinian was lower than the thickness which could force the system to change its internal kinematics. The increasing sedimentation rate during the Messinian Salinity Crisis forced the system to reshape the wedge quickly, resulting in internal out-of-sequence thrusting. The wedge's erosion and the rapid deposition of the kilometers-thick Messinian evaporites in a short timespan in the Herodotus Basin (about 640 kyr – Krijgsman et al., 1999) led to a significant reduction in the α-angle, so the system had to restore its equilibrium.

Since the pre-Messinian strata in the Antalya Basin are eroded on the apex of the anticlines, this deformation began before the inception of the Messinian Salinity Crisis.

The formation of the out-of-sequence (inner) thrusts contributed to the northward tilting of the pre-Messinian, Messinian, and Plio-Quaternary units. The seafloor is also gently folded by these two splay faults (Fig.31) confirming that they are still active structures.

The resulting landward tilt caused the northward gravity gliding of the Messinian evaporites and the consequent development of intra-evaporites N-verging reverse faults. In addition, the rigid backstop represented by the Inner Deformation Zone and the "buried block" also contributed to developing the north-verging reverse faults within the evaporites, acting as a rigid backstop.

Another important phase in the development of the Florence Rise is the formation of the backthrusts. These backthrusts deformed the Messinian sequence. When the Messinian and Plio-Quaternary sediments were deposited, the Florence Rise already was a structural high, resulting in the Messinian and Plio-Quaternary deposits being thinner compared to other areas crossed by the Western Transect. In fact, at the top of Florence Rise, the Plio-Quaternary and Messinian deposits reach a maximum of tens of meters.

5.2.2 – Central Transect

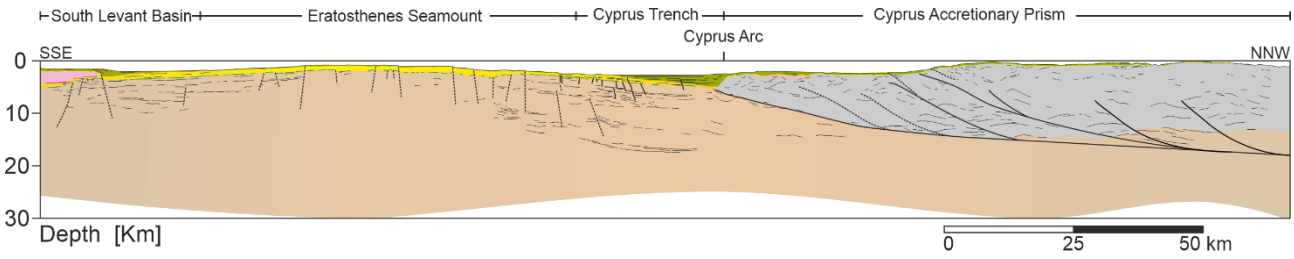

Figure 48: Geological model of the Western Transect created after interpreting the depth-migrated seismic section by projecting the geological sections from Fernández -Blanco et al. (2019) and McPhee et al. (2022), the seismological model from Merry et al. (2022), the seismic refraction data from Feld et al. (2017) and the lower crust-mantle discontinuity from Smaily (2017). See also Figure Supplementary Material 2 for bigger image.

From the previous paragraphs, a geological section through the Eratosthenes Seamount and the Cyprus deformation front has been obtained (i.e., the Central Transect – Fig.48). The Cyprus accretionary prism is still active as shown by the growth strata in its trench, the active extensional faults affecting the Eratosthenes Seamount and the seismicity in the area (Fig. seismicity). A new earthquake catalogue of the last 2 years of monitoring of the island of Cyprus (i.e., the TROODOS catalogue of Merry – 2022, Ph.D. thesis) has recently been published. It highlights a northward

dipping band of earthquakes beneath the island, ranging from about 20 to 70 km depth. The focal mechanisms of the earthquakes within the slab are all consistent with trench-parallel compression, clearly indicating the presence of the African slab subducting beneath Cyprus. Seismicity on the island during the TROODOS catalogue was dominated by earthquakes in an elongated zone south of the Troodos ophiolite at about 15-25 km depth, consistent with plate-interface deformation. These earthquakes decrease in depth in the center of the island, where uplift is greater. Suppose these earthquakes correspond to undulation in the plate interface. In that case, this suggests that the slab's topography correlates with the upper plate's uplift, which is consistent with arguments that the uplift on Cyprus is caused by underthrusting of the continental Eratosthenes Seamount. Thus, at the base of the accretionary prism, there is the underthrusting of the continental crust of Eratosthenes Seamount, indicating thick-skinned tectonics and incipient collision (Fig.48b). As the continental crust of the seamount is thicker than the surrounding thinned continental crust of the Levant Basin and more buoyant of the oceanic crust of the Herodotus Basin, it slows the southward propagation of the wedge and has triggered the uplift of the prism and the island itself. Therefore, the deeper reflectors beneath the Cyprus accretionary prism can be associated with the underthusting of the Eratosthenes continental crust, as testified by the model proposed by Merry (2022). While the deeper reflectors interpreted in the Cyprus trench can be associated with the subduction interface as evinced by the model proposed by Feld et al. (2017). The flattening of the upper Plio-Quaternary reflectors can be explained in this framework as a record of the recent uplift of Cyprus against its southward propagation.

5.2.3 – Eastern Transect

The Eastern Transect has the best seismic imaging among the analyzed seismic profiles. As mentioned before, we could distinguish the Miocene from the Paleogene seismic package in this section. Unfortunately, the MS56 is the best profile, but in an area where there is a need for more direct information and other models; the available bibliographic data are less than in the surrounding areas. Therefore, to better constrain our geological model and to check if the proposed geological section is viable and balanced, we reconstruct it in three-time steps, which are essential to understand the main tectonic phases that affected the area during the Cenozoic.

The main problem in reconstructing the Cenozoic evolution of the Eastern Transect arising from our 2D model because during the Cenozoic all the tectonic structures caused out-of-plane movements with respect to our section due to their transpressional-transtensional kinematics. Moreover, the

movements of the evaporites could also be out-of-plane. Therefore, the main assumption is that what exits the section should be equal to what enters it. Considering this constraint, the visualization of the main tectonic phase of the area can be helpful to subtract the shortening along the profile.

We propose three reconstructions (Fig.49). The first (Fig.49a) shows how the area looked at the end of the Paleogene when the main contractional phase ended. The second (Fig.49b) and the third (Fig.49c) reconstructions show the area during the transpression phase, before and after the Messinian Salinity Crisis.

To begin with the sketch of the Paleogene (Fig.49a), we observe a well-developed accretionary wedge in the southern sector, with normal faults cutting the Levant Basin, due to the flexure of the lower plate (Africa) under the weight of the upper plate (Eurasia - Anatolia microplate). The overriding plate shows an accretionary prism already formed. The Cyprus Basin was affected by compression and represents the outer wedge of this system, while extensional structures are visible in the Latakia Basin north of the Larnaka Ridge. The Latakia Basin, therefore, represents the forearc basin of this convergent system. We need more information about the Kyrenia Ridge to interpret it back to Paleogene time.

At the end of the Tortonian (Fig.49b), the Levant Basin remained undeformed, the Latakia Ridge was further compressed, and out-of-sequence reverse faulting took place. The latter could be explained by the great thickness of the sediments deposited in front of it, which prevented the expected forward propagation and favored the development of new structures inwards, such as back thrusts in the Cyprus Basin, while extension continued in the Latakia Basin.

At the end of the Messinian (Fig.49c), strike-slip kinematics set in, resulting in areas of transpression and transtension. Flexural normal faults were reactivated in the Levant Basin. From the Latakia Ridge to the Kyrenia Ridge, transpressional kinematics dominated in this area. The result was an uplift of the Latakia Ridge, a positive tectonic inversion of the Larnaka Ridge and the development of a thrust system in front of the Kyrenia Ridge. Meanwhile, the Cilicia Basin continued to be dominated by extension. Messinian evaporites were deposited in local basins separated by structural highs and eroded during the rapid sea-level drop of the Messinian Salinity Crisis. This is a critical time lag because present-day tectonic activity began during this phase.

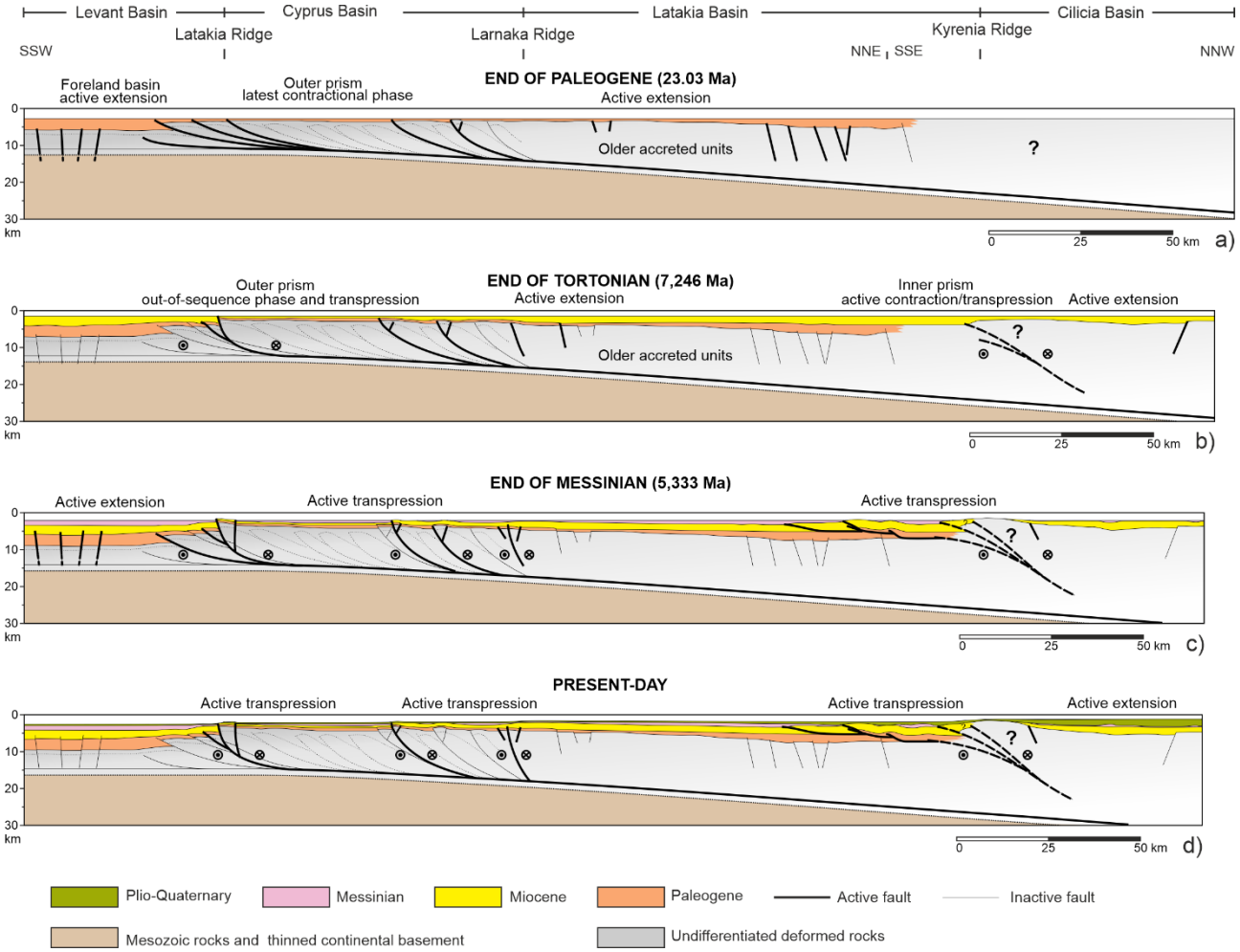

Figure 49: a) Restored section at the end of the Paleogene (~23.03 Ma). b) Restored section at the end of the Tortonian (~7.246 Ma). c) Restored section at the end of the Messinian (~5.333 Ma). d) Present-day geological section.

Based on the interpretation of the Cenozoic structures, we can propose a tectonic evolution of the study area and reconcile our results with the major geodynamic events that shaped the eastern Mediterranean.

Our restoration in figure 46 shows a small shortening during the Cenozoic, as the main shortening occurred during the previous northward Tethys subduction that structured the convergent margin (Woodside, 1977; Biju-Duval et al., 1977; Ben-Avraham et al., 1995; Robertson et al., 1998; Hall et al., 2005 a/b; Calon et al., 2005; Bowman, 2011; Symeou et al., 2018).

At the end of the Paleogene (Fig.49a), the oceanic crust north of the Levant Basin had been completely subducted: the collision with the thinned continental crust of the Levant Basin created the Latakia Ridge. During the Oligocene, the flexure of the downgoing African Plate was

accompanied by high-angle normal faults cutting the tilted foreland. On the upper plate, the overlying Eurasian Plate developed an accretionary prism corresponding to the present-day Latakia Ridge-Cyprus Basin sector. The present-day Latakia Ridge consists of a deep reverse fault with a low dip angle cutting the Mesozoic sequence, followed by a series of inner steeper reverse faults (Fig.49a). In the northern part, we interpret the region of the Latakia forearc Basin to have been formed by extensional faults that formed a northward thickening wedge of chalk, marl and turbidite deposits.

The forearc extension could be attributed to a "soft collision" (terminology from Darin & Umhoefer, 2022) between the migrating arc and the Levant foreland Basin. On the back, the seismic recordings do not allow a clear understanding of the Kyrenia Ridge reflectors: the opaque seismic facies can be attributed, at least in part, to the Late Cretaceous - Paleogenic volcanic rocks analyzed by Chen & Robertson (2021) in the Kyrenia Mountains: According to these authors, these formations could be attributed to an incipient marginal basin formed in an oblique-convergent setting before the Miocene suture with the Arabian plate. In this view, the Kyrenia Ridge could represent a poorly-developed volcanic arc, while the Cilicia Basin would be the back-arc basin.

Furthermore, during the Paleogene, the African and Arabian plates were progressively separated by the northward propagation of the Dead Sea Transform Fault. With the convergence between the Eurasian and Arabian plates, a “soft collision” occurred (Hempton, 1987). The collision propagated diachronically both eastward and westward. Today, the remaining oceanic crust of the Southern Neo-Tethys Ocean is actively subducting beneath the Makran Trench (Darin & Umhoefer, 2022) to the east and the Antalya Basin (Güvercin et al., 2021 – Western Transect) to the west. Between these two subduction zones, a “hard collision” (terminology from Darin & Umhoefer, 2022) occurred at the northern margin of the Arabian Plate. As for the Arabian foreland, the late Paleogene collision of the frontal chain with the thinned crust of the Levant Basin triggered the “soft collision” and slowed down the convergent phase.

During the Miocene (Fig.49b), a thick pile of sediment was deposited in a deep-water foreland of the Levant Basin, contributing to inhibiting the forward propagation of deformation, and creating out-of-sequence and back thrusting in the outer wedge (Fig.49b). Meanwhile, N-verging extensional tectonics in the Latakia Basin produced the thick sequence of Miocene turbidites. Extension at this time has also been documented in the surrounding sector (i.e., Cyprus, Syrian Coastal Range, and

Adana Basin - Robertson, 1998; Brew et al., 2001; Harrison et al., 2004; Harrison et al., 2008). A dramatic change occurred in the late Miocene before the Messinian Salinity Crisis. The back thrusts evolved into a transpressive flower structure in the outer wedge. Positive tectonic inversion affected the forearc basin in the Larnaka Ridge zone (Fig.49c). As a result, significant thicknesses of Messinian evaporites were deposited in the deep Levant Basin, in local minor basins of the outer wedge and, more continuously, in the Latakia Basin. At the same time, the prominent ridges were exposed to erosion, as were the fold and thrust structures in front of the Kyrenia Ridge, which prove that they predate Messinian evaporite deposition.

Since the Messinian, strike-slip dominates the kinematics of the study area (Fig.49c and Fig.49d) that have been influenced by the westward tectonic escape of the Anatolian microplate by the Hellenic rollback and the subsequent formation of the Northern and Eastern Anatolian Fault Zones (Schildgen et al., 2014).

During the Pliocene transgression, the marine water reflooded the entire Mediterranean Sea, giving it the present configuration (Fig.49c). At the same time, transpressive movements prevailed and continued to shape this part of the northeastern Mediterranean Sea. This active tectonics is reflected in strong folding and faulting on the seafloor, with more symmetrical and prominent forms of the former compressional structure, notably the Latakia Ridge and, to some extent, the Margat (i.e., a minor ridge in the middle of the Cyprus Basin) and Larnaka Ridges. Compressive activity continued and led to the formation of a thrust system and growth strata in front of the Kyrenia Ridge. Back-arc extension continues in the Cilicia Basin until the present day as the basin is experiencing a high subsidence rate (Aksu et al., 2005) and has an enormous thickness of Plio-Quaternary deposits.

5.3 – Linking the transects

The three geological sections (Fig.50) proposed cross three different sectors of the Cyprus Arc system: the Florence Rise (i.e., Western Transect – Fig.50a), the Cyprus Arc s.s. (i.e., Central Transect – Fig50b), and the Latakia Ridge (i.e., Eastern Transect – Fig.50c). These three transects shown how different types of crust along a single convergence boundary influence the structure and kinematics of the deformation fronts, depicting an oblique and diachronous closure.

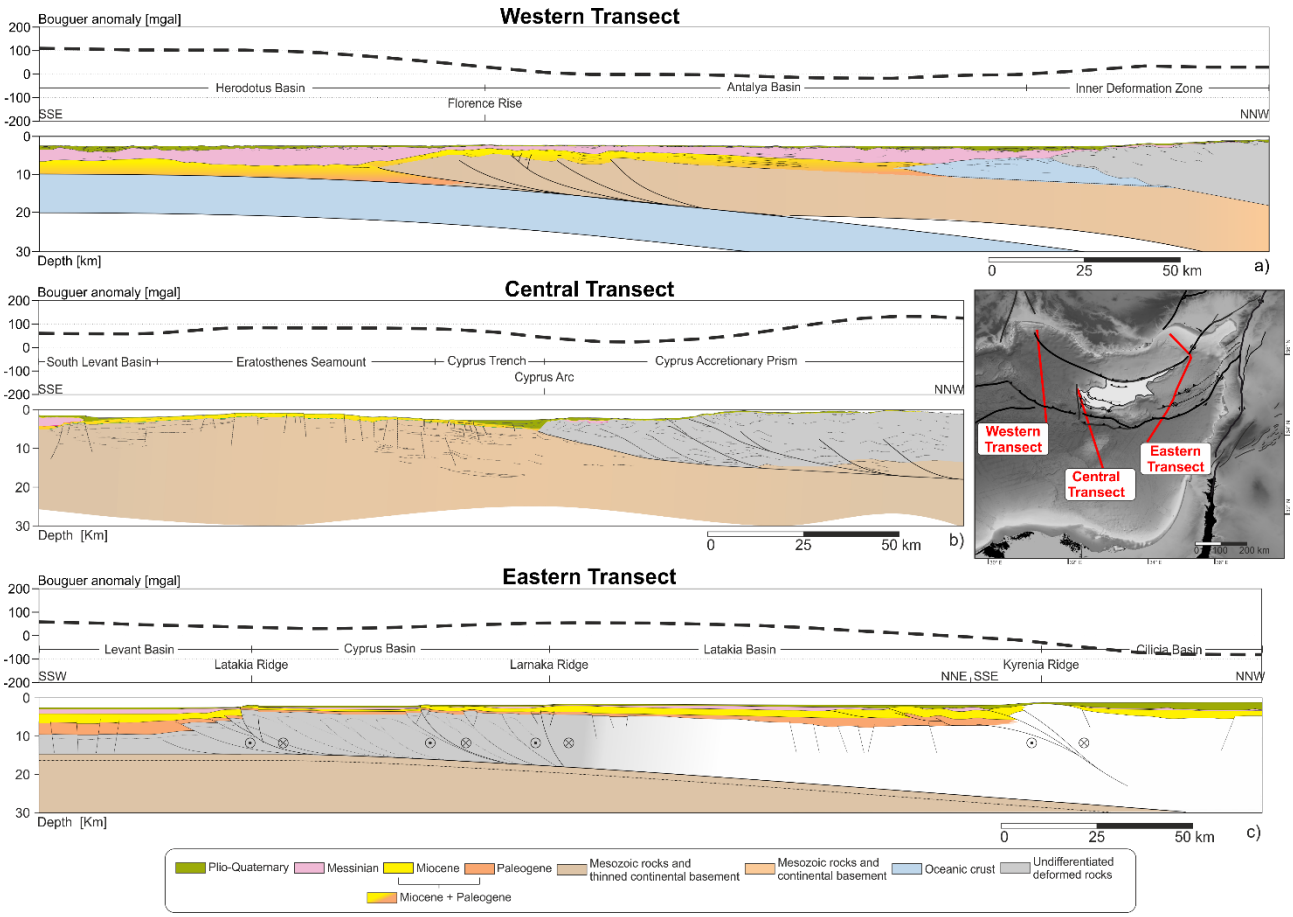

Figure 50: Final geological sections. a) Western Transect. b) Central Transect. c) Eastern Transect. Each transect has the corresponding Bouguer anomaly value plotted on it. The Bouguer anomaly grid is taken from Zingerle et al. (2020) with the terrain correction of Rexer et al. (2016). See also Figure Supplementary Material 4 for bigger image.

The system has been in compression since the Cretaceous to the present day: beneath the Florence Rise, the Southern Neo-Tethys' oceanic crust continues to subduct (Fig. 50a). Moving towards east, the oceanic crust south of Cyprus is completely consumed, leading to an incipient collision with the thicker continental crust of the Eratosthenes Seamount (Fig.50b). To the east, the front is affected by suture thickening due to transpressional kinematics resulting from the obliquity of the stress

vectors (Fig.50c) and underthrusting of the northern sector of the Levant Basin, which is characterized by thinned continental crust.

We have not modeled the gravimetric anomalies but by plotting the Bouguer anomalies (Zingerle et al., 2020) on our transects (Fig.50) some consideration can be made:

- On the Western Transect (Fig.50a), the values of the Bouguer anomaly in the Herodotus Basin are relatively high, which is related to the underlying oceanic crust, which is denser than the continental crust and shallower here. The Antalya Basin is characterised by a decrease in Bouguer anomaly values, which then increase again in correspondence of the Inner Deformation Zone, indicating an excess of mass or a denser lithology.
- On the Central Transect (Fig.50b), the relatively high Bouguer values are on the Eratosthenes Seamount and the Cyprus accretionary prism, which is due to their thicker crust. The trench, on the other hand, is characterised by lower Bouguer values because the sedimentary fill is less dense than the surrounding rock and deflects the curve.
- On the Eastern Transect (Fig.50c), a relative minimum value of the Bouguer anomaly curve is in agreement with the extinct trench but it is more evident in the Cilicia Basin. The Cilicia Basin has a high subsidence rate (Aksu et al., 2005), so a large thickness of Plio-Quaternary sediments has been deposited causing this lower Bouguer value. In the Latakia Basin, on the other hand, there is a local maximum in Bouguer values. This higher Bouguer value could be explained by a thicker basement or by a strand of obducted ophiolites over the thinned continental crust of the northern African margin.

The nature of the bedrock beneath the deformed basins is still controversial, as few boreholes have been drilled. Bowman (2011) published some borehole data from the Syrian margin where Cretaceous carbonates were drilled, as well as the Ayse-1 borehole in the Iskenderun Basin where the Kilzildag ophiolites were directly overlain by Miocene sediments. Rybakov et al. (2011) published the latest findings on the source of magnetic anomalies in the northeastern Mediterranean, delineating anomalies associated with volcanic intrusions from those of obducted ophiolites. Their result is the most detailed map of magnetic anomalies in the study area. Therefore, they were able to identify smaller anomalies and subdivide different buried bodies, neglecting a unique massive obducted ophiolite beneath the deformed basins. On the MS56 seismic section, some sparse deep reflections could be interpreted as a carbonate platform and its basin fill (Fig.40). Also, on the MS53,

some deep reflectors have a different acoustic impedance contrast than the acoustic basement surrounding them, which makes it possible to guess the nature of the different basements' nature. Thus, it can be assumed that the basement consists of a mixture of obducted ophiolites and rocks of continental origin (Ben-Avraham et al., 1995, Vidal et al., 2000; Symeou et al., 2018). Moreover, if we consider the distribution of Tethyan ophiolites along the entire convergent margin, it is impossible to find a single ophiolite body hundreds of kilometres wide like the one that is supposed to lie beneath the basins around Cyprus. It is more likely that some pieces were obducted onto the old passive margin, as is also modelled under the Antalya Basin by Ergün et al. (2005).

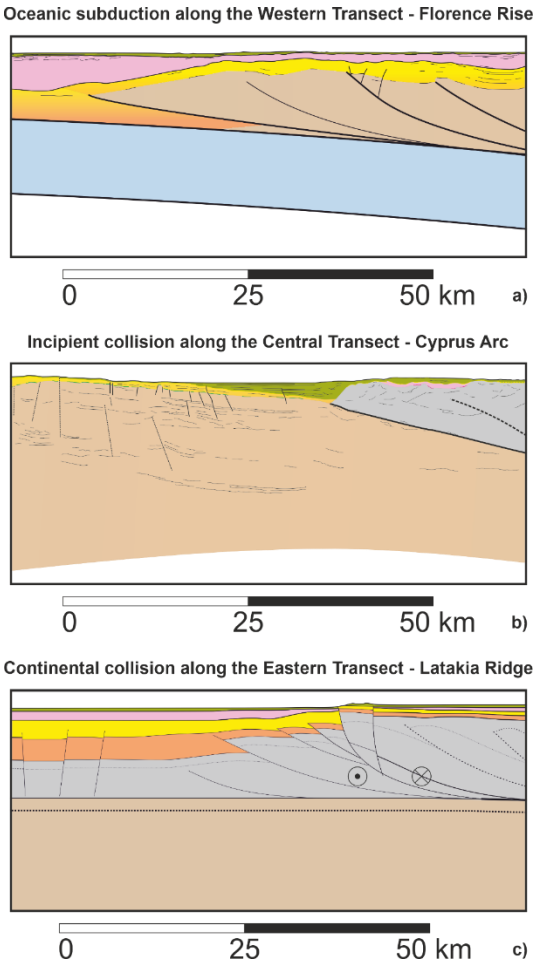

Figure 51: a) Detail of the Western Transect centered on the Florence Rise. b) Detail of the Central Transect centered on the Cyprus Arc. c) Detail of the Eastern Transect centered on the Latakia Ridge.

Figure 51 shows the main differences between the three transects, i.e., their trenches and the shape of the deformation zones. The Western Transect trench (Fig.51a) is poorly developed due to the absence of a major river in southern Turkey and sediments coming from the north accumulate in the northern Antalya Basin. Therefore, only a few sediments can reach the trench in the Herodotus

Basin, unlike its southern part, which is fed by the large amounts of sediments transported by the Nile and forming the Nile Delta.

Instead, the Cyprus Trench (Fig.51b) is well developed as the source of sediment is the island of Cyprus and the eroded sediments of the prism.

Towards the east, along the Eastern Transect (Fig.51c), the trench is no longer active as subduction has ceased. The classic wedge shape is also no longer present as strike-slip movements tend to create more symmetrical ridges, represented by flower structures.

In our geodynamic model, the Cyprus Arc system began to close diachronically after the collision of the Arabian promontory in the east, so that at least the northeastern corner was affected by a component of the strike-slip from then on. Figure 52 shows the Cenozoic tectonic evolution of the study area based on the three sections proposed in this study.

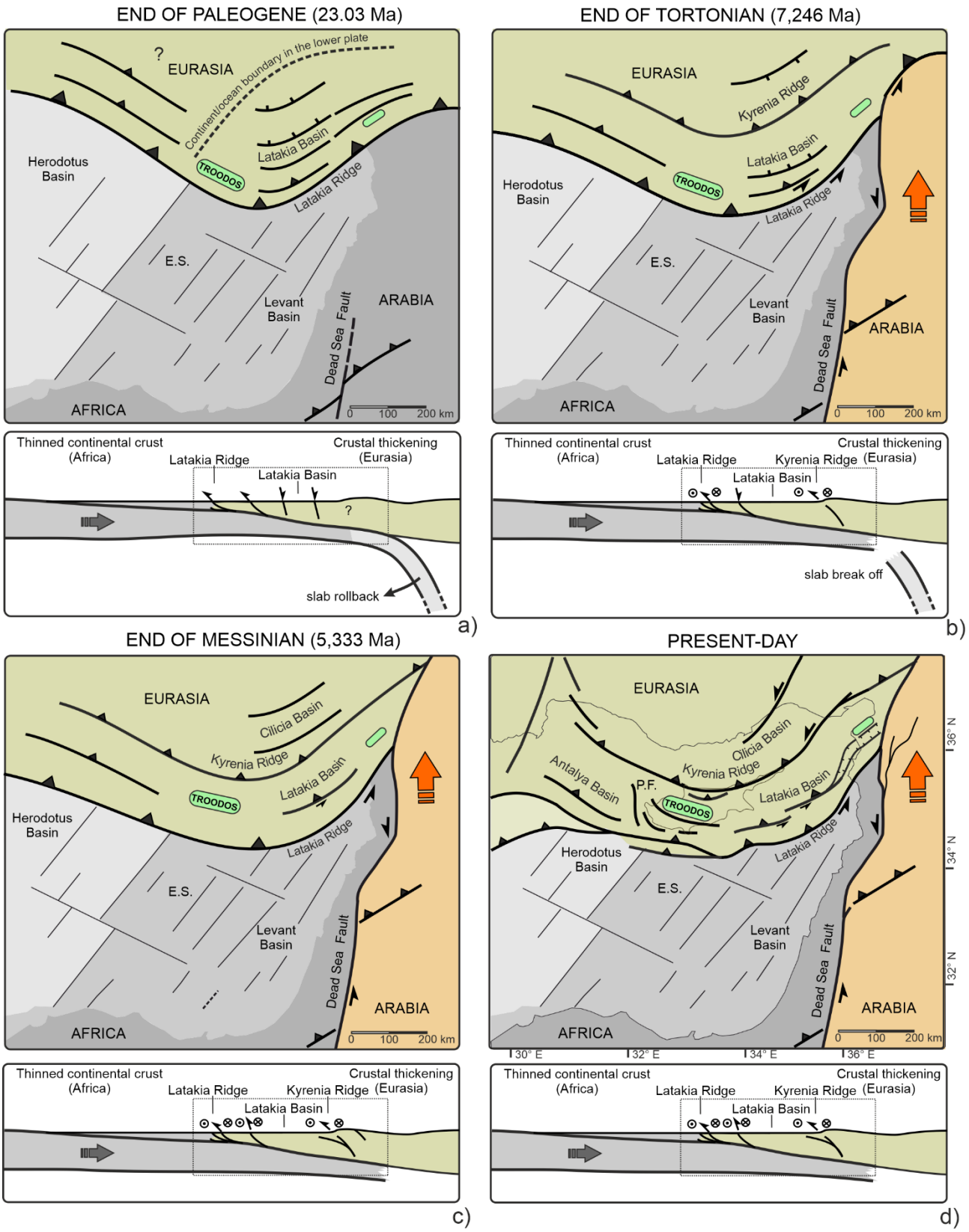

Figure 52: Sketch of the Cenozoic tectonic evolution of the northeastern Mediterranean in map and the corresponding sketch of the restored Eastern Transect. The green area represents the deformed Eurasian plate. The light grey area represents the oceanic crust of the Herodotus Basin. The grey area represents the thinned continental crust of the Levant Basin. The dark grey area represents - in

panel-a - the Afro-Arabia continental crust. Then, the two plates were divided by the propagation of the Dead Sea Transform Fault. Hence, the orange area represents the Arabian Plate continental crust, and the dark grey one the African Plate continental crust. Red arrows represent the Arabian plate movements. Grey tectonic lineaments are the inherited normal faults of the Tethyan rifting. Black lineaments represent the major tectonic structures. E.S. = Eratosthenes Seamount, P.F. = Paphos Fault.

Figure 52 shows that the Florence Rise must have moved faster than the Cyprus Arc s.s. and the Latakia Ridge to cover a major "radial" distance. The front's migration could be hypothesized to be a counterclockwise motion broadly centered near the triple junction between the Cyprus Arc system, the Dead Sea Transform Fault, and the Eastern Anatolian Fault meet. Beneath Cyprus and its deformed eastern basins, the oceanic slab has now detached, while beneath the Antalya Basin it is still connected to the African oceanic plate domain (Fig.53).

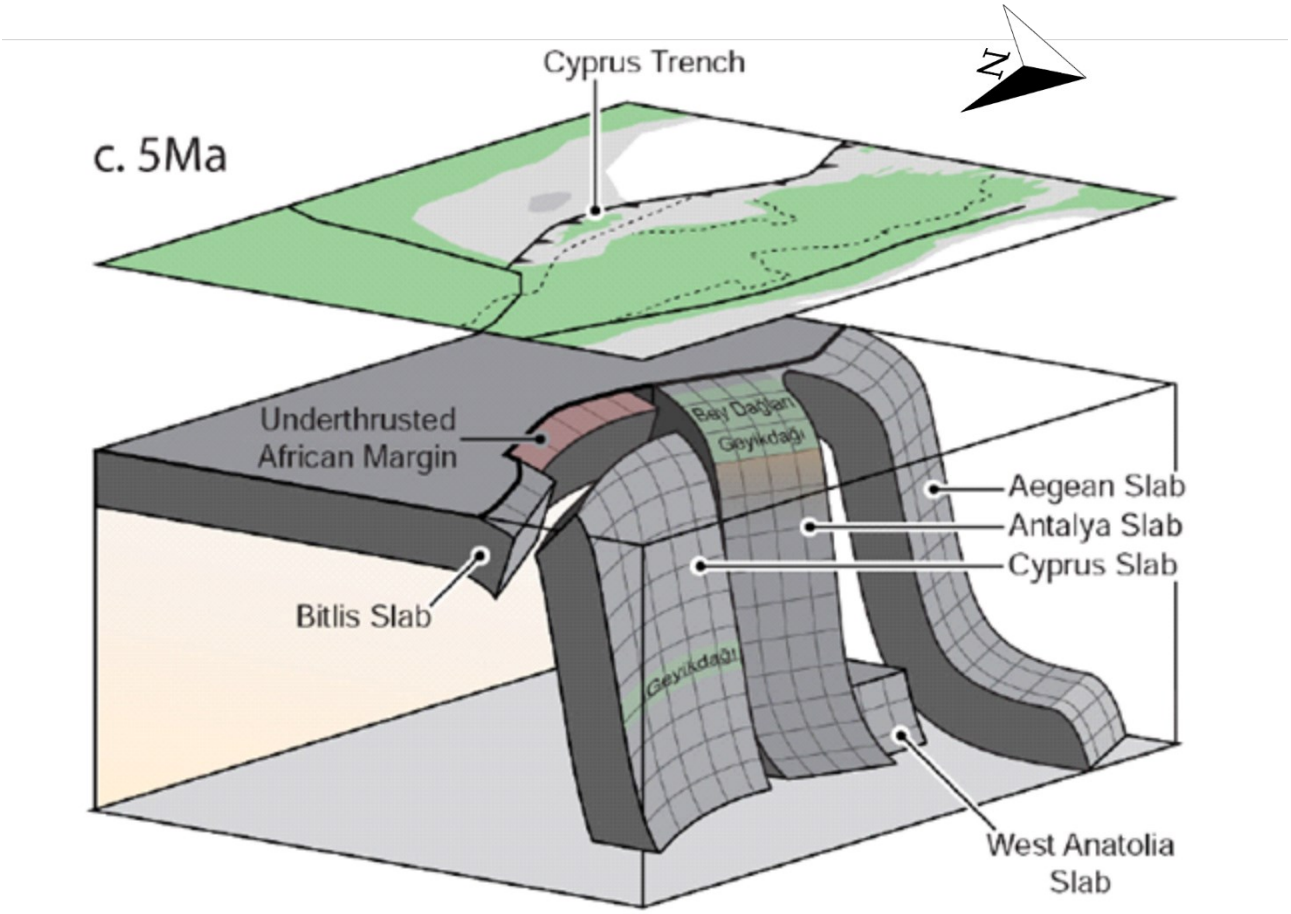

Figure 53: Slabs geometry beneath the eastern Mediterranean and surrounding areas. The Bitlis and Western Anatolian slabs have entered the lower mantle. The Cyprus slab has broken off, and the

lithosphere of the African margin is subducting. The Antalya Slab continues to steepen and slowly delaminates the western Central Taurides. Figure modified from McPhee et al. (2022).

Present-day tectonics is thus influenced by the subducted ocean-continent boundary, which played and continues to play a role in driving the deformation and led to a pivotal motion of the Cyprus Arc system during the Cenozoic.

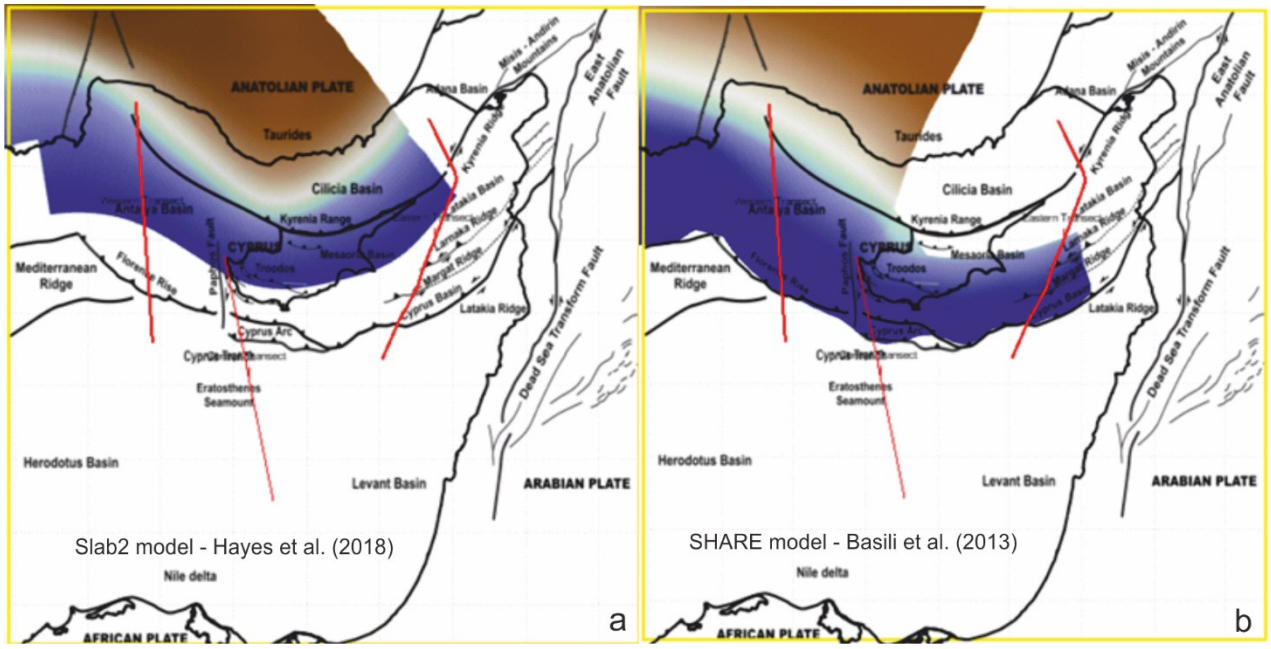

Figure 54: a) Slab2 model form Hayes et al. (2018). b) SHARE model from the European Database of Seismogenic Faults, Basili et al. (2013).

Figure 54 shows the comparison between the Hayes et al. (2018) – Slab2 model (Fig.54a) and the Basili et al. (2013) – SHARE subduction interface model (Fig.54b). The Slab2 model predicts the convergence front to be located northward with respect to both our finding and the SHARE geometries. Both models involved active subduction along almost the entire Cyprus Arc system except for its easternmost (Syrian) part. Our interpretation is in good agreement with the SHARE model about the front position but differ in two main aspects: 1) our model predicts the subduction to stop immediately east of the Cyprus Arc s.s. and the Latakia Ridge is seen as a positive flower structure where oceanic subduction ceased; 2) the dip of the modeled subduction interface.

Figure 55 shows a 3D view of the SHARE subduction interface model plotted on our three geological sections across the study area. The Western Transect fits well with the modeled slab interface, while moving eastward the differences increase. On the Central Transect the two reconstructions are still in good agreement but the major bias in on the Eastern Transect, due to different plate kinematics proposed.

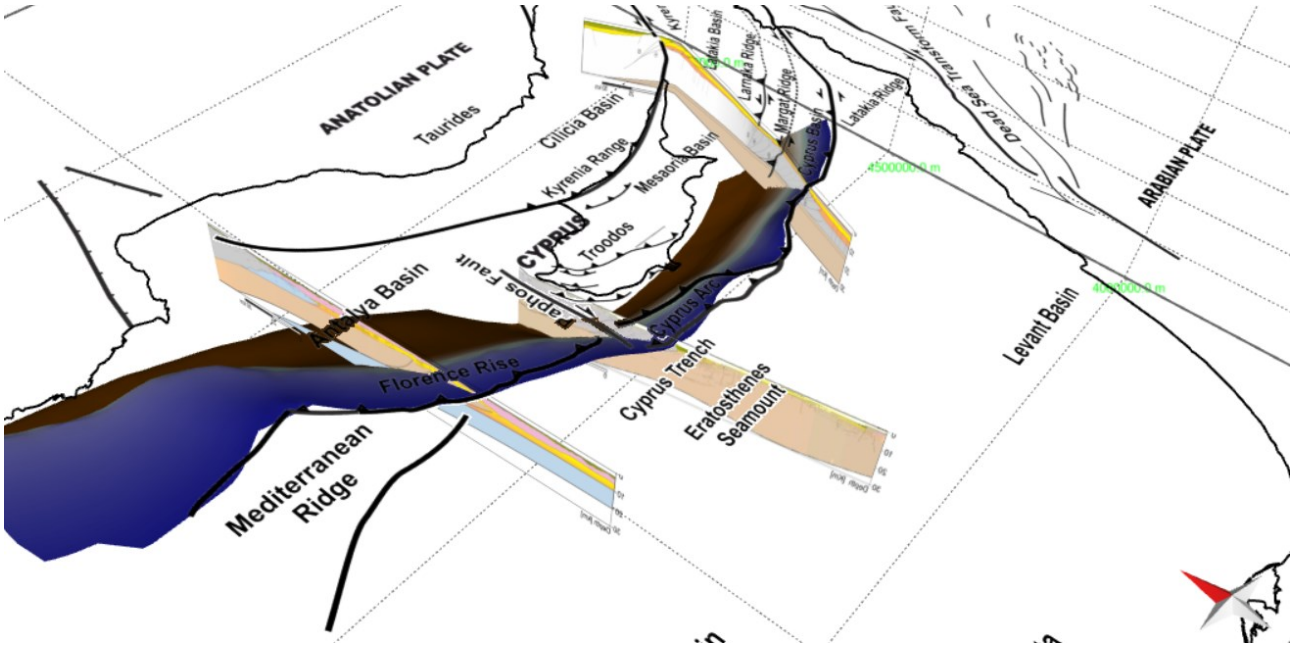

Figure 55: 3D view of the SHARE subduction interface model and our three transects along the Cyprus Arc system. The front's position fits well the dip of the subduction interface is in good agreement on the western side and differ moving toward the east due to different tectonic setting proposed: continued oceanic subduction vs suture thickening and transpression.

The SHARE slab model assumes that subduction is still active below the Latakia Ridge, while our model points out that the subduction stopped in that sector and the Cyprus slab is detached from the underridding African plate. East of Cyprus suture thickening and transpressional kinematics dominates the now-a-days tectonics with a more buoyant and thinner continental crust involved in this part of the Cyprus Arc system.

As a result, a tearing between these two descending slabs occurred, creating the Paphos Fault (Fig.52d). The Paphos fault is not visible on our seismic sections, but it is highlighted by a cluster of seismicity where the Cyprus Arc s.s. and the Florence Rise meet. The seismicity to the south/southwest of Cyprus is dominated by dextral strike-slip focal mechanism with minor compressional and extensional ones, as an expression of this deep lithospheric tearing (Mercier et al., 1973; Papazachos & Papaioannou, 1999). Analogous examples of similar tear faults in the Mediterranean Sea are the Calabrian STEP fault (Goves & Wortel, 2005; Gallais et al., 2013; Maesano et al. 2020), where the same oceanic crust subducts beneath the Calabrian Arc, or the Kefalonia Transform Fault at the western end of the Hellenic Arc (Özbakir et al., 2020) and the Finike Basin at the eastern junction between the Hellenic Arc and the Florence Rise.

CHAPTER 6: CONCLUSION

The interpretation of the three transects across the Cyprus Arc system and the integration with the surrounding geological evidence allow us to shed light on the deeper structures and deposits of the northern part of the eastern Mediterranean Sea. Depth conversion, sequential restoration and creation of deep geological sections allow the description of a tectonostratigraphic model to explain the Cenozoic evolution of the study area.

Our data enable us to reconstruct the evolution of this convergent margin: from the Messinian to the Quaternary along the Western and Central transects, and from the Paleogene along the Eastern Transect. By moving from west to east with Cyprus in the center, it was possible to analyze the evolution of this convergent margin, from oceanic subduction to continent-continent collision. The characteristic features are a thinner accretionary wedge to the west and a thicker and more deformed wedge towards the east. The trenches also vary along strike: the Herodotus Basin has a poorly developed trench due to the small amount of sediment that can reach it, as the Florence Rise is a structural barrier. South of Cyprus, the trench is well developed, testifying the recent evolution of this system, while on the Eastern Transect, there is no trench as strike-slip movements dominate today and subduction ceased. This interpretation is also supported by the relocation of the earthquakes, which become shallower from west to east and by gravimetric and magnetic anomalies.

Our tectonic model can be summarized as follows:

- The Cretaceous convergent phase created the Cyprus Arc system and the associated accretionary complexes.
- During the Paleogene, the suture propagated diachronically from east to west. The continental collision in the area of the Arabian promontory influenced the evolution in the study area as on the Eastern Transect the thinned continental crust of the Levant Basin entered the convergent margin. Therefore, we interpreted a few shortenings during the Cenozoic. We related this to a component of strike-slip, while out-of-sequence thrusting and backthrusting occurred in the eastern Cyprus offshore. Meanwhile, south and west of Cyprus, the convergence phase continued.

- During the Miocene, strike-slip kinematics continued in the eastern sectors, with some areas affected by transtension and others by transpression, while accretionary complexes continued to develop on the Central and Western transects.
- Before the Messinian Salinity Crisis, on the Eastern Transect, we hypothesize the positive tectonic inversion of the Larnaka Ridge, namely from extensional to transpressional kinematics, while the other ridges continued their transpressional evolution. On the Central Transect, convergence continued. On the Western Transect, out-of-sequence thrusting took place with the development of backthrusts and internal thrusting that tilted the Antalya Basin northwards.
- From the latter phase to the present, the tectonic escape of the Anatolian microplate has influenced the movements of the study area, and strike-slip dominates on the Eastern Transect. On the Central Transect, we interpret a slowdown in the forward propagation of the deformation front associated with the underthrusting of the Eratosthenes Seamount, which triggered the recent uplift of the island of Cyprus. On the Western Transect, oceanic subduction has continued, and the strain is partitioned between the Florence Rise and the Inner Deformation Zone as both structures are still active.

The main conclusions can be summarized as follows:

- The subdivision of the Cyprus Arc system into three main segments with their respective geometries and kinematics is directly related to the type of plates involved in the convergence.
- For the first time, a regional, viable and balanced geological section that crosses the deformed basins east of Cyprus has been proposed. The Cenozoic tectonic evolution is characterized by few shortenings, out-of-sequence thrusting, positive tectonic inversion of the Larnaka Ridge and the switch from compressive to strike-slip kinematics.
- The regional arrangement was initially driven by north-south compression. During the Cenozoic, the gradual rotation of the arc led to a current ENE-WSW compression, particularly effective and visible in the western sector, combined with transpression in the central sector, up to almost pure strike-slip tectonics in the eastern sector of the arc.
- The long and complex geological evolution of the area has produced various types of faults that were generally reactivated by following tectonic phases.

6.1 - Future perspectives

Our model, based on the interpretation of multichannel seismic reflection sections, is consistent with the published observations. However, deep features are not clearly shown on the available seismic profiles and further work is needed to better understand the geological evolution of the eastern Mediterranean:

- drilling in the deformed basins to confirm our age estimate of the reflectors or not;
- improving the density of the seismic network in Middle Eastern countries to better monitor and correlate earthquakes and structures;
- publishing the private data of oil and gas companies will help the academic world enormously because open-access seismic and borehole data are rare.

REFERENCES

- Agard, P., Omrani, J., Jolivet, L., Whitechurch, H., Vrielynck, B., Spakman, W., ... & Wortel, R. (2011). Zagros orogeny: a subduction-dominated process. *Geological Magazine*, *148*(5-6), 692-725.
- Aksu, A. E., Calon, T. J., Hall, J., Mansfield, S., & Yaşar, D. O. Ğ. A. N. (2005). The Cilicia–Adana basin complex, Eastern Mediterranean: Neogene evolution of an active fore-arc basin in an obliquely convergent margin. *Marine Geology*, *221*(1-4), 121-159.
- Aksu, A. E., Hall, J., Calon, T. J., Barnes, M. C., Güneş, P., & Cranshaw, J. C. (2018). Messinian evaporites across the Anaximander mountains, Sırrı Erinç Plateau and the Rhodes and Finike basins, eastern Mediterranean Sea. *Marine Geology*, *395*, 48-64.
- Aksu, A. E., Walsh-Kennedy, S., Hall, J., Hiscott, R. N., Yaltırak, C., Akhun, S. D., & Çifçi, G. Ü. N. A. Y. (2014). The Pliocene–Quaternary tectonic evolution of the Cilicia and Adana basins, eastern Mediterranean: Special reference to the development of the Kozan Fault zone. *Tectonophysics*, *622*, 22-43.
- Bagnall, P. S. (1960). *The geology and mineral resources of the Pano Lefkara-Larnaca area*. authority of the Government of Cyprus.
- Barrier, E., & Vrielynck, B. (2008). Palaeotectonic maps of the Middle East. *Atlas of*, *14*.
- Basili, R., Kastelic, V., Demircioglu, M. B., Garcia Moreno, D., Nemser, E. S., Petricca, P., ... & Wössner, J. (2013). The European Database of Seismogenic Faults (EDSF) compiled in the framework of the Project SHARE.
- Ben-Avraham, Z., Ginzburg, A., Makris, J., & Eppelbaum, L. (2002). Crustal structure of the Levant Basin, eastern Mediterranean. *Tectonophysics*, *346*(1-2), 23-43.
- Ben-Avraham, Z., Tibor, G., Limonov, A. F., Leybov, M. B., Ivanov, M. K., Tokarev, M. Y., & Woodside, J. M. (1995). Structure and tectonics of the eastern Cyprean Arc. *Marine and Petroleum Geology*, *12*(3), 263-271.
- Ben-Avraham, Z., Woodside, J., Lodolo, E., Gardosh, M., Grasso, M., Camerlenghi, A., & Vai, G. B. (2006). Eastern Mediterranean basin systems. *Geological Society, London, Memoirs*, *32*(1), 263-276.
- Biju-Duval, B., & Montadert, L. (1977). Introduction to the structural history of the Mediterranean basins. In *Structural history of the Mediterranean Basins* (pp. 1-12). Technip Paris.

- Bilim, F., Aydemir, A., & Ates, A. (2017). Tectonics and thermal structure in the Gulf of Iskenderun (southern Turkey) from the aeromagnetic, borehole and seismic data. *Geothermics*, *70*, 206-221.
- Bowman, S. A. (2011). Regional seismic interpretation of the hydrocarbon prospectivity of offshore Syria. *GeoArabia*, *16*(3), 95-124.
- Brancatelli, G., Forlin, E., Bertone, N., Del Ben, A., & Geletti, R. (2022). Time to depth seismic reprocessing of vintage data: A case study in the Otranto Channel (South Adriatic Sea). In *Interpreting Subsurface Seismic Data* (pp. 157-197). Elsevier.
- Brew, G., Barazangi, M., Al-Maleh, A. K., & Sawaf, T. (2001). Tectonic and geologic evolution of Syria. *GeoArabia*, *6*(4), 573-616.
- Brian Meyer; Richard Saltus; and Arnaud Chulliat. 2017: EMAG2v3: Earth Magnetic Anomaly Grid (2-arc-minute resolution). Version 3. NOAA National Centers for Environmental Information - https://www.ncei.noaa.gov/access/metadata/landing-page/bin/iso?id=gov.noaa.ngdc.mgg.geophysical_models:EMAG2_V3
- Bridge, C., Calon, T. J., Hall, J., & Aksu, A. E. (2005). Salt tectonics in two convergent-margin basins of the Cyprus arc, Northeastern Mediterranean. *Marine Geology*, *221*(1-4), 223-259.
- Burton-Ferguson, R., Aksu, A. E., Calon, T. J., & Hall, J. (2005). Seismic stratigraphy and structural evolution of the Adana Basin, eastern Mediterranean. *Marine Geology*, *221*(1-4), 189-222.
- Calon, T. J., Aksu, A. E., & Hall, J. (2005). The Neogene evolution of the outer Latakia Basin and its extension into the eastern Mesaoria Basin (Cyprus), eastern Mediterranean. *Marine Geology*, *221*(1-4), 61-94.
- Camerlenghi, A., Del Ben, A., Hübscher, C., Forlin, E., Geletti, R., Brancatelli, G., ... & Facchin, L. (2020). Seismic markers of the Messinian salinity crisis in the deep Ionian Basin. *Basin Research*, *32*(4), 716-738.
- Chen, G., & Robertson, A. H. (2021). Evidence from Late Cretaceous-Paleogene volcanic rocks of the Kyrenia Range, northern Cyprus for the northern, active continental margin of the Southern Neotethys. *Lithos*, *380*, 105835.
- Çiftçí, S. Y., Haciköylü, P., Geze Kalanyuva, Y., Kansu, E., & Aktepe, A. (2012). Exploration plays in the Mersin Basin, Turkish Mediterranean Sea. *The Leading Edge*, *31*(7), 832-845.

- Civile, D., Brancolini, G., Lodolo, E., Forlin, E., Accaino, F., Zecchin, M., ... & Billi, A. (2021). Morphostructural setting and tectonic evolution of the central part of the Sicilian channel (Central Mediterranean). *Lithosphere*, *2021*(1).
- Collin, P. Y., Mancinelli, A., Chiocchini, M., Mroueh, M., Hamdam, W., & Higazi, F. (2010). Middle and Upper Jurassic stratigraphy and sedimentary evolution of Lebanon (Levantine margin): Palaeoenvironmental and geodynamic implications. *Geological Society, London, Special Publications*, *341*(1), 227-244.
- Dahlen, F. A., Suppe, J., & Davis, D. (1984). Mechanics of fold-and-thrust belts and accretionary wedges: Cohesive Coulomb theory. Journal of Geophysical Research: Solid Earth, 89(B12), 10087-10101.
- Davis, D., Suppe, J., & Dahlen, F. A. (1983). Mechanics of fold-and-thrust belts and accretionary wedges. Journal of Geophysical Research: Solid Earth, 88(B2), 1153-1172.
- Darin, M. H., & Umhoefer, P. J. (2022). Diachronous initiation of Arabia–Eurasia collision from eastern Anatolia to the southeastern Zagros Mountains since middle Eocene time. *International Geology Review*, 1-29.
- Dewey, J. F., PITMAN III, W. C., Ryan, W. B., & Bonnin, J. (1973). Plate tectonics and the evolution of the Alpine system. *Geological society of America bulletin*, *84*(10), 3137-3180.
- Druckman, Y., Buchbinder, B., Martinotti, G. M., Tov, R. S., & Aharon, P. (1995). The buried Afiq Canyon (eastern Mediterranean, Israel): a case study of a Tertiary submarine canyon exposed in Late Messinian times. Marine Geology, 123(3-4), 167-185.
- Eppelbaum, L., & Katz, Y. (2015). Eastern Mediterranean: combined geological–geophysical zonation and paleogeodynamics of the Mesozoic and Cenozoic structural-sedimentation stages. *Marine and Petroleum Geology*, *65*, 198-216.
- Ergün, M., Okay, S., Sari, C., Oral, E. Z., Ash, M., Hall, J., & Miller, H. (2005). Gravity anomalies of the Cyprus Arc and their tectonic implications. *Marine Geology*, *221*(1-4), 349-358.
- Euro-Mediterranean Seismological Center - https://www.emsc-csem.org/#2
- Evans, S. L., & Jackson, C. A. L. (2021). Intra-salt structure and strain partitioning in layered evaporites: implications for drilling through Messinian salt in the eastern Mediterranean. *Petroleum Geoscience*, *27*(4), petgeo2020-072.
- Feld, C., Mechie, J., Hübscher, C., Hall, J., Nicolaides, S., Gurbuz, C., ... & Weber, M. (2017). Crustal structure of the Eratosthenes Seamount, Cyprus and S. Turkey from an amphibian wide-angle seismic profile. *Tectonophysics*, *700*, 32-59.

- Feng, Y. E., & Reshef, M. (2016). The Eastern Mediterranean Messinian salt-depth imaging and velocity analysis considerations. *Petroleum Geoscience*, *22*(4), 333-339.
- Fernández-Blanco, D., Bertotti, G., Aksu, A., & Hall, J. (2019). Monoclinal flexure of an orogenic plateau margin during subduction, south Turkey. *Basin Research*, *31*(4), 709-727.
- Fernández-Blanco, D., Mannu, U., Cassola, T., Bertotti, G., & Willett, S. D. (2021). Sedimentation and viscosity controls on forearc high growth. *Basin Research*, *33*(2), 1384-1406.
- Finetti, I., & Morelli, C. (1973). Geophysical exploration of the Mediterranean Sea.
- Finetti, I., Del Ben, A., Forlin, E., & Prizzon, A. (2005). Review of the main results of the pioneering MS seismic exploration programme in the deep water of the Mediterranean Sea (OGS, 1969–1980). *CROP project, deep seismic exploration of the central mediterranean and Italy*, 1-30.
- Follows, E. J., & Robertson, A. H. F. (1990). Sedimentology and structural setting of Miocene reefal limestones in Cyprus. In *Troodos 1987. Symposium* (pp. 207-215).
- Fuller, C. W., Willett, S. D., & Brandon, M. T. (2006). Formation of forearc basins and their influence on subduction zone earthquakes. *Geology*, *34*(2), 65-68.
- Gallais, F., Graindorge, D., Gutscher, M. A., & Klaeschen, D. (2013). Propagation of a lithospheric tear fault (STEP) through the western boundary of the Calabrian accretionary wedge offshore eastern Sicily (Southern Italy). *Tectonophysics*, *602*, 141-152.
- Gardosh, M. A., & Druckman, Y. (2006). Seismic stratigraphy, structure and tectonic evolution of the Levantine Basin, offshore Israel. *Geological Society, London, Special Publications*, *260*(1), 201-227.
- Gardosh, M. A., Garfunkel, Z., Druckman, Y., & Buchbinder, B. (2010). Tethyan rifting in the Levant Region and its role in Early Mesozoic crustal evolution. *Geological Society, London, Special Publications*, *341*(1), 9-36.
- Gardosh, M., Druckman, Y., Buchbinder, B., & Rybakov, M. (2008). *The Levant Basin offshore Israel: stratigraphy, structure, tectonic evolution and implications for hydrocarbon exploration* (p. 119). Geophysical Institute of Israel.
- Garfunkel, Z. (1998). Constrains on the origin and history of the Eastern Mediterranean basin. *Tectonophysics*, *298*(1-3), 5-35.

- Garfunkel, Z., & Derin, B. (1984). Permian-early Mesozoic tectonism and continental margin formation in Israel and its implications for the history of the Eastern Mediterranean. *Geological Society, London, Special Publications*, *17*(1), 187-201.
- GeoMappApp - *http://www.geomapapp.org*
- Ghalayini, R., Daniel, J. M., Homberg, C., Nader, F. H., & Comstock, J. E. (2014). Impact of Cenozoic strike-slip tectonics on the evolution of the northern Levant Basin (offshore Lebanon). *Tectonics*, *33*(11), 2121-2142.
- Ghalayini, R., Nader, F. H., Bou Daher, S., Hawie, N., & Chbat, W. E. (2018). Petroleum systems of Lebanon: An update and review. *Journal of Petroleum Geology*, *41*(2), 189-214.
- Gökçen, S. L., Kelling, G., Gökçen, N., & Floyd, P. A. (1988). Sedimentology of a late Cenozoic collisional sequence: the Misis Complex, Adana, southern Turkey. *Sedimentary Geology*, *59*(3-4), 205-235.
- Gorini, C., Montadert, L., & Rabineau, M. (2015). New imaging of the salinity crisis: Dual Messinian lowstand megasequences recorded in the deep basin of both the eastern and western Mediterranean. *Marine and Petroleum Geology*, *66*, 278-294.
- Govers, R., & Wortel, M. J. R. (2005). Lithosphere tearing at STEP faults: Response to edges of subduction zones. *Earth and Planetary Science Letters*, *236*(1-2), 505-523.
- Granot, R. (2016). Palaeozoic oceanic crust preserved beneath the eastern Mediterranean. *Nature Geoscience*, *9*(9), 701-705.
- Güneş Özer, P. (2009). *Miocene to recent stratigraphy, structural arcitecture and tectonic evolution of the florence rise, Eastern Mediterranean sea* (Doctoral dissertation, DEÜ Fen Bilimleri Enstitüsü).
- Güneş, P., Aksu, A. E., & Hall, J. (2018). Structural framework and deformation history of the western Cyprus Arc. *Tectonophysics*, *744*, 438-457.
- Güvercin, S. E., Konca, A. Ö., Özbakır, A. D., Ergintav, S., & Karabulut, H. (2021). New focal mechanisms reveal fragmentation and active subduction of the Antalya slab in the Eastern Mediterranean. *Tectonophysics*, *805*, 228792.
- Gvirtzman, Z., Manzi, V., Calvo, R., Gavrieli, I., Gennari, R., Lugli, S., ... & Roveri, M. (2017). Intra-Messinian truncation surface in the Levant Basin explained by subaqueous dissolution. *Geology*, *45*(10), 915-918.

- Hall, J. K., Krasheninnikov, V. A., Hirsch, F., Benjamini, C., & Flexer, A. (2005)c. Geological framework of the Levant, volume II: the Levantine Basin and Israel. *Geological Framework of the Levant; Historical Productions-Hall: Jerusalem, Israel*.
- Hall, J., Aksu, A. E., Calon, T. J., & Yaşar, D. (2005)a. Varying tectonic control on basin development at an active microplate margin: Latakia Basin, Eastern Mediterranean. *Marine Geology*, *221*(1-4), 15-60.
- Hall, J., Aksu, A. E., King, H., Gogacz, A., Yaltırak, C., & Çifçi, G. Ü. N. A. Y. (2014). Miocene–Recent evolution of the western Antalya Basin and its linkage with the Isparta Angle, eastern Mediterranean. *Marine Geology*, *349*, 1-23.
- Hall, J., Calon, T. J., Aksu, A. E., & Meade, S. R. (2005)b. Structural evolution of the Latakia Ridge and Cyprus Basin at the front of the Cyprus Arc, eastern Mediterranean Sea. *Marine Geology*, *221*(1-4), 261-297.
- Haq, B., Gorini, C., Baur, J., Moneron, J., & Rubino, J. L. (2020). Deep Mediterranean's Messinian evaporite giant: how much salt?. *Global and Planetary Change*, *184*, 103052.
- Harrison, R. W. (2008, September). A model for the plate tectonic evolution of the eastern Mediterranean region that emphasizes the role of transform (strike-slip) structures. In *1st WSEAS International Conference on Environmental and Geological Science and Engineering (EG'08) Malta*.
- Harrison, R. W., Newell, W. L., Batıhanlı, H., Panayides, I., McGeehin, J. P., Mahan, S. A., ... & Necdet, M. (2004). Tectonic framework and Late Cenozoic tectonic history of the northern part of Cyprus: implications for earthquake hazards and regional tectonics. *Journal of Asian Earth Sciences*, *23*(2), 191-210.
- Hayes, G. P., Moore, G. L., Portner, D. E., Hearne, M., Flamme, H., Furtney, M., & Smoczyk, G. M. (2018). Slab2, a comprehensive subduction zone geometry model. Science, 362(6410), 58-61.
- Hawie, N., Gorini, C., Deschamps, R., Nader, F. H., Montadert, L., Granjeon, D., & Baudin, F. (2013). Tectono-stratigraphic evolution of the northern Levant Basin (offshore Lebanon). *Marine and petroleum geology*, *48*, 392-410.
- Hempton, M. R. (1987). Constraints on Arabian plate motion and extensional history of the Red Sea. *Tectonics*, *6*(6), 687-705.

- Hsü, K. J.; Montadert, L.; Bernoulli, D.; Bizon, G.; Cita, M. B.; Erickson, A. J.; Fabricius, F. H.; Garrison, R. E.; Kidd, R. B.; Melieres, F.; Mueller, C.; Wright, R. C. (1978). Sites 375 and 376, Florence Rise. DSDP Volume XLII, 219-304.
- IODP / https://www.iodp.org/
- ISC International Seismological Center / http://www.isc.ac.uk/
- Işler, F. I., Aksu, A. E., Hall, J., Calon, T. J., & Yaşar, D. (2005). Neogene development of the Antalya Basin, Eastern Mediterranean: An active forearc basin adjacent to an arc junction. *Marine geology*, *221*(1-4), 299-330.
- Klaeschen, D., Vidal, N., Kopf, A. J., von Huene, R., & Krasheninnikov, V. A. (2005). Reflection seismic processing and images of the eastern Mediterranean from the Cruise 5 of the Research Vessel" Akademik Nicolaj Strakhov". Historical Productions-Hall.
- Krijgsman, W., Hilgen, F. J., Raffi, I., Sierro, F. J., & Wilson, D. S. (1999). Chronology, causes and progression of the Messinian salinity crisis. Nature, 400(6745), 652-655.
- Lofi J., Déverchère J., Gaullier V., Gillet H., Gorini C., Guennoc P., Loncke L., Maillard A., Sage F., Thinon I. (2011) Seismic Atlas of the "Messinian Salinity Crisis" markers in the Mediterranean and Black Seas. Commission for the Geological Map of the World. Société Géologique de France, 179, pp.1-72, 2011, Mémoires de la Société Géologique de France.
- Loncke, L., Vendeville, B. C., Gaullier, V., & Mascle, J. (2010). Respective contributions of tectonic and gravity-driven processes on the structural pattern in the Eastern Nile deep-sea fan: insights from physical experiments. *Basin Research*, *22*(5), 765-782.
- Longacre, M., Bentham, P., Hanbal, I., Cotton, J., & Edwards, R. (2007, April). New crustal structure of the Eastern Mediterranean basin: detailed integration and modeling of gravity, magnetic, seismic refraction, and seismic reflection data. In *EGM 2007 International Workshop* (pp. cp-166). European Association of Geoscientists & Engineers.
- Maesano, F. E., Tiberti, M. M., & Basili, R. (2020). Deformation and fault propagation at the lateral termination of a subduction zone: the Alfeo Fault System in the Calabrian Arc, southern Italy. *Frontiers in Earth Science*, *8*, 107.
- Maffione, M., van Hinsbergen, D. J., de Gelder, G. I., van der Goes, F. C., & Morris, A. (2017). Kinematics of Late Cretaceous subduction initiation in the Neo-Tethys Ocean reconstructed from ophiolites of Turkey, Cyprus, and Syria. *Journal of Geophysical Research: Solid Earth*, *122*(5), 3953-3976.

- Maillard, A., Hübscher, C., Benkhelil, J., & Tahchi, E. (2011). Deformed Messinian markers in the Cyprus Arc: tectonic and/or Messinian Salinity Crisis indicators?. *Basin Research*, *23*(2), 146-170.
- Makris, J., Wang, J., Odintsov, S. D., & Udintsev, G. B. (1994). The magnetic field of the eastern Mediterranean Sea. *Geological Structure of the North-Eastern Mediterranean: Jerusalem (Historical Productions-Hall Ltd.)*, 75-85.
- Mcclusky, S., Balassanian, S., Barka, A., Demir, C., Ergintav, S., Georgiev, I., ... & Veis, G. (2000). Global Positioning System constraints on plate kinematics and dynamics in the eastern Mediterranean and Caucasus. *Journal of Geophysical Research: Solid Earth*, *105*(B3), 5695-5719.
- McPhee, P. J., Koç, A., & van Hinsbergen, D. J. (2022). Preparing the ground for plateau growth: Late Neogene Central Anatolian uplift in the context of orogenic and geodynamic evolution since the Cretaceous. *Tectonophysics*, *822*, 229131.
- Mercier, J., Vergely, P., & Delibassis, N. (1973). Comparison between deformation deduced from the analysis of recent faults and from focal mechanisms of earthquakes (an example: the Paphos region, Cyprus). Tectonophysics, 19(4), 315-332.
- Merry, T., Bastow, I., Green, D., Ugo, F., Bell, R., Pilidou, S., & Dimitriadis, I. (2022). *The seismicity of Cyprus* (No. EGU22-5732). Copernicus Meetings.
- Merry (2022) - Upper mantle seismic anisotropy in the eastern Mediterranean and seismicity in Cyprus – Ph.D. thesis. Imperial College London. Department of Earth Science and Engineering.
- Montadert, L., Nicolaides, S., Semb, P. H., & Lie, Ø. (2014). Petroleum systems offshore Cyprus.
- Morris, A., & Maffione, M. (2016). Is the Troodos ophiolite (Cyprus) a complete, transform fault–bounded Neotethyan ridge segment?. *Geology*, *44*(3), 199-202.
- Netzeband, G. L., Gohl, K., Hübscher, C. P., Ben-Avraham, Z., Dehghani, G. A., Gajewski, D., & Liersch, P. (2006). The Levantine Basin—crustal structure and origin. *Tectonophysics*, *418*(3-4), 167-188.
- Nichols, G. (2009). Sedimentology and stratigraphy. John Wiley & Sons.
- Noda, A. (2016). Forearc basins: Types, geometries, and relationships to subduction zone dynamics. *Bulletin*, *128*(5-6), 879-895.

- Özbakır, A. D., Govers, R., & Fichtner, A. (2020). The Kefalonia Transform Fault: A STEP fault in the making. *Tectonophysics*, *787*, 228471.
- Ozel, E., Ulug, A., & Pekcetinoz, B. (2007). Neotectonic aspects of the northern margin of the Adana-Cilicia submarine basin, NE Mediterranean. *Journal of Earth System Science*, *116*(2), 113-124.
- Papadimitriou, N., Gorini, C., Nader, F. H., Deschamps, R., Symeou, V., & Lecomte, J. C. (2018). Tectono-stratigraphic evolution of the western margin of the Levant Basin (offshore Cyprus). *Marine and Petroleum Geology*, *91*, 683-705.
- Papazachos, B. C., & Papaioannou, C. A. (1999). Lithospheric boundaries and plate motions in the Cyprus area. Tectonophysics, 308(1-2), 193-204.
- Reiche, S., Hübscher, C., & Ehrhardt, A. (2016). The impact of salt on the late Messinian to recent tectonostratigraphic evolution of the Cyprus subduction zone. *Basin Research*, *28*(5), 569-597.
- Rexer, M., Hirt, C., Claessens, S., & Tenzer, R. (2016). Layer-based modelling of the Earth's gravitational potential up to 10-km scale in spherical harmonics in spherical and ellipsoidal approximation. Surveys in Geophysics, 37, 1035-1074.
- Robertson, A. H. (1998). Tectonic significance of the Eratosthenes Seamount: a continental fragment in the process of collision with a subduction zone in the eastern Mediterranean (Ocean Drilling Program Leg 160). *Tectonophysics*, *298*(1-3), 63-82.
- Robertson, A. H. (2002). Overview of the genesis and emplacement of Mesozoic ophiolites in the Eastern Mediterranean Tethyan region. *Lithos*, *65*(1-2), 1-67.
- Robertson, A. H. F. (1976). Pelagic chalks and calciturbidites from the lower Tertiary of the Troodos Massif, Cyprus. *Journal of Sedimentary Research*, *46*(4), 1007-1016.
- Robertson, A. H., Parlak, O., & Ustaömer, T. (2012). Overview of the Palaeozoic–Neogene evolution of neotethys in the Eastern Mediterranean region (southern turkey, cyprus, Syria). *Petroleum Geoscience*, *18*(4), 381-404.
- Rybakov, M., Goldshmidt, V., Hall, J. K., Ben-Avraham, Z., & Lazar, M. (2011). New insights into the sources of magnetic anomalies in the Levant. *Russian Geology and Geophysics*, *52*(4), 377-397.
- Sagy, Y., Gvirtzman, Z., Reshef, M., & Makovsky, Y. (2015). The enigma of the Jonah high in the middle of the Levant basin and its significance to the history of rifting. *Tectonophysics*, *665*, 186-198.

- Sarhan, M. A. (2015). High resolution sequence stratigraphic analysis of the late Miocene Abu Madi Formation, northern Nile Delta Basin. *NRIAG Journal of Astronomy and Geophysics*, *4*(2), 298-306.
- Schattner, U. (2010). What triggered the early-to-mid Pleistocene tectonic transition across the entire eastern Mediterranean?. *Earth and Planetary Science Letters*, *289*(3-4), 539-548.
- Schildgen, T. F., Yıldırım, C., Cosentino, D., & Strecker, M. R. (2014). Linking slab break-off, Hellenic trench retreat, and uplift of the Central and Eastern Anatolian plateaus. *Earth-Science Reviews*, *128*, 147-168.
- Segev, A., & Rybakov, M. (2010). Effects of Cretaceous plume and convergence, and Early Tertiary tectonomagmatic quiescence on the central and southern Levant continental margin. *Journal of the Geological Society*, *167*(4), 731-749.
- Segev, A., Sass, E., & Schattner, U. (2018). Age and structure of the Levant basin, Eastern Mediterranean. *Earth-Science Reviews*, *182*, 233-250.
- Sellier, N. C., Loncke, L., Vendeville, B. C., Mascle, J., Zitter, T., Woodside, J., & Loubrieu, B. (2013). Post-messinian evolution of the florence ridge area (western Cyprus arc), Part I: morphostructural analysis. *Tectonophysics*, *591*, 131-142.
- Skiple, C., Anderson, E., & Fürstenau, J. (2012). Seismic interpretation and attribute analysis of the Herodotus and the Levantine Basin, offshore Cyprus and Lebanon. *Petroleum Geoscience*, *18*(4), 433-442.
- Smaily, L. I. (2017). *Lithosphere dynamics and architecture of the Levant basin margins: integrated geophysical approach* (Doctoral dissertation, Université Pierre et Marie Curie-Paris VI; Université Saint-Joseph (Beyrouth). Ecole supérieure d'ingénieurs de Beyrouth).
- Stampfli, G. M., & Borel, G. D. (2002). A plate tectonic model for the Paleozoic and Mesozoic constrained by dynamic plate boundaries and restored synthetic oceanic isochrons. *Earth and Planetary science letters*, *196*(1-2), 17-33.
- Steinberg, J., Gvirtzman, Z., Folkman, Y., & Garfunkel, Z. (2011). Origin and nature of the rapid late Tertiary filling of the Levant Basin. *Geology*, *39*(4), 355-358.
- Symeou, V., Homberg, C., Nader, F. H., Darnault, R., Lecomte, J. C., & Papadimitriou, N. (2018). Longitudinal and temporal evolution of the tectonic style along the Cyprus Arc system, assessed through 2-D reflection seismic interpretation. *Tectonics*, *37*(1), 30-47.

- Tugend, J., Chamot-Rooke, N., Arsenikos, S., Blanpied, C., & Frizon de Lamotte, D. (2019). Geology of the Ionian Basin and margins: A key to the East Mediterranean geodynamics. *Tectonics*, *38*(8), 2668-2702.
- Van Hinsbergen, D. J., Torsvik, T. H., Schmid, S. M., Maţenco, L. C., Maffione, M., Vissers, R. L., ... & Spakman, W. (2020). Orogenic architecture of the Mediterranean region and kinematic reconstruction of its tectonic evolution since the Triassic. *Gondwana Research*, *81*, 79-229.
- Van Simaeys, S., Janszen, A., Hardy, C., Garnier, E., Sullivan, M., Fabuel-Perez, I., ... & Twigg, T. (2019, June). Unravelling the Tectono-Stratigraphy of the Eratosthenes Continental Block. In *81st EAGE Conference and Exhibition 2019* (Vol. 2019, No. 1, pp. 1-5). European Association of Geoscientists & Engineers.
- Verschuur, D. J., Berkhout, A. J., & Wapenaar, C. P. A. (1992). Adaptive surface-related multiple elimination. *Geophysics*, *57*(9), 1166-1177.
- Vidal, N., Klaeschen, D., Kopf, A., Docherty, C., Von Huene, R., & Krasheninnikov, V. A. (2000). Seismic images at the convergence zone from south of Cyprus to the Syrian coast, eastern Mediterranean. *Tectonophysics*, *329*(1-4), 157-170.
- Wdowinski, S., Ben-Avraham, Z., Arvidsson, R., & Ekström, G. (2006). Seismotectonics of the Cyprian arc. *Geophysical Journal International*, *164*(1), 176-181.
- Wiggins, J. W. (1988). Attenuation of complex water-bottom multiples by wave-equation-based prediction and subtraction. *Geophysics*, *53*(12), 1527-1539.
- Woodside, J. M. (1977). Tectonic elements and crust of the eastern Mediterranean Sea. *Marine Geophysical Researches*, *3*(3), 317-354.
- Zingerle, P., Pail, R., Gruber, T., & Oikonomidou, X. (2020). The combined global gravity field model XGM2019e. Journal of Geodesy, 94, 1-12.

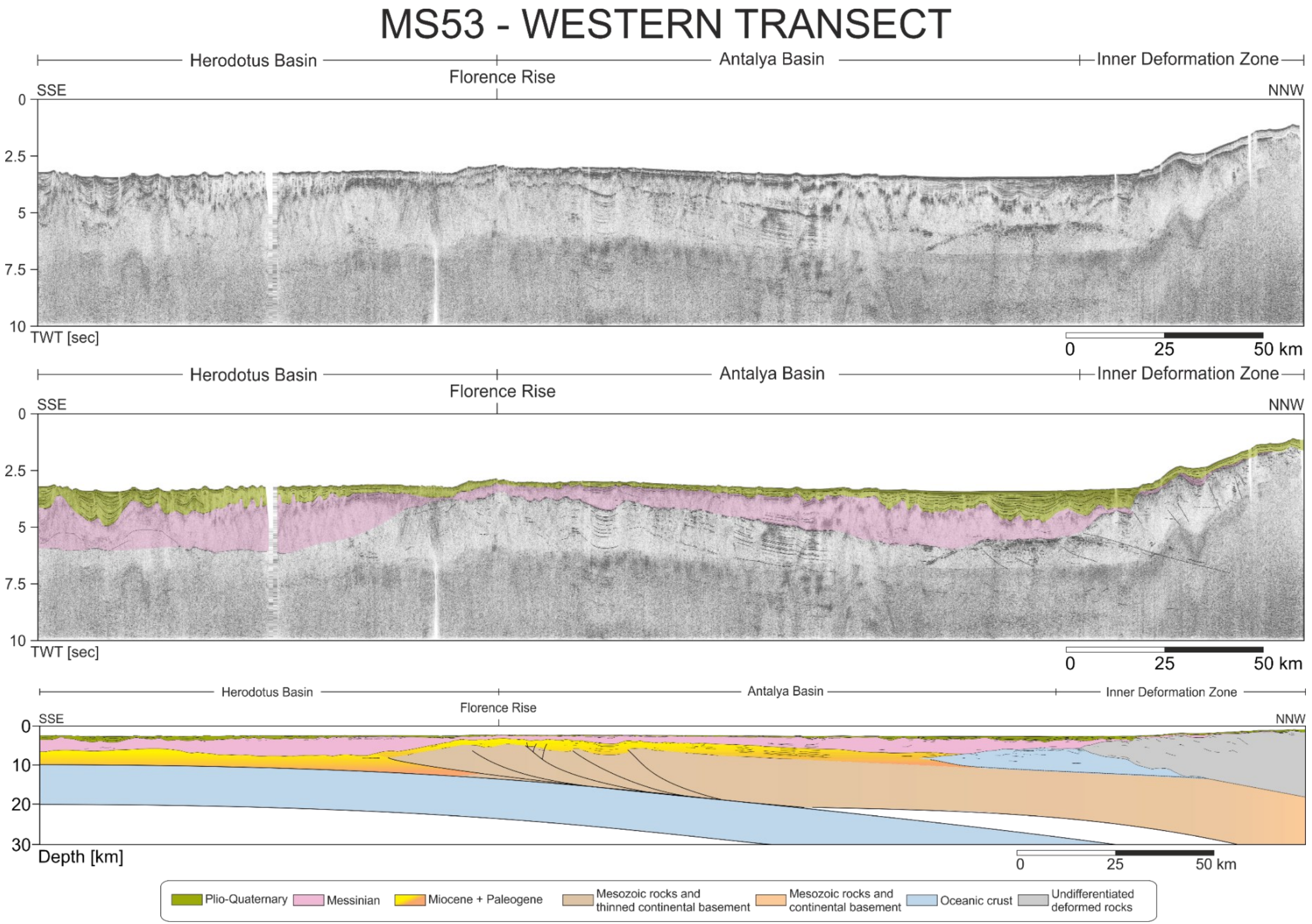

Figure Supplementary Materials 1: Top: MS53 time-migrated with 6x vertical exaggeration. Center: Interpreted MS53 time-migrated with 6x vertical exaggeration. Bottom: Western Transect geological model.

STRAKHOV-8 - CENTRAL TRANSECT

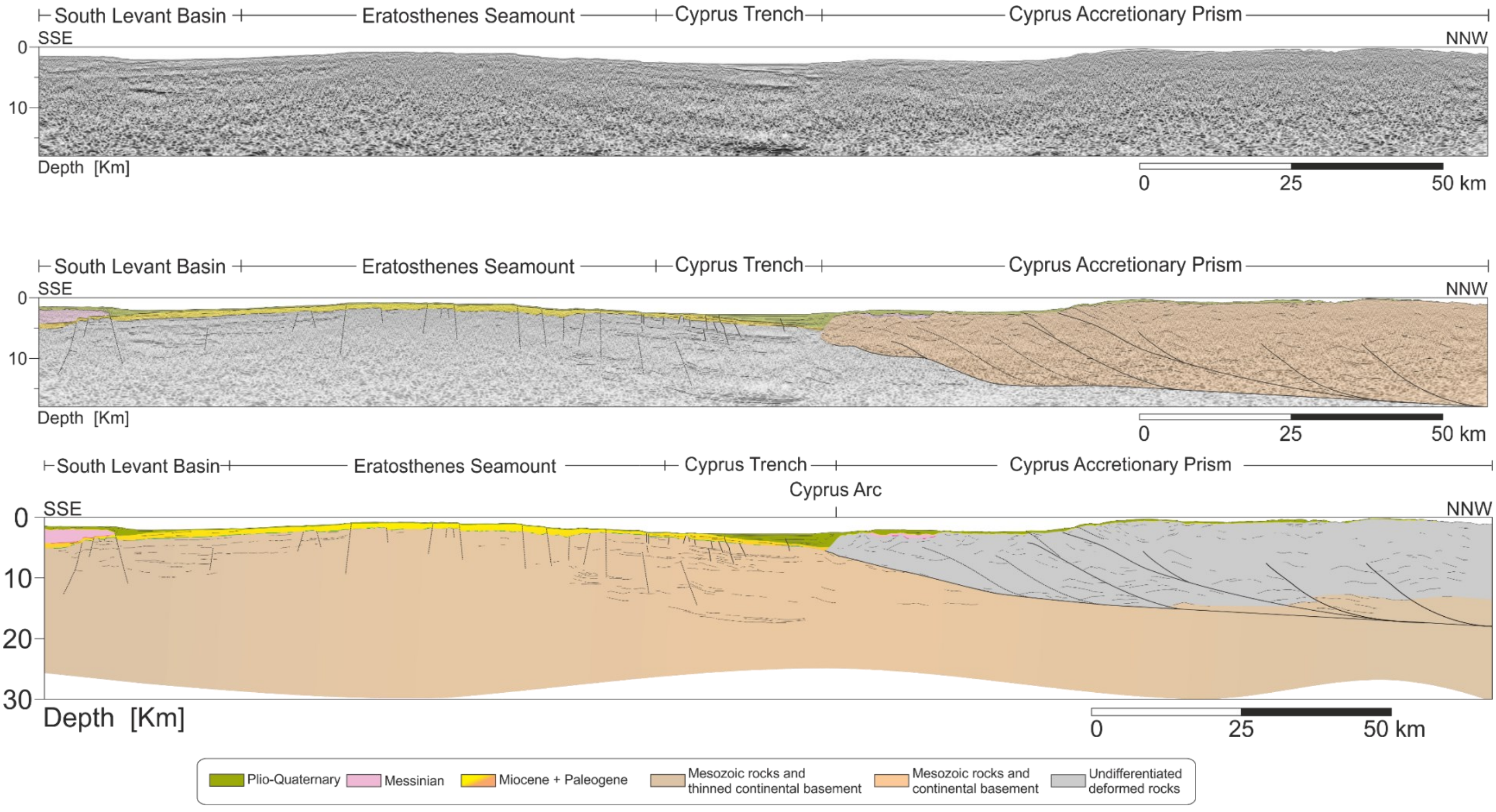

Figure Supplementary Materials 2: Top: Strakhov8 depth-migrated without vertical exaggeration. Bottom: Central Transect geological model.

MS56 - EASTERN TRANSECT

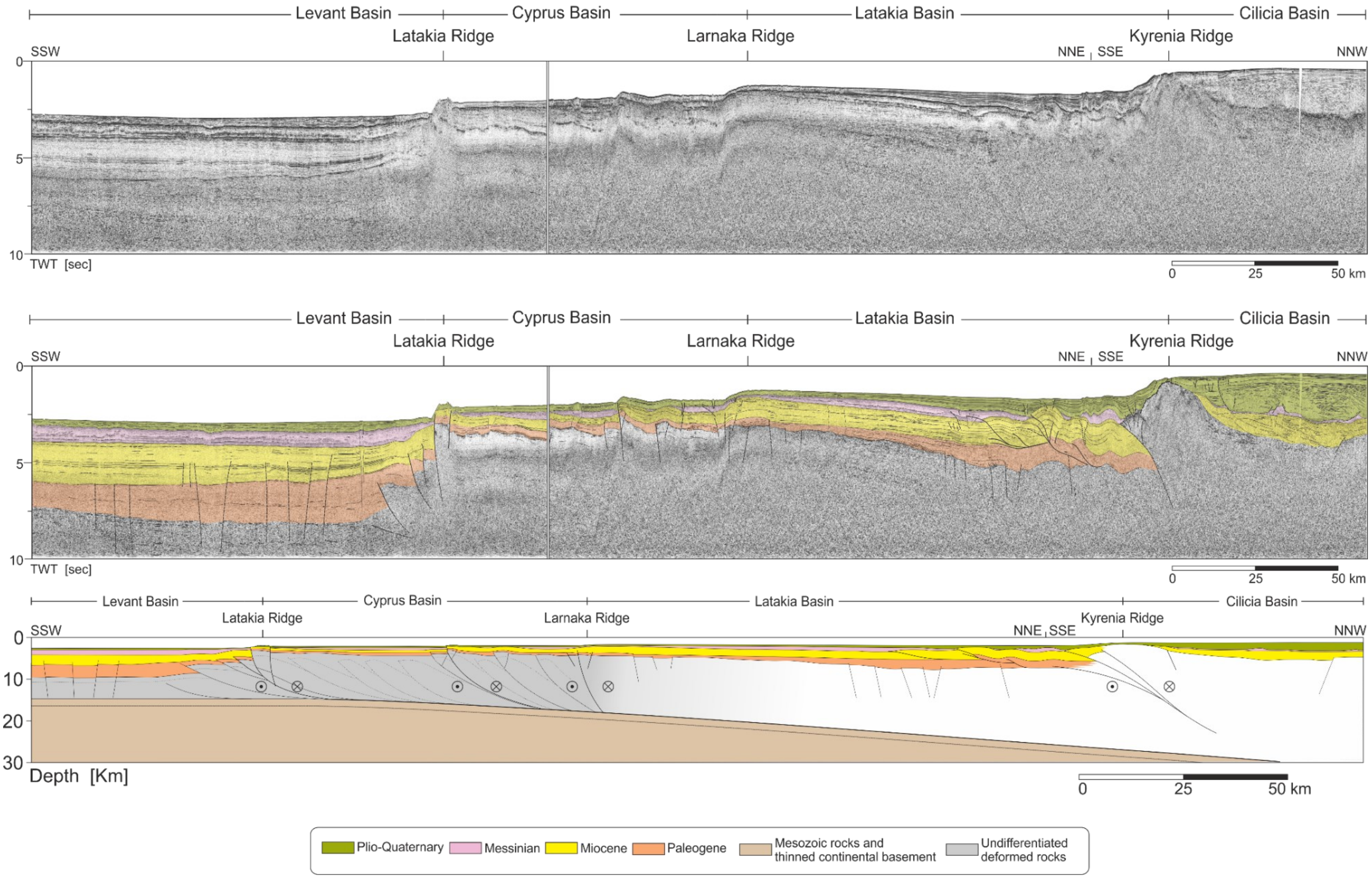

Figure Supplementary Materials 3: Top: MS56 time-migrated with 6x vertical exaggeration. Center: Interpreted MS56 time-migrated with 6x vertical exaggeration. Bottom: Eastern Transect geological model.

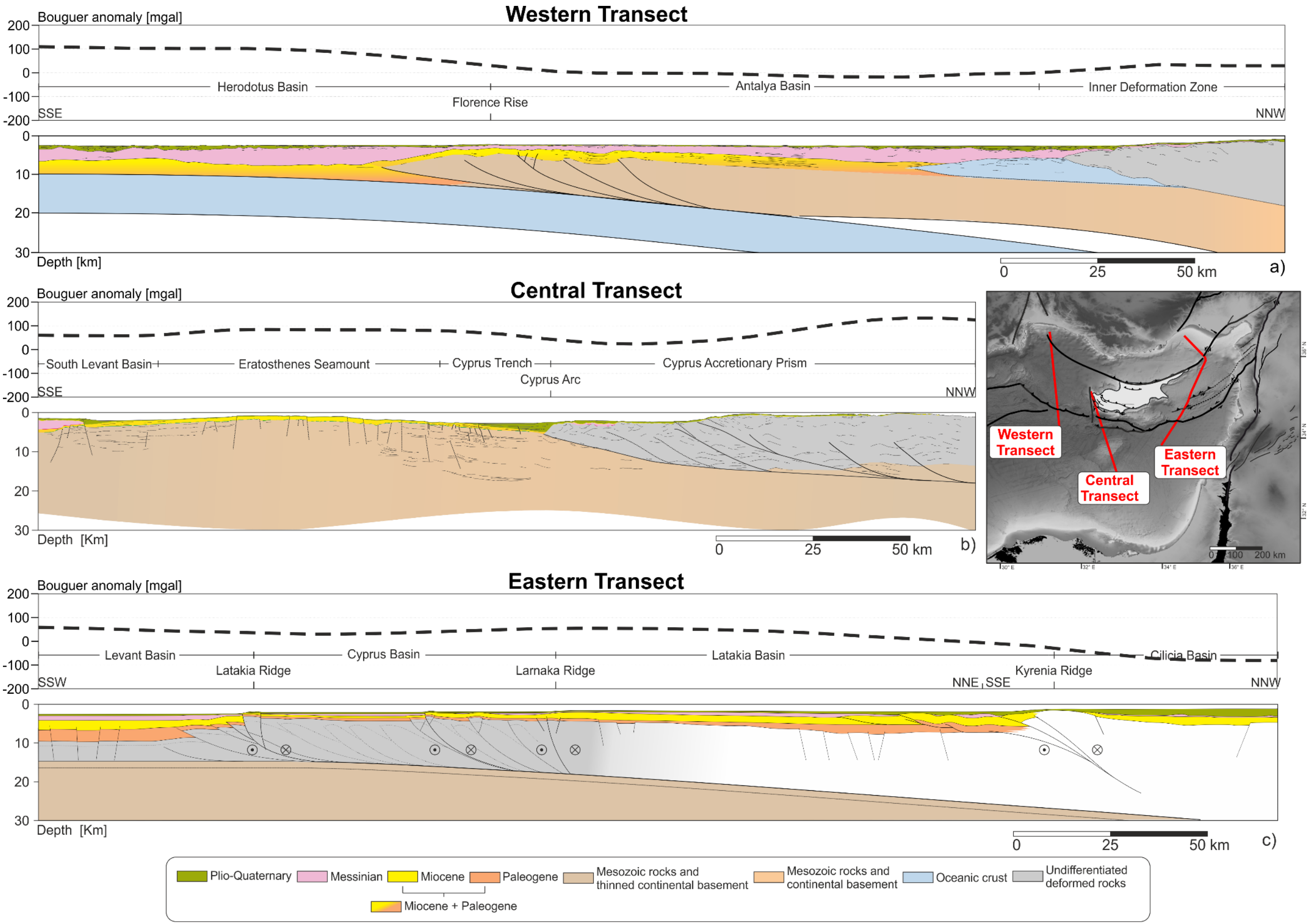

Figure Supplementary Materials 4: a) Western Transect with the corresponding Bouguer anomaly curve. b) Central Transect with the corresponding Bouguer anomaly curve. c) Eastern Transect with the corresponding Bouguer anomaly curve. The Bouguer anomaly grid derived from Ziengerle et al. (2020) with applied a terrain correction from Rexer et al. (2016).

Acknowledgment

First of all, of course, a big thank you to my supervisors: Gian Andrea, Anna and Lorenzo.

Gian Andrea Pini for encouraging discussions about everything but the PhD project. A break is always needed!

Anna Del Ben for the help during the interpretation phase and for the long discussions about the field of study, which always ended with us talking about everything everywhere in the world that could be related to the field of study. She really sprays passion and dedication!

Lorenzo Bonini for the extensive support he gave me from the beginning to the end of this PhD. Lorenzo gave me the best tools and practise to tackle this difficult project. During these years he was really my academic mentor. I learned from him everything about analogue modelling, something about structural modelling and I hope to have enriched his knowledge about seismic reflection methods.

I would also like to thank the reviewers Giovanni Toscani and Roberto Basili for their time and effort; their comments greatly improved the quality of this manuscript.

Many thanks to Dirk Klaeschen (GEOMAR) for providing the fundamental Strakhov dataset and finding old papers not available online.

I would also like to acknowledge the students I helped and who helped me with their BSc and MSc work: Agnese, Eugenia and Michelle. They assisted me in carrying out some aspects of my research topic. Special thanks to Eugenia, the best student I had the honour to supervise.

OGS is acknowledged for providing the MS dataset, especially Giuseppe (Beppe) Brancatelli, Edy Forlin and Angelo Camerlenghi. Beppe was my co-supervisor during the Master's thesis and continued to support me during the PhD. He is really the best when it comes to processing the MS vintage dataset and provided me with the seismic data of course, but also technical support.

Thank you to Christian Gorini and Christian Blanpied who helped me during the "blocking phase". I felt isolated during the PhD because no one here in Italy is studying this part of the Mediterranean and no one here in Trieste is doing similar research. Therefore, they encouraged me through long discussions and brought me field information that I did not have access to.

A big thank you to Carlotta, the best girlfriend in the world. She always supports me and encourages me to keep going even in difficult times. At the end I really thought about giving up, but I finally managed to finish the PhD, mainly thanks to her positive spirit.

Of course, I thank all my friends who made me feel relaxed, chill, and have a good time during these years. I also had the opportunity to meet other excellent friends at congresses or summer schools. Some of them have inspired me in my research, others have given me nice conversations and interesting ideas, and still others have given me a smile. Friends really are the family we choose!

I thank my family for their emotional and economic support, without which I could not afford to be here.

And finally, I would like to thank my willpower for making it possible for me to complete this hard and sometimes tedious journey!